Electronic Thesis and Dissertation Repository

8-1-2018 10:00 AM

Toward optimization of target planning for magnetic resonance image-targeted, 3D transrectal ultrasound-guided fusion prostate biopsy

Peter Martin
The University of Western Ontario

Supervisor
Ward, Aaron D.
The University of Western Ontario

Recommended Citation

Abstract

The current clinical standard for diagnosis of prostate cancer (PCa) is 2D transrectal ultrasound (TRUS)-guided biopsy. However, this procedure has a false negative rate of 21-47% and therefore many patients return for repeat biopsies. A potential solution for improving upon this problem is "fusion" biopsy, where magnetic resonance imaging (MRI) is used for PCa detection and localization prior to biopsy. In this procedure, tumours are delineated on pre-procedural MRI and registered to the 3D TRUS needle guidance modality. However, fusion biopsy continues to yield false negative results and there remains a gap in knowledge regarding biopsy needle target selection. Within-tumour needle targets are currently chosen ad hoc by the operating clinician without accounting for guidance system and registration errors. The objective of this thesis was to investigate how the choice of target selection strategy and number of biopsy attempts made per lesion may affect PCa diagnosis in the presence of needle delivery error.

A fusion prostate biopsy simulation software platform was developed, which allowed for the investigation of how needle delivery error affects PCa diagnosis and cancer burden estimation. Initial work was conducted using 3D lesions contoured on MRI by collaborating radiologists. The results indicated that more than one core must be taken from the majority of lesions to achieve a sampling probability $\geq$ 95% for a biopsy system with needle delivery error $\geq$ 3.5 mm. Furthermore, it was observed that the optimal targeting scheme depends on the relative levels of systematic and random needle delivery errors inherent to the specific fusion biopsy system. Lastly, PCa tumours contoured on digital histology images by

genitourinary pathologists were used to conduct biopsy simulations. The results

demonstrated that needle delivery error has a substantial impact on the biopsy core

involvement observed, and that targeting of high-grade lesions may result in higher core

involvement variability compared with lesions of all grades.

This work represents a first step toward improving the manner in which lesions are targeted

using fusion biopsy. Successful integration of these findings into current fusion biopsy

system operation could lead to earlier PCa diagnosis with the need for fewer repeat biopsy

procedures.

Keywords

Co-Authorship Statement

This thesis is presented in an integrated article format, wherein the chapters are based on the following publications, which are either currently published or in preparation for submission to a peer-reviewed journal. As the first author on these peer-reviewed manuscripts, I was a substantial contributor to all aspects of the studies, including manuscript preparation and publication. I was responsible for experiment design, including the planning, implementation and analysis of all experiments, including development of many of the software tools used for analysis. I was also responsible for drafting, submission and revisions of all manuscripts. All work was performed under the supervision of Dr. Aaron Ward, who is the senior author on all manuscripts. Dr. Ward was responsible for study conception, development of key research questions, experiment design, interpretation of results, and the revision of all manuscripts.

Chapter 2, "Magnetic resonance imaging-targeted, 3D transrectal ultrasound-guided fusion biopsy for prostate cancer: quantifying the impact of needle delivery error on diagnosis," was published in *Medical Physics* in May 2014. This work was co-authored by Derek Cool, Cesare Romagnoli, Aaron Fenster and Aaron Ward. Derek Cool and Cesare Romagnoli were responsible for lesion contouring on MRI performed for this study, generating tumour volumes for analysis. Aaron Fenster was responsible for design of the clinical trial wherein all ultrasound and MR images used for analysis were obtained.

Chapter 3, "A comparison of prostate tumour targeting strategies using magnetic resonance imaging-targeted, transrectal ultrasound-guided fusion biopsy," was published in *Medical Physics* in March 2018. This work was co-authored by Derek Cool, Aaron Fenster

and Aaron Ward. Derek Cool was responsible for lesion contouring on MRI performed for this study, generating tumour volumes for analysis. Aaron Fenster was responsible for design of the clinical trial wherein all ultrasound and MR images used for analysis were obtained.

Chapter 4, "Investigating the impact of prostate biopsy guidance error on pathologic cancer risk assessment," is in preparation for submission to *SPIE Journal of Medical Imaging*. This work was coauthored by Mena Gaed, Jose Gómez, Madeleine Moussa, Derek Cool, Joseph Chin, Stephen Pautler, Aaron Fenster and Aaron Ward. Mena Gaed, Jose Gómez and Madeleine Moussa were responsible for the collection and analysis of the histology data. Derek Cool was responsible for lesion contouring on MRI performed for this study, generating tumour volumes for analysis. Joseph Chin and Stephen Pautler recruited subjects and performed prostatectomies, generating histology specimens for analysis. Aaron Fenster was responsible for design of the clinical trial wherein all ultrasound, MR and histology images used for analysis were obtained.

Dedicated to the memory of my grandfather, Thomas Marshall, a man whose unrivaled

humour and charisma is dearly missed;

and to Neil Young, for *Tell Me Why*

Acknowledgments

There are many people whose support and guidance were instrumental to the completion of this thesis.

First and foremost, I would like to thank my supervisor Dr. Aaron Ward for his mentorship throughout my graduate studies, you are an inspiring example of the type of researcher that I aspire to be. The support you have provided me throughout these past few years has allowed me to develop into a better scientist, communicator and leader. I cannot begin to express the full extent of my gratitude for all that you have done for both my personal and career development.

I have been immensely fortunate to collaborate throughout my research project with Dr. Aaron Fenster, Dr. Derek Cool and the late Dr. Cesare Romagnoli. Without you, none of the work in this thesis would have been possible. I would also like to thank Dr. Charlie McKenzie for your support and guidance as a member of my advisory committee.

To our collaborators from the Image Guidance in Prostate Cancer team, Dr. Glenn Bauman, Dr. José Gómez, Dr. Madeleine Moussa, Dr. Joseph Chin and Dr. Stephen Pautler, thank you for your continued support and interest in this work. I would also like to thank Dr. Mena Gaed and Cathie Crukley, for somehow finding a way to make tedious days of specimen processing thoroughly enjoyable.

Thank you to Dr. Terry Peters, Dr. George Hajdok, Dr. Ashley Mercado and Dr. Parvin Mousavi, you have my utmost gratitude for the time and effort you have spent in evaluating my thesis and for sharing this day with me.

years of my life. For making our home a loving environment full of music and laughter, for the long drives and the tranquil Algonquin sunsets, you have had a more profound effect on my life than words can express.

Table of Contents

List of Tables

List of Figures

List of Abbreviations

2D	Two-dimensional
3D	Three-dimensional
ADC	Apparent diffusion coefficient
AE	Axial error
BPH	Benign prostatic hyperplasia
DCE	Dynamic contrast-enhanced
DRE	Digital rectal examination
DWI	Diffusion-weighted imaging
GTV	Gross tumour volume
MHz	Megahertz
mpMRI	Multi-parametric magnetic resonance imaging
MR	Magnetic resonance
MRI	Magnetic resonance imaging
P	Tumour sampling probability
PCa	Prostate cancer
PCF	Positive core fraction
PI-RADS	Prostate Imaging Reporting and Data System
PSA	Prostate-specific antigen

PZ	Peripheral zone
RMS	Root mean square
RMSE	Root mean square error
SD	Standard deviation
SystMag	Systematic error magnitude
SystAngle	Systematic error angle
TRE	Target registration error
TRUS	Transrectal ultrasound
T2W	T2-weighted
T1W	T1-weighted
TNM	Tumour, Node, Metastasis Classification of Malignant Tumours

Chapter 1

1 Introduction

The work in this thesis is primarily concerned with modifications to the strategies used in performing magnetic resonance imaging-targeted, 3D transrectal ultrasound (TRUS)-guided "fusion" prostate biopsy. "Fusion" biopsy refers to the use of MRI-3D TRUS fusion to allow targeting of MRI-defined lesions using a 3D TRUS biopsy system. Such biopsy systems were developed as a potential solution to the high false negative rate of clinical standard 2D transrectal ultrasound-guided biopsy. However, while such systems have shown an increase in cancer detection rate of prostate biopsy, fusion biopsy continues to yield false negative results. Therefore, a need remains for improvement in detection rate for timely diagnosis of PCa while it is still small and curable. There exists substantial research into prostate imaging and biopsy needle guidance, but there remains a gap in knowledge regarding biopsy plan optimization. Within-tumour needle targets are chosen ad hoc in fusion biopsy without accounting for uncertainties due to guidance system and registration errors, and irregular tumour sizes and shapes. Therefore, the work presented in this thesis is intended further investigate whether optimization of needle target planning with appropriate uncertainty propagation may lead to an improved prostate cancer detection rate.

1.1 Prostate cancer epidemiology and impact

Prostate cancer (PCa) is the most commonly diagnosed non-cutaneous cancer in North American men[1]. Approximately one in seven Canadian men will develop PCa and 1 in 29 men will die from the disease. In Canada, 21300 new cases of PCa were projected for 2017[1].

While PCa is a highly treatable disease, with a 5 year net survival of 95% for those diagnosed[1], those who receive treatment often face substantial costs to quality of life as a result of the treatment. Regardless of patient age, the anatomical location of the prostate relative to the neurovascular bundles, bladder, rectum and urethra means that conventional treatments such as prostatectomy, external beam radiation therapy and brachytherapy lead to decreased urinary, bowel and sexual health[2].

Perhaps one of the largest challenges with PCa is that its aggressiveness can vary widely, as measured by the Gleason grade of the cancer[3]. Due to this variety of PCa grades, some PCa patients need urgent care while others have indolent cancers that are unlikely to be fatal.

1.2   Prostate cancer diagnosis

1.2.1   Digital rectal examination

Digital rectal exam (DRE) is an exam in which a physician palpates the prostate gland through the rectal wall. DRE generally performs poorly in the detection of PCa with a positive predictive value between 17-38%[4]; however it is more sensitive to detection of PCa in the peripheral zone (PZ) of the prostate, as the PZ is adjacent to the rectal wall. In cases of PCa in the PZ (where 70-80% of prostate cancers form[5]), the physician may detect a hardening of tissue that would be particularly suspicious if it is asymmetric with the contralateral side of the gland. As this test suffers from a generally poor sensitivity outside of the PZ and misses most early stage tumours[6], it is often used in conjunction with the prostate specific antigen (PSA) test.

1.2.2   Prostate specific antigen test

Prostate specific antigen (PSA) is a glycoprotein produced by the prostate gland. It was shown by Stamey et al[7] that the PSA levels in the blood correlated with PCa stage. Generally, a PSA level of 4.0 ng/mL or higher is considered suspicious for the presence of PCa[8]. However, the PSA test suffers from numerous sources of inaccuracy, as sources other than PCa can cause elevated PSA levels in the blood. Some examples include benign prostatic hyperplasia (BPH), prostatitis and previous prostate biopsies[9]. In order

to detect cancers at an early and treatable stage, a combination of DRE and PSA testing is used in Canada to screen asymptomatic men. This method of PCa screening remains controversial due to the balance of benefit achieved through treating aggressive cancer early versus the decreased quality of life for men with indolent cancers who receive treatment.

1.2.3   2D transrectal ultrasound (TRUS)-guided biopsy

If there is suspicion that a patient has PCa, they will be referred for a prostate biopsy, the current standard for definitive diagnosis of PCa. In this procedure, tissue samples are taken from the prostate using a biopsy needle, either through the rectal wall (transrectally) or through the perineum (transperineally) and the samples are then sent to pathology in order to assess the presence and Gleason grade of cancer[3]. In particular, 2D transrectal ultrasound (TRUS)-guided biopsy is the current clinical standard for PCa diagnosis. However, as PCa is generally not detectable on ultrasound[10-12], 6-12 biopsy cores are taken using a systematic targeting scheme which primarily samples the peripheral zone of the gland where most cancers are located (Fig. 1-1). However, this approach has been shown to have upwards of a 21-47% false negative rate in terms of PCa diagnosis[13, 14], and therefore many patients are required to return to the clinic for repeat biopsies. Furthermore, this method may lead to an underestimation or an overestimation of a PCa patient's true Gleason score[15].
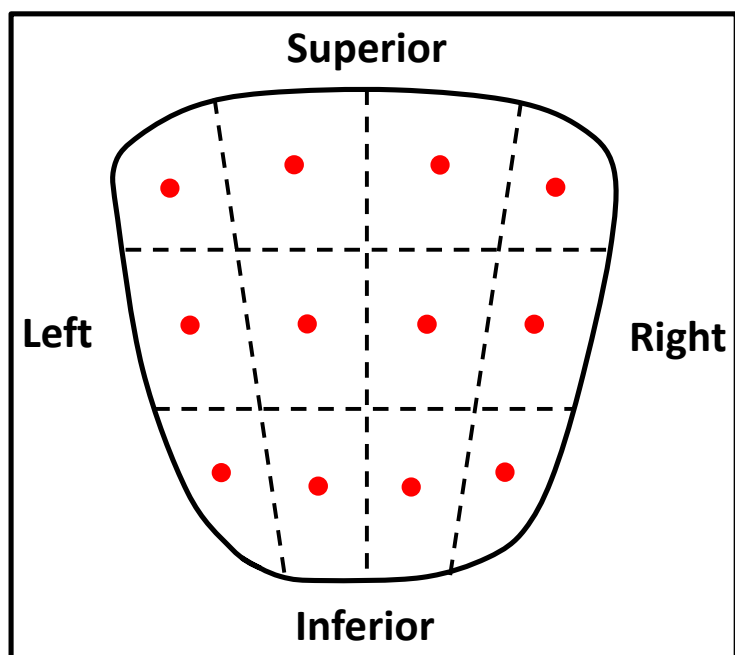
Figure 1-1: 12 needle target locations for an "extended-sextant" prostate biopsy targeting scheme.

After biopsy, tissue from each core is examined under a microscope in order to estimate cancer burden for the patient using the TNM Classification of Malignant Tumours system[8] (where TNM stands for tumours, nodes and metastases). In this system, PCa of the primary tumour is classified into stages T1 – T4. The criteria for stages T1 through T4 are described in Table 1-1. Additional to TNM staging of PCa, three other important measures for estimation of cancer burden include the Gleason scores of tumours sampled through biopsy, the number of biopsy cores containing cancer tissue, and the core involvement obtained (i.e. the proportion of the biopsy core which contains tumour tissue)[8].

Table 1-1: TNM staging system for PCa: primary tumour (T)

Stage	Sub-stage	Criteria
T1	-	Clinically inapparent tumour, not palpable or visible by imaging.
-	T1a	Tumour incidental histologic finding in 5% or less of resected tissue.
-	T1b	Tumour incidental histologic finding in more than 5% of resected tissue.
	T1c	Tumour identified by needle biopsy
T2	-	Tumour confined within prostate
-	T2a	Tumour involves one half of one lobe or less
-	T2b	Tumour involves more than one half of one lobe, but not both lobes.
-	T2c	Tumour involves both lobes
T3	-	Tumour extends through prostatic capsule
-	T3a	Extracapsular extension
-	T3b	Tumour invades the seminal vesicles.
T4	-	Tumour invades structures other than seminal vesicles: bladder, pelvic wall and/or levator muscles.

However, grading biopsy tissue is a challenging issue, and may contribute to the problem of overtreatment of men with indolent PCa[16, 17]. In an attempt to reduce the overtreatment of PCa, there has been a push in the past two decades to place men with low risk cancers on active surveillance. However, it has been shown that 25-37% of men who are placed on active surveillance after receiving 2D TRUS-guided biopsy are removed from surveillance to receive treatment within 5 years[18, 19]. This may be due to underestimation of tumour grade on initial biopsy, interval changes in the tumour histology, and/or patients opting for definitive treatment, however this indicates that improved methods for per-patient estimation of PCa burden are needed.

1.2.4   Prostate cancer imaging techniques

1.2.4.1   Ultrasound Imaging

Due its portability, inherent real-time nature, and relatively low cost compared to magnetic resonance imaging, transrectal ultrasound (TRUS) is currently the most commonly used modality for image guided prostate biopsy and other needle-based therapies such as brachytherapy. TRUS allows easy visualization of zonal anatomy and is also important for estimation of prostate volume primarily for calculation of PSA density for cancer staging[8]. In this imaging modality, a transducer which contains transmitting elements generates ultrasonic waves[20], which in the context of TRUS imaging operate in the range of 5-10 MHz. As discussed further in Section 1.2.5.1, some

TRUS systems contain enhanced functionality which allows for the reconstruction of a full 3D volume using multiple single-plane 2D TRUS images. The acquisition rate of 2D TRUS imaging is generally 10-20 frames per second, while acquisition of a 3D TRUS image can take upwards of 13 seconds[21]. A labelled 2D TRUS image of a prostate is shown in Figure 1-2.
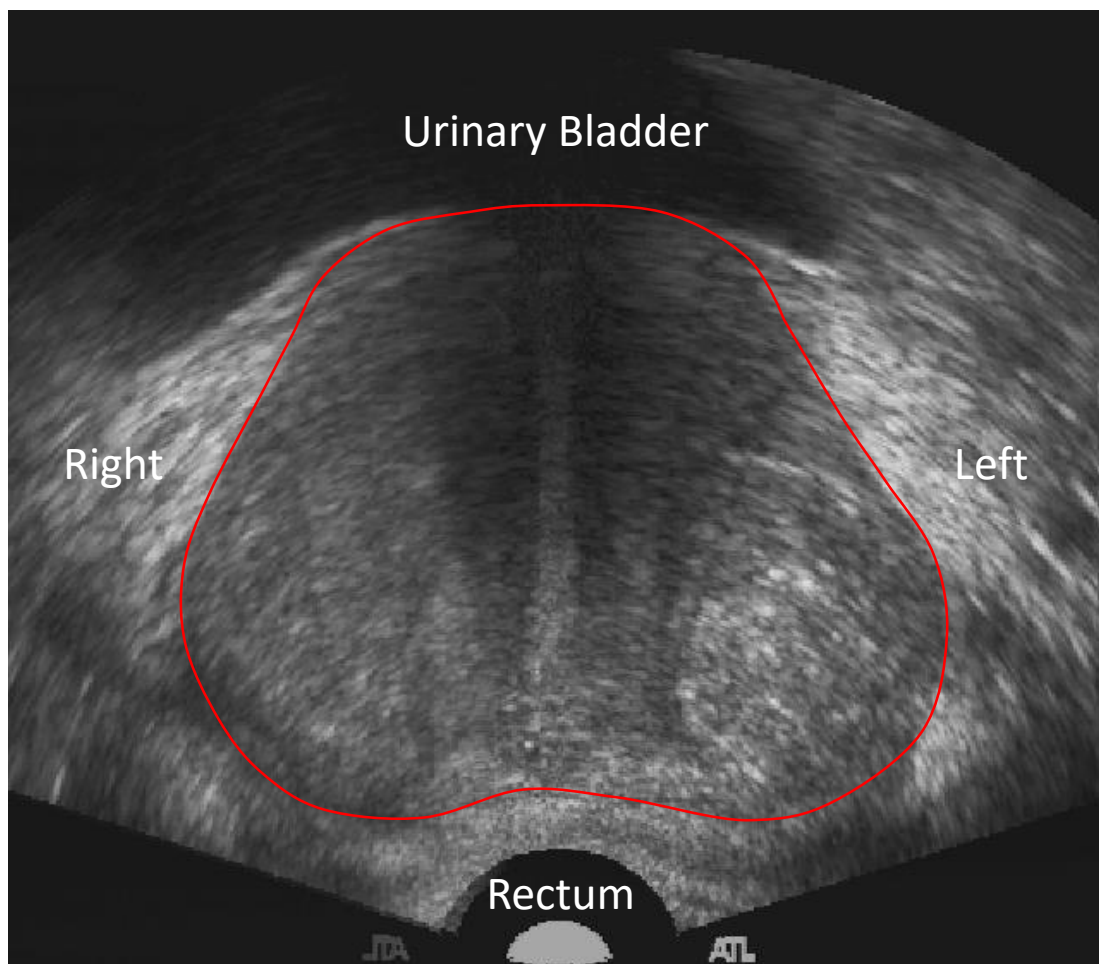
Figure 1-2: An in vivo 2D TRUS image of the prostate. The outline of the prostate is shown in red. Patient left and right are indicated, as well as the locations of the urinary bladder and rectum.

In-vivo ultrasound images are produced by detecting ultrasound waves that are reflected as they penetrate through tissue and anatomical structures of varying density. The degree of reflectance is dependent on the acoustic impedance between two different layers of material or tissue. The structures which reflect the most ultrasound waves

appear bright in the resultant image (hyperechoic), while the structures which reflect the least amount of ultrasound waves appear dark (hypoechoic). In the context of prostate imaging, two examples of structure which appear hyperechoic are the pubic bone and calcifications within the gland. Conversely, fluid filled structures such as the seminal vesicles, bladder and cysts appear hypoechoic.

While in some instances PCa in the PZ can appear hypoechoic on TRUS[22], it generally has a low sensitivity (35-91%) and specificity (24-81%) with respect to detection of PCa[10-12, 23-26]. As discussed in Section 1.2.5.2, due to the limitations of PCa imaging using TRUS, there have been systems developed for MR-guidance of prostate biopsies. However, due to the upfront cost, time and technical challenges required to perform biopsies using these systems, TRUS-guided biopsy remains the standard for prostate biopsy guidance in North America.

1.2.4.2   Magnetic resonance imaging

Magnetic resonance imaging (MRI) has shown to be effective for detection, localization and staging of PCa[27]. A major advantage of MRI compared to TRUS is that it allows for high contrast between soft tissues using different image acquisition sequences, therefore providing richer anatomical detail compared to what can be achieved using TRUS. However, the performance of specific MRI sequences for detection and localization of PCa can vary widely depending on which sequence is used.

Currently the most common MRI sequences used in PCa imaging are T2-weighted imaging, T1-weighted dynamic contrast enhanced imaging and diffusion weighted imaging. Examples of these image sequences are shown in Figure 1-3. These three sequences are the cornerstones of the Prostate Imaging Reporting and Data System (PI-RADS), designed for assessment of PCa risk on MRI[28, 29].

T2-weighted (T2W) MR imaging is one of the most common anatomical MRI sequences, and is sensitive to transverse relaxation of precessing protons after a radio frequency pulse. T2W prostate images provide detailed anatomical maps of prostate zonal anatomy, allowing clear differentiation between the peripheral zone, transition zone and central zone[30]. In terms of detection and localization of PCa, T2W sequences are most useful in the peripheral zone, where cancer can be detected as a region of hypointensity (i.e. appearing dark on T2W MRI) compared to the contralateral side of the PZ. It has been shown that the greater the contrast between the hypointense region and the typically bright normal tissue in the PZ, the higher the Gleason grade of the detected cancer [30, 31]. Overall, T2W interpretation for PCa detection is limited by the similar appearance of cancerous and non-cancerous tissue abnormalities, including BPH, atrophy, chronic prostatitis and also hemorrhaging following prostate biopsy[32].

A common functional technique for the detection of PCa is T1-weighted (T1W) dynamic contrast enhanced (DCE) sequences. In a standard DCE scan, the patient is injected with a contrast agent (such as gadolinium) and imaged using a T1W imaging sequence, typically with a high temporal resolution (<10 seconds). This imaging starts

before the contrast agent is injected, allowing the full "wash-in" and "wash-out" of the contrast agent to be observed. It has been shown that cancerous tissues exhibit an earlier enhancement (i.e. wash-in) and earlier wash-out compared to normal healthy tissue. The qualitative analysis of DCE-MRI in the context of prostate imaging is based on the general assumption that tumour blood vessels are leaky and more readily enhance are injection of the contrast agent, expressed by a fast exchange of blood and contrast agent between capillaries and tumour tissue[33]. This is thought to be caused by higher permeability of new blood vessels formed due to angiogenesis associated with PCa[34].

While qualitative analysis of DCE-MRI is widely practiced, quantitative analysis of these images has been increasing in popularity as well, due to more widely available software designed to perform this analysis, and a growing consensus of the utility of this approach. Several pharmacokinetic models have been proposed for quantitative analysis of DCE-MRI[35-38], and in general these models are based on determining the rate of contrast exchange between plasma and the extracellular space using transfer rate constants, which are known to be elevated in many cancers, including PCa[39, 40]. These quantitative methods have the potential for standardization across various imaging sequences and parameters.

Another functional technique that is now a critical component of prostate MRI is diffusion weighted imaging (DWI). Unlike the dynamic DCE sequence, DWI is a static sequence that does not require injection of a contrast agent, as it used to produce image contrast that is proportional to the diffusion of water molecules. A decrease in the

magnitude of water diffusion is observed with increased cellular density associated with PCa. By acquiring multiple diffusion weighted images with different b-values (which is a parameter that adjusts the level of diffusion weighting), this allows the computation of post-processed apparent diffusion coefficient (ADC) maps. It has been shown that PCa appears as a hyperintense region on high b-level DWI, while it appears as a hypointense region on ADC maps[28]. Furthermore, ADC values are correlated with the Gleason score of PCa, potentially allowing for improved diagnosis of more aggressive cancers[41-44].
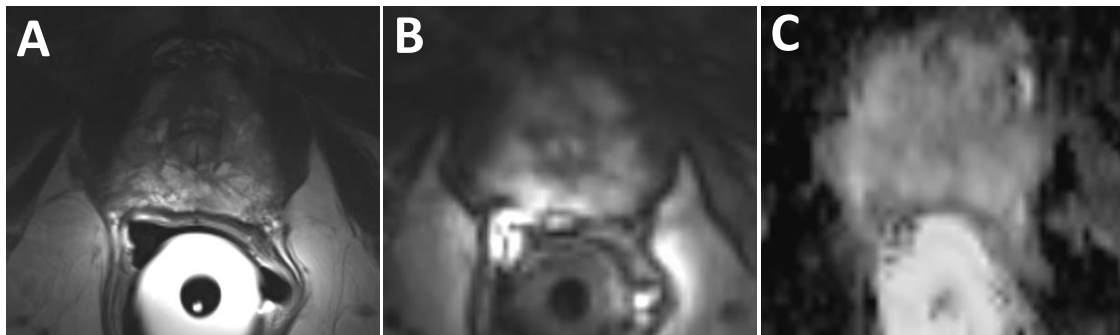
Figure 1-3: In vivo MR imaging showing the same axial slice within a prostate, showing **(A)** a T2W image, **(B)** an image from the T1W DCE sequence, and **(C)** an ADC map calculated from the DWI sequence.

1.2.4.3   Challenges with lesion delineation on imaging

Despite the consensus of utility of MRI in PCa imaging, prostate volumes estimated by radiologists on multi-parametric MRI (mpMRI) consistently overestimate

histological reference volumes[45]. This disagreement between lesions contoured on MRI and histologic cancer leads to challenges in how to best target lesions with biopsy needles, as well as defining gross volumes and clinical target volumes for PCa treatment.

However, despite mpMRI overestimating volume compared with histologic reference volumes, in the context of prostate focal therapy, 95% histologic coverage margins were 8 mm (Gleason score $\geq$ 6) and 6 mm (Gleason score $\geq$ 7) expansions from the gross tumour volumes (GTVs) defined by radiologists on MRI[46]. This is likely due to fact that when considering histologic coverage of clinical treatment volumes, the shape of the lesion must also be considered, as it is possible to overestimate lesion volume on MRI while also not achieving complete coverage of the lesion with the MR-defined contour.

While expansion of the GTV is a promising means to achieve better coverage for prostate therapy, this does not address the challenge of how to adjust biopsy needle targeting to deal with the disagreement between MRI contours and histologic cancer coverage. This is a field of research which requires further investigation.

1.2.5   3D-guided biopsy systems

1.2.5.1   MR-3D TRUS fusion biopsy

The Artemis (Eigen, Grass Valley, CA) is a biopsy system developed by Aaron Fenster's research group at Robarts Research Institute[47], and involves attaching any

standard end-fire 2D TRUS probe to a mechanical tracking device which monitors the real-time 3D orientation of the probe. A 3D TRUS image is then acquired by rotating the probe around its axis. An example of a 3D TRUS fusion biopsy system interface is shown in Fig. 1-4. As this mechanical tracking mechanism can only track the location of the probe itself, an additional motion compensation algorithm is required to compensate for patient motion[48]. While Artemis is one commercially available fusion biopsy system, there now exist numerous other MRI-targeted, 3D TRUS guided biopsy systems for PCa detection. UroNav (Invivo, Gainesville, FL), bkFusion (bk Ultrasound, Peabody, MA), and TargetScan (Envisioneering Medical Technologies, St. Louis, MO) are three examples of other systems developed for fusion prostate biopsy.

The development of 3D TRUS-guided biopsy systems allows for improved spatial information relative to 2D-TRUS, by providing a 3D volume image as opposed to solely a 2D plane. As defined in the beginning of this Chapter, a 3D TRUS biopsy system with MRI-3D TRUS fusion of biopsy targets is known as "fusion" biopsy. In this approach, suspicious regions to be targeted by biopsy are delineated on MRI, and then registered onto the 3D TRUS image volume. Cool et al. showed that fusion biopsy produced significantly higher (p < 0.01) positive biopsy core rates, mean Gleason scores and volumes sampled, compared to 2D TRUS-guided 12-core systematic biopsy[49]. Roethke et al. observed a 29% cancer-positive core rate for targeted fusion prostate biopsy, with cancer detected in 42% of patients[50]. Puech et al. determined that cancer was detected in 69% of patients when undergoing fusion biopsy compared to 50% of patients for systematic TRUS-guided biopsy[51], while Natarajan et al. determined that 33% of targeted

fusion biopsy cores contained cancer-positive tissue compared to 7% of biopsy cores for non-targeted TRUS guided biopsy[52]. Volkin et al. investigated the effectiveness of fusion biopsy specifically for anterior lesions, and observed a cancer detection rate of 40% for fusion biopsy compared to a 26% detection rate for systematic TRUS-guided biopsy cores taken from the equivalent anatomic sextent of the prostate[53]. Conversely, Tonttila et al. did not observe any significant improvement in terms of clinically significant cancer detection rate from the use of MRI-TRUS fusion targeted biopsy vs. the extended sextant standard for target selection[54]. However, it is worth noting that of the three operating clinicians in their study (with 5, 10 and 15 years of 2D-TRUS guided prostate biopsy experience respectively), none had any prior experience with targeted biopsies.
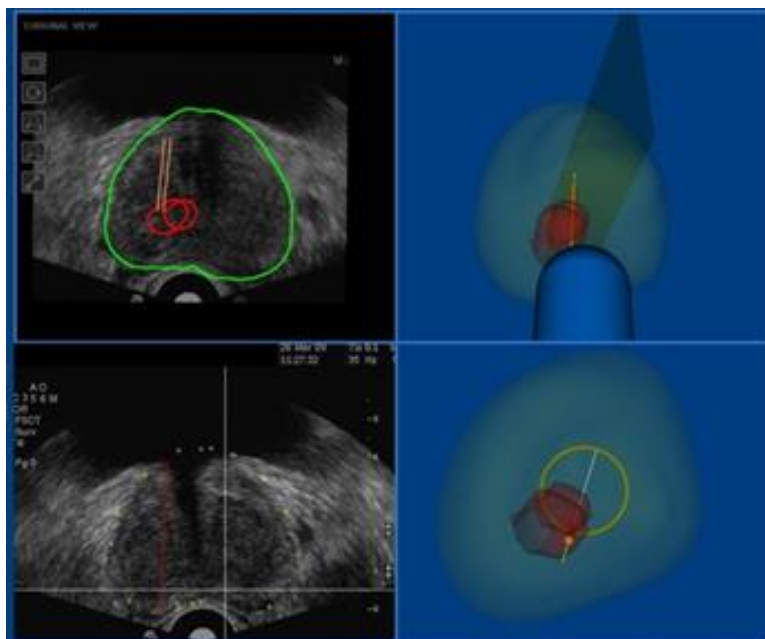
Figure 1-4: The software interface of the prototype for the Artemis biopsy system, described in Bax, J., et al., Med. Phys. 35(12), 2008.[47]

1.2.5.2 MR only-guided biopsy systems

An alternative to MR-3D TRUS "fusion" biopsy is MR-targeted, MR-guided biopsy, wherein both lesion delineation and biopsy targeting are done under MR-guidance[55, 56]. An advantage of these systems over fusion biopsy is that they remove the need to perform image registration between modalities, removing some sources of registration error. However, MR-TRUS fusion biopsy has the advantage of low cost, widespread availability, real-time imaging, and is compatible with standard biopsy needles. Contrary to MR-targeted, MR-guided biopsy, fusion biopsy is also compatible

with the close access to the TRUS probe entry point required to accurately position

biopsy needles, with patient positioning that is concordant with the usual training of the

urologist.

Numerous studies have been conducted which show the clinical feasibility of

MR-only systems[57-64]. One such system has a mean procedure time of 80 minutes[57],

indicating that procedure cost and patient comfort may be the leading impediments of

widespread availability of such systems. However, further studies of clinical usefulness

of MR-guided biopsy versus TRUS-guided biopsy are warranted[57]. Furthermore, a study

has shown that MR-guided prostate biopsy is also characterized by substantial needle

placement error, with a mean and standard deviation of 6.5 ± 3.5 mm for targeted

biopsies[58], while further phantom experiments showed significant needle placement error

due to needle deflection while using a needle with an asymmetrically beveled tip ($4.6 \pm$

0.4 mm in gelatin, 8.7 ± 0.8 in bovine muscle tissue). However, needle deflection error

was greatly reduced through using a symmetrically beveled needle (0.8 ± 0.6 mm in

gelatin, 1.1 ± 0.5 in bovine muscle tissue). Misalignment of the needle template guide

used for transperineal insertion also contributed a needle placement error of 1.5 ± 0.3

mm. These results indicate that further studies must be completed to determine if there

are any potential benefits in needle placement error achieved through MRI-only guided

prostate biopsy over MRI-targeted, 3D TRUS-guided fusion biopsy.

1.3 Histological examination and prostate cancer

1.3.1 Prostate biopsy histology

Histological analysis of biopsy tissue is necessary for obtaining definitive diagnosis of PCa in patients with suspicious screening results. It is also highly important for disease burden monitoring in active surveillance populations and for confirmation of disease recurrence in some post-treatment patients experiencing biochemical recurrence. The value of histology in the workflow of PCa diagnosis and treatment selection is due to the high prognostic importance of the Gleason grading of PCa[3]. Since it was initially developed in the 1960s, this system for assessing the aggressiveness of PCa has been incorporated into numerous internationally recognized guidelines for PCa treatment[8, 65] . Considered conjointly with the Gleason score and anatomical location of biopsy-confirmed PCa, the core involvement (as described in Section 1.2.3), or proportion of each biopsy core which contains tumour tissue, is an important measure for estimation of tumour burden and therefore treatment selection for patients. The percent core involvement is measured with respect to an 18 mm long biopsy core, as detailed by the National Comprehensive Cancer Network Practice Guidelines in Oncology: Prostate Cancer[8]. In general, a core involvement of 50% is an important threshold, as a lesion with a Gleason score < 7 and core involvement $< 50\%$ may be deemed to be clinically insignificant, while a lesion with Gleason score < 7 and core involvement $\geq 50\%$ could be deemed clinically significant[8, 65].

However, due to the finite nature of biopsy needle cores (on average biopsy samples account for approximately 0.2% of total prostate volume), histological analysis of biopsy tissue may not always reflect the true grade and extent of PCa for the patient. In fact, it is reported to have a 30-40% risk of under sampling clinically significant lesions[66-68]. Therefore, histological analysis of biopsy tissue may lead to underestimation of cancer burden for many patients.

1.3.2   Clinical relevance of post-prostatectomy histology

Compared to biopsy cores, histological analysis of the entire prostate gland obtained after prostatectomy can provide a complete picture of the extent and Gleason grade of all PCa within a given patient's prostate. While this is very useful for predicting disease progression after prostatectomy for patients, this method requires a whole-gland prostatectomy before histological analysis. Therefore, this inherently limits the study population to men who have already received prostatectomy for diagnosed PCa, potentially leading to an overrepresentation of high-grade PCa in the dataset compared with low-grade.

Despite this limitation, histological data of post-prostatectomy tissue provides a highly useful reference standard for grade and location of PCa[31, 39, 44, 46, 69-72]. However, these data are inherently biased toward patients with high-risk PCa (as these are the patients who generally receive prostatectomy), and do not provide generalizable findings related to men in low-risk PCa cohorts.

1.3.3   Image registration of post-prostatectomy histology and in-vivo MRI

As discussed in Section 1.2.4.3, there are often disagreement between lesions contoured on MRI and histologic cancer. While whole-gland histology can only be obtained from patients who have already received a prostatectomy to treat their diagnosed prostate cancer, such histological data also provide a useful method for validation of MR-defined lesions. As MR-defined lesions are used to determine needle sampling locations for fusion biopsy systems, their validation against prostate histology may provide useful lessons with respect to how lesion targeting can be improved for fusion biopsy.

Our group has developed a method for registration of post-prostatectomy midgland histology with in-vivo MRI, with a target registration error (TRE) ≤ 2 mm[46, 73, 74]. In order to perform this registration, in-vivo MRI images were obtained from each patient prior to surgery. After surgery, excised prostate specimens were pierced with three hollow needles with cotton threads lined within them such that the threads remain when the needles are removed. Seven strands of lamb kidney were also fixed to the surface of the gland. Both the thread and lamb kidney were treated with a gadolinium-based contrast agent to be used as MRI-visible fiducial markers, while the thread was also treated with ink. An ex-vivo MRI scan was then performed on the specimen before histological processing. After the ex vivo scan, the internal threads were removed and the prostate midgland was sliced into approximately 4 mm transverse slices, while both the apex and base were sliced sagitally. As the internal threads were also treated with

ink, this ink can be seen around the edge of each hole created by an internal thread, allowing them to be distinguished from other tears or luminal areas. All slices were scanned using a slide scanner and then contoured for PCa by a physician trained in PCa morphology. All contours were subsequently confirmed by a genitourinary pathologist.

The co-registration of contoured midgland histology with in-vivo MRI was completed in two main steps. Registration of the histology slices to ex-vivo MRI was completed using a semi-automatic affine transformation algorithm which mapped each histology slice to the best matching plane on the ex vivo image, using the relative locations of the external and internal fiducial strands. The ex-vivo to in-vivo MRI registration step was then completed using a custom-built, interactive thin-plate spline transformation extension for 3D Slicer. This registration involved manual placement of 30-50 fiducial points on corresponding regions of interest in both the in-vivo and ex-vivo image volumes. After fiducials were placed, the ex-vivo volume (and hence the histology slices matched with the ex-vivo volume) was deformed to match the in-vivo volume.

This dataset of prostate histology aligned with in-vivo MRI allows for direct comparison of delineated cancer on histology and in-vivo imaging obtained for the patient prior to surgery. This also allows for comparison of radiologist delineated regions of suspicion on MRI with locations of cancerous tissue as confirmed by histology. As discussed further in Chapter 5, this data can be used to evaluate the Gleason score and

core involvement of PCa contained within a simulated biopsy core, when MR-defined lesions are used to select biopsy needle target locations.

1.4 3D TRUS-guided fusion biopsy challenges

1.4.1 Previous work in this field

3D TRUS-guided "fusion" biopsy systems allow for improved spatial information relative to 2D TRUS and allow for MRI targeting via image registration[47, 75-78]. One fusion biopsy system has shown improved positive core rates of 30.4% (compared to 7.1% for 2D TRUS) and 42.3% (compared to 25.6% for 2D TRUS) for moderate and high suspicion lesions respectively[49]. There exists research into accurate multi-modal image registration from MRI-3D TRUS, as well as algorithms for compensation of prostate motion during the biopsy procedure[48, 75, 79]. A systematic review was conducted by Valerio et al, collecting 14 papers which compared MRI-TRUS fusion targeted biopsy versus 2D TRUS-guided systematic biopsy. They found that MRI-TRUS fusion biopsy detected more clinically significant cancers using fewer cores compared with systematic biopsy (median 33%, range 13-50% for fusion biopsy; median 24%, range 5%-52% for systematic biopsy). Fusion biopsy also led to the detection of some clinically significant cancers that would have been missed by standard biopsy alone (median 9%, range 5-16%)[80].

While this work focuses on MRI-TRUS fusion using image registration software, another approach to TRUS-guided biopsy of prostate MRI-defined lesions is "cognitive registration." This approach involves intuitive visual alignment between MRI lesions and TRUS guidance[81]. However, consensus has not yet been reached regarding the superiority of the cognitive vs. software fusion approaches. Two studies reporting that biopsy targeting of clinically significant MRI lesions using cognitive registration resulted in inferior cancer detection rates compared with MRI-TRUS fusion[82, 83], while another study found no significant difference in cancer detection rates between the two approaches[54]. It should be noted that in the study which saw no significant difference in detection rates, the three collaborating urologists (with 5, 10 and 15 years of TRUS-guided biopsy experience respectively) had no prior experience performing MRI-targeted fusion biopsies. Further investigation is warranted, as it may be that small but still clinical significant tumours may benefit more from MRI-TRUS fusion over cognitive registration, compared with larger tumours.

The volume of research cited in this section indicates the value of MRI-targeted biopsy and motivates our goal to further optimize this procedure. In particular, there remains a lack of knowledge in terms of target optimization for placement fusion biopsy needles. While errors leading to uncertainty in biopsy needle placement can be measured for any commercially available fusion biopsy system, these errors are not apparent to an operating physician using these machines to perform prostate biopsy. At the time of the writing of this thesis, the author is aware of only one other study, by van de Ven et al.[84], which provides insight into a potential avenue for further improvement of the positive

core rate. The authors estimated the maximum allowable TRE of MRI-3D TRUS registration for correct grading of 95% of ADC-determined high Gleason grade tumour components of peripheral zone PCa with fusion biopsy of sphere-shaped tumours[84]. The results of that study lead to the observation that the positive core rate is related to the biopsy system error in delivering the needle to the intended tumour target.

Based on this observation, one point of view is that a fusion biopsy system must deliver needles to targets with no more than some maximum needle delivery error to provide a clinically useful positive core rate for all tumours of clinically significant sizes. Another perspective is that for a fusion biopsy system with a given needle delivery error, some (larger) tumours can be sampled with a clinically desired probability (e.g. 95%) in a single biopsy core, and other (smaller) tumours will require more than one attempt in order to achieve the clinically desired probability of sampling the tumour in at least one of the cores taken. In principle, if the number of biopsy samples required for each tumour in a practical biopsy scenario is determined (within a reasonable limit for the number of biopsy cores), the positive yield of contemporary fusion biopsy systems could be increased by optimizing the number and within-tumour placement of targets for each tumour. The research presented in this thesis takes the latter perspective, investigating varying numbers of biopsy attempts and targeting strategies for fusion prostate biopsy.

1.4.2 Clinical challenges

While touched on in Sections 1.2 and 1.4.1, this section enumerates the specific clinical challenges in prostate biopsy that are addressed by this thesis.

1.4.2.1 Uncertainties in biopsy needle delivery

As mentioned in Section 1.4.1, 3D TRUS-guided fusion biopsy systems utilize accurate multi-modal image registration from MRI-3D TRUS, as well as motion compensation algorithms used during the biopsy procedure. However, each step in the fusion biopsy pipeline is inherently characterized by non-zero error. Four main sources of error include (1) MRI-TRUS registration, (2) Intersessional TRUS-TRUS registration, (3) intraprocedural registration for compensation of prostate motion and (4) biopsy needle guidance error of the system. The errors associated with each of these steps for the Artemis system are as follows. (1) A 3D nonrigid MRI-TRUS registration method was shown to have a median whole-gland target registration error (TRE) of 1.76 mm[75]. (2) An intersession TRUS-TRUS registration method has been shown to have a mean whole gland TRE of 2.15 mm[79]. (3) An intrasession rigid registration to compensate for prostate motion during fusion biopsy was shown to have a mean TRE of 1.63 mm[48]. (4) The average needle delivery error for the Artemis fusion biopsy system was estimated to be 1.2 mm[47].

Therefore, without accounting for the uncertainties associated with the registration and needle delivery errors described above, the biopsy needle of a fusion biopsy system may not be sampling the exact location intended by the operating clinician. The work presented in Chapter 2 investigates how these errors in biopsy needle placement affect the probability of successfully sampling prostatic tumours when making only one biopsy attempt.

1.4.2.2 Lesion targeting approaches

As discussed in Sections 1.2.5.1 and 1.3.3, it has been found that fusion prostate biopsy detects more clinically significant cancers using fewer cores compared with 2D TRUS-guided systematic biopsy, and led to the detection of clinically significant lesions that would have been missed by systematic biopsy alone[80]. However, in the numerous studies comparing the two prostate biopsy approaches, the intended within-lesion biopsy needle targets were selected in an ad-hoc manner, where the errors associated with biopsy needle delivery were not considered when deciding the placement of targeted biopsies[51-60].

Chapter 3 compares two different prostate lesion targeting strategies in the presence of practical needle delivery errors of 3D TRUS fusion biopsy systems, and how they affect both the probability of obtaining any amount of tumour tissue in the biopsy core, and the probability of obtaining a core involvement $\geq 50\%$.

1.4.2.3   Lesion delineation on multi-parametric MRI

As discussed in Section 1.2.4.3, prostate volumes estimated by radiologists on MRI consistently overestimate histological reference volumes[45], while also the gross tumour volumes defined by radiologists require an 8 mm expansion in order to achieve 95% histological coverage[46]. This shows that while MR-defined lesions volumes are consistently larger than the histological reference volumes, they still generally do not cover the entirety of the tumour as confirmed by histology.

While expansion of the GTV allows for better coverage of the lesion for prostate therapy, due to the finite nature of biopsy needle sampling and the small diameter of each needle, a GTV expansion alone does not address the challenge of how to adjust biopsy needle targeting to deal with the disagreement between MRI contours and histologic cancer coverage Chapter 4 investigates how needle delivery error affects the sampling probabilities of PCa of all Gleason grades and high grade-only cancer, using lesions as delineated on prostate midgland histology.

1.5   Thesis hypothesis and objectives

In order to address key gaps in knowledge with regards to biopsy needle target selection for MRI-targeted, 3D TRUS-guided fusion prostate biopsy, the central

hypotheses of this thesis detailed in Section 1.5.1 were tested through the completion of the specific research objectives listed in Section 1.5.2. In doing so, this work has led to first steps toward improving the manner in which lesions are targeted using fusion biopsy, potentially supporting earlier diagnosis and more accurate characterization of PCa while it remains localized to the gland and curable.

1.5.1   Hypothesis

The two central hypotheses of this work are enumerated as follows:

1) The majority of clinically significant prostate lesions require more than one biopsy attempt to achieve a probability $\geq 95\%$ of obtaining a PCa-positive sample for practical needle delivery errors observed in MRI-targeted, 3D-TRUS-guided fusion biopsy guidance.

2) More than one biopsy attempt is required to achieve a probability $\geq 95\%$ of obtaining a PCa-positive sample with core involvement $\geq 50\%$ (see Section 1.3.1) from clinically significant prostate lesions which are large enough for such a core involvement to be obtained.

1.5.2   Research objectives

1) Adaptable biopsy simulation platform: to develop a software platform allowing for the simulation of multiple biopsy attempts and varying targeting strategies, given biopsy system error characteristics and 3D tumour shapes.

2) Impact of biopsy needle delivery errors on probability of obtaining a tumour sample: to determine how the probability of sampling 3D tumour shapes in one biopsy attempt is affected by various amounts of needle delivery error characterizing fusion biopsy systems.

3) Impact of targeting strategy on biopsy sampling: to determine the impact of using a ring versus a centroid targeting scheme on tumour sampling probabilities and tumour core involvement obtained when making multiple biopsy attempts, in the presence of both systematic and random errors.

4) Impact of biopsy needle delivery error on pathologic cancer risk assessment: to investigate how biopsy needle delivery error affects the measure of core involvement and estimation of Gleason score from simulated biopsy cores contents evaluated using post-prostatectomy prostate histology.

1.6 Outline of this thesis

1.6.1 Chapter 2: Magnetic resonance imaging-targeted, 3D transrectal ultrasound-guided fusion biopsy for prostate cancer: Quantifying the impact of needle delivery error on diagnosis

Magnetic resonance imaging (MRI)-targeted, 3D transrectal ultrasound (TRUS)-guided "fusion" prostate biopsy aims to reduce the 21–47% false negative rate of clinical 2D TRUS-guided sextant biopsy, but still has a substantial false negative rate. This could be improved via biopsy needle target optimization, by accounting for uncertainties due to guidance system errors, image registration errors, and irregular tumour shapes. This chapter takes an initial step toward the broader goal of improved prostate biopsy targeting. In particular, it elucidates the impact of biopsy needle delivery error on the probability of obtaining a tumour sample as determined by suspicious lesions contoured by radiologists on MRI.

Prior to this work, there had been only one study providing insight into a potential avenue for further improvement of the positive core rate of fusion biopsy[84]. The authors of that work estimated the maximum allowable target registration error (TRE) of MRI-3D TRUS registration for correct grading of 95% of ADC-determined high Gleason grade tumour components of peripheral zone PCa with fusion biopsy of sphere-shaped tumours.

However, another perspective is that for a fusion biopsy system with a given needle delivery error, some (larger) tumours can be sampled with a clinically desired probability (e.g., 95%) in a single biopsy core and other (smaller) tumours will require more than one attempt in order to achieve the clinically desired probability of sampling the tumour in at least one of the cores taken. This latter perspective is the one taken throughout this thesis.

In this chapter, I estimated the probability of obtaining a positive tumour sample from 81 3D suspicious regions contoured on MRI by experts, in a single biopsy core. The findings from this work were critical for the justification of development of the biopsy simulation software platform which allowed the simulation of multiple biopsy attempts and different targeting schemes for each lesion, as discussed in Chapter 3.

1.6.2   Chapter 3: A comparison of prostate tumour targeting strategies using magnetic resonance imaging-targeted, transrectal ultrasound-guided fusion biopsy

In Chapter 2, it was determined that for a fusion biopsy system with a given needle delivery error, some larger tumours can be sampled with a clinically desired probability (e.g. 95%) in a single biopsy core, and other smaller tumours will require more than one targeted core to achieve the clinically desired probability of sampling the tumour in at least one of the cores taken. The rationale for this perspective is that in

principle, the positive yield of contemporary fusion biopsy systems can be increased by optimizing the number and within-tumour placement of targets for each tumour, with consideration given to taking a reasonable number of cores in a practical biopsy scenario.

The previous study was intended as a preliminary step toward the overarching goal of increasing the positive yield of fusion prostate biopsy systems, and therefore experiments were built on a set of assumptions that must be relaxed to more accurately reflect the uncertainties involved in a fusion biopsy procedure. The previous error model assumed an overall needle delivery error that was isotropic and contained no systematic components. However, both systematic and random errors have been measured in fusion biopsy systems, and it is reasonable to consider that such errors could be present in any percutaneous needle delivery device. It is the purpose of the work in this chapter to relax these assumptions, and investigate the effects of this more complex error model on predicted tumour sampling probabilities. For the purpose of the experiments performed in this chapter, I developed a generalizable biopsy simulation software platform which allows repeated simulations of biopsy attempts on tumour segmentations, given the desired targeting strategy and an error distribution used to model the needle delivery error of any given fusion biopsy system. A detailed description of the simulator algorithm is provided in Section 3.2.4.

In this chapter, a "ring" targeting strategy was investigated, with the intention of compensating for a systematic error of known magnitude, but unknown direction. While this paper represents a step toward improving the manner in which lesions are targeted

using fusion biopsy, a prospective trial will ultimately be needed to determine the improvement in positive yield achieved through optimization of needle target selection. The data presented in this paper could potentially be incorporated into an onboard software module that provides automatic selection of biopsy target locations given the error characteristics of any particular biopsy system.

1.6.3   Chapter 4: Investigating the impact of prostate biopsy needle delivery error on pathologic cancer risk assessment

An important limitation of the studies described in Chapters 2 and 3 is that MRI-defined regions of suspicion were used as biopsy simulation targets, without histologic confirmation of the core involvements and high-grade cancer yield resulting from biopsy simulation. In the work presented in Chapter 4, I addressed this issue by using histologically confirmed PCa tumours as contoured on digital histology images by genitourinary pathologists to conduct biopsy simulations and report core involvement and high-grade cancer yield as a function of biopsy system error. By using histology image contours to define tumour targeting, this work modeled idealized tumour targeting, wherein boundary delineation on the planning image is exactly concordant with lesions on histopathology.

Although the use of histology imaging for simulated biopsy affords the ability to characterize percent core involvement and distribution of cancer grades in the core using

a recognized gold standard, due to clinical limitations histology images are 2D, sliced approximately in the axial orientation, and acquired sparsely throughout the midgland. Thus, the findings of this study were made under the assumption that apparent prostate tumour size and shape are invariant to tissue slicing orientation.

This study provides a precursor to the ongoing work in the project, described in Section 5.4. In this continuing work, my biopsy simulation platform will be used to determine how the biopsy needle delivery errors and targeting schemes discussed in this thesis affect tumour sampling probabilities when radiologist-defined contours on MR are used to select biopsy target locations, while co-registered whole-mount histopathology is used to confirm the contents of the simulated biopsy cores.

1.6.4 Chapter 5: Conclusions and Future Work

This chapter is dedicated to the overall conclusions of the major chapters in this thesis, while providing speculation for future work that could address remaining challenges stemming from this project.

References

1   "Canadian Cancer Statistics," Canadian Cancer Society, 2017.

2   D.T. Eton and S.J. Lepore, "Prostate cancer and health-related quality of life: a review of the literature," Psycho-oncology **11**(4), 307-326 (2002).

3   D.F. Gleason, "Classification of prostatic carcinomas," Cancer Chemotherapy Reports **50**(3), 125-128 (1966).

4   J.P. Richie, W.J. Catalona, F.R. Ahmann, M.A. Hudson, P.T. Scardino, R.C. Flanigan, J.B. Dekernion, T.L. Ratliff, L.R. Kavoussi, B.L. Dalkin, W.B. Waters, M.T. MacFarlane and P.C. Southwick, "Effect of patient age on early detection of prostate cancer with serum prostate-specific antigen and digital rectal examination," Urology **42**(4), 365-374 (1993).

5   M.E. Chen, D.A. Johnston, K. Tang, R.J. Babaian and P. Troncoso, "Detailed mapping of prostate carcinoma foci: biopsy strategy implications," Cancer **89**(8), 1800-1809 (2000).

6   J.I. Epstein, P.C. Walsh, M. Carmichael and C.B. Brendler, "Pathologic and clinical findings to predict tumour extent of nonpalpable (stage T1c) prostate cancer," JAMA, The Journal of the American Medical Association **271**(5), 368-374 (1994).

7   T.A. Stamey, N. Yang, A.R. Hay, J.E. McNeal, F.S. Freiha and E. Redwine, "Prostate-specific antigen as a serum marker for adenocarcinoma of the prostate," The New England Journal of Medicine **317**(15), 909-916 (1987).

8   National Comprehensive Cancer Network Clinical Practice Guidelines in Oncology: Prostate Cancer (2017).

9   J.I. Izawa, L. Klotz, D.R. Siemens, W. Kassouf, A. So, J. Jordan, M. Chetner and A.E. Iansavichene, "Prostate cancer screening: Canadian guidelines 2011," Canadian Urological Association Journal **5**(4), 235-240 (2011).

10   R. Clements, "Ultrasonography of prostate cancer," European Radiology **11**(11), 2119-2125 (2001).

11   R. Clements, "The role of transrectal ultrasound in diagnosing prostate cancer," Current Urology Reports **3**(3), 194-200 (2002).

12   M. Norberg, L. Egevad, L. Holmberg, P. Sparen, B.J. Norlen and C. Busch, "The sextant protocol for ultrasound-guided core biopsies of the prostate underestimates the presence of cancer," Urology **50**(4), 562-566 (1997).

13   H. Singh, E.I. Canto, S.F. Shariat, D. Kadmon, B.J. Miles, T.M. Wheeler and K.M. Slawin, "Predictors of prostate cancer after initial negative systematic 12 core biopsy," Urology **171**(5), 1850-1854 (2004).

14   A.V. Taira, G.S. Merrick, R.W. Galbreath, H. Andreini, W. Taubenslag, R. Curtis, W.M. Butler, E. Adamovich and K.E. Wallner, "Performance of transperineal template-guided mapping biopsy in detecting prostate cancer in the initial and repeat biopsy setting," Prostate Cancer and Prostatic Diseases **13**(1), 71-77 (2010).

15   A. Rajinikanth, M. Manoharan, C.T. Soloway, F.J. Civantos and M.S. Soloway, "Trends in Gleason score: concordance between biopsy and prostatectomy over 15 years," Urology **72**(1), 177-182 (2008).

16   S. Loeb, M.A. Bjurlin, J. Nicholson, T.L. Tammela, D.F. Penson, H.B. Carter, P. Carroll and R. Etzioni, "Overdiagnosis and overtreatment of prostate cancer," European Urology **65**(6), 1046-1055 (2014).

17   J.I. Epstein, M.J. Zelefsky, D.D. Sjoberg, J.B. Nelson, L. Egevad, C. Magi-Galluzzi, A.J. Vickers, A.V. Parwani, V.E. Reuter, S.W. Fine, J.A. Eastham, P. Wiklund, M. Han, C.A. Reddy, J.P. Ciezki, T. Nyberg and E.A. Klein, "A contemporary prostate cancer grading system: a validated alternative to the Gleason score," European Urology **69**(3), 428-435 (2016).

18   L. Klotz, D. Vesprini, P. Sethukavalan, V. Jethava, L. Zhang, S. Jain, T. Yamamoto, A. Mamedov and A. Loblaw, "Long-term follow-up of a large active surveillance cohort of patients with prostate cancer," Journal of Clinical Oncology **33**(3), 272-277 (2015).

19   J.J. Tosoian, M. Mamawala, J.I. Epstein, P. Landis, S. Wolf, B.J. Trock and H.B. Carter, "Intermediate and longer-term outcomes from a prospective active-surveillance program for favorable-risk prostate cancer," Journal of Clinical Oncology **33**(30), 3379-3385 (2015).

20   S. Jones, *Prostate cancer diagnosis: PSA, biopsy and beyond*. (Springer, 2012).

21   A. Fenster, D.B. Downey and H.N. Cardinal, "Three-dimensional ultrasound imaging," Physics in Medicine and Biology **46**(5), R67-99 (2001).

22   E.A. Singer, D.J. Golijanin, R.S. Davis and V. Dogra, "What's new in urologic ultrasound?," Urologic Clinics of North America **33**(3), 279-286 (2006).

23   F. Lee, S.T. Torp-Pedersen, D.B. Siders, P.J. Littrup and R.D. McLeary, "Transrectal ultrasound in the diagnosis and staging of prostatic carcinoma," Radiology **170**(3), 609-615 (1989).

24   P. Hammerer and H. Huland, "Systematic sextant biopsies in 651 patients referred for prostate evaluation," Urology **151**(1), 99-102 (1994).

25   J.L. Sauvain, P. Palascak, D. Bourscheid, C. Chabi, A. Atassi, J.M. Bremon and R. Palascak, "Value of power doppler and 3D vascular sonography as a method for diagnosis and staging of prostate cancer," European Urology **44**(1), 21-31, (2003).

26   W.J. Ellis, M.P. Chetner, S.D. Preston and M.K. Brawer, "Diagnosis of prostatic carcinoma: the yield of serum prostate specific antigen, digital rectal examination and transrectal ultrasonography," Urology **152**(5), 1520-1525 (1994).

27   J.J. Futterer, S.W. Heijmink, T.W. Scheenen, J. Veltman, H.J. Huisman, P. Vos, C.A. Hulsbergen-van de Kaa, J.A. Witjes, P.F. Krabbe, A. Heerschap and J.O. Barentsz, "Prostate cancer localization with dynamic contrast-enhanced MR imaging and proton MR spectroscopic imaging," Radiology **241**(2), 449-458 (2006).

28   J.O. Barentsz, J. Richenberg, R. Clements, P. Choyke, S. Verma, G. Villeirs, O. Rouviere, V. Logager and J.J. Futterer, "ESUR prostate MR guidelines 2012," European Radiology **22**(4), 746-757 (2012).

29   J.C. Weinreb, J.O. Barentsz, P.L. Choyke, F. Cornud, M.A. Haider, K.J. Macura, D. Margolis, M.D. Schnall, F. Shtern, C.M. Tempany, H.C. Thoeny and S. Verma, "PI-RADS Prostate Imaging - Reporting and Data System: 2015, Version 2," European Urology **69**(1), 16-40 (2016).

30   C.M. Hoeks, M.G. Schouten, J.G. Bomers, S.P. Hoogendoorn, C.A. Hulsbergen-van de Kaa, T. Hambrock, H. Vergunst, J.P. Sedelaar, J.J. Futterer and J.O. Barentsz, "Three-Tesla magnetic resonance-guided prostate biopsy in men with increased prostate-specific antigen and repeated, negative, random, systematic, transrectal ultrasound biopsies: detection of clinically significant prostate cancers," European Urology **62**(5), 902-909 (2012).

31   L. Wang, Y. Mazaheri, J. Zhang, N.M. Ishill, K. Kuroiwa and H. Hricak, "Assessment of biologic aggressiveness of prostate cancer: correlation of MR signal intensity with Gleason grade after radical prostatectomy," Radiology **246**(1), 168-176 (2008).

32   A.B. Rosenkrantz and S.S. Taneja, "Radiologist, be aware: ten pitfalls that confound the interpretation of multiparametric prostate MRI," AJR: American Journal of Roentgenology **202**(1), 109-120 (2014).

33   S. Verma, B. Turkbey, N. Muradyan, A. Rajesh, F. Cornud, M.A. Haider, P.L. Choyke and M. Harisinghani, "Overview of dynamic contrast-enhanced MRI in

prostate cancer diagnosis and management," AJR: American Journal of Roentgenology **198**(6), 1277-1288 (2012).

34   H. Hricak, P.L. Choyke, S.C. Eberhardt, S.A. Leibel and P.T. Scardino, "Imaging prostate cancer: a multidisciplinary perspective," Radiology **243**(1), 28-53 (2007).

35   P.S. Tofts, D.A. Wicks and G.J. Barker, "The MRI measurement of NMR and physiological parameters in tissue to study disease process," Progress in Clinical and Biological Research **363**(1), 313-325 (1991).

36   G. Brix, W. Semmler, R. Port, L.R. Schad, G. Layer and W.J. Lorenz, "Pharmacokinetic parameters in CNS Gd-DTPA enhanced MR imaging," Journal of Computer Assisted Tomography **15**(4), 621-628 (1991).

37   H.B. Larsson, M. Stubgaard, J.L. Frederiksen, M. Jensen, O. Henriksen and O.B. Paulson, "Quantitation of blood-brain barrier defect by magnetic resonance imaging and gadolinium-DTPA in patients with multiple sclerosis and brain tumours," Magnetic Resonance in Medicine **16**(1), 117-131 (1990).

38   W.T. Hrinivich, E. Gibson, M. Gaed, J.A. Gomez, M. Moussa, C. Mckenzie, G.S. Bauman, A.D. Ward, A. Fenster and E. Wong, "A dimensionless dynamix contrast enhanced MRI parameter for intra-prostatic tumour target volume delineation: Initial comparison with histology," SPIE Medical Imaging Proceedings 9036, 90362I (2014).

39   F.A. van Dorsten, M. van der Graaf, M.R. Engelbrecht, G.J. van Leenders, A. Verhofstad, M. Rjipkema, J.J. de la Rosette, J.O. Barentsz and A. Heerschap, "Combined quantitative dynamic contrast-enhanced MR imaging and (1)H MR spectroscopic imaging of human prostate cancer," Journal of Magnetic Resonance Imaging **20**(2), 279-287 (2004).

40   M.V. Knopp, F.L. Giesel, H. Marcos, H. von Tengg-Kobligk and P. Choyke, "Dynamic contrast-enhanced magnetic resonance imaging in oncology," Topics in Magnetic Resonance Imaging **12**(4), 301-308 (2001).

41   H.A. Vargas, O. Akin, T. Franiel, Y. Mazaheri, J. Zheng, C. Moskowitz, K. Udo, J. Eastham and H. Hricak, "Diffusion-weighted endorectal MR imaging at 3T for prostate cancer: tumour detection and assessment of aggressiveness," Radiology **259**(3), 775-784 (2011).

42   T. Hambrock, D.M. Somford, H.J. Huisman, I.M. van Oort, J.A. Witjes, C.A. Hulsbergen-van de Kaa, T. Scheenen and J.O. Barentsz, "Relationship between apparent diffusion coefficients at 3.0-T MR imaging and Gleason grade in peripheral zone prostate cancer," Radiology **259**(2), 453-461 (2011).

43   S. Verma, A. Rajesh, H. Morales, L. Lemen, G. Bills, M. Delworth, K. Gaitonde, J. Ying, R. Samartunga and M. Lamba, "Assessment of aggressiveness of prostate cancer: correlation of apparent diffusion coefficient with histologic grade after radical prostatectomy," AJR: American Journal of Roentgenology **196**(2), 374-381 (2011).

44   B. Turkbey, V.P. Shah, Y. Pang, M. Bernado, S. Xu, J. Kruecker, J. Locklin, A.A. Baccala, A.R. Rastinehad, M.J. Merino, J.H. Shih, B.J. Wood, P.A. Pinto and P.L. Choyke., "Is apparent diffusion coefficient associated with clinical risk scores for prostate cancers that are visible on 3-T MR images?," Radiology **258**(2), 488-495 (2011).

45   M.G. Salarian, M. Shahedi, M. Gaed, J.A. Gomez, M. Moussa, C. Romagnoli, D.W. Cool, M. Bastian-Jordan, J.L. Chin, S. Pautler, G.S. Bauman and A.D. Ward, "Accuracy and variability of tumour burden measurement on multi-parametric MRI," SPIE Medical Imaging Proceedings 9041, 90410I (2014).

46   E. Gibson, G.S. Bauman, C. Romagnoli, D.W. Cool, M. Bastian-Jordan, Z. Kassam, M. Gaed, M. Moussa, J.A. Gomez, S.E. Pautler, J.L. Chin, C. Crukley, M.A. Haider, A. Fenster and A.D Ward, "Toward prostate cancer contouring guidelines on magnetic resonance imaging: dominant lesion gross and clinical target volume coverage via accurate histology fusion," International Journal of Radiation Oncology, Biology, Physics **96**(1), 188-196 (2016).

47   J. Bax, D. Cool, L. Gardi, K. Knight, D. Smith, J. Montreuil, S. Sherebrin, C. Romagnoli and A. Fenster, "Mechanically assisted 3D ultrasound guided prostate biopsy system," Medical Physics **35**(12), 5397-5410 (2008).

48   T. De Silva, A. Fenster, D.W. Cool, L. Gardi, C. Romagnoli, J. Samarabandu and A.D. Ward, "2D-3D rigid registration to compensate for prostate motion during 3D TRUS-guided biopsy," Medical Physics **40**(2), 022904 (2013).

49   D.W. Cool, J. Bax, C. Romagnoli, A.D. Ward, L. Gardi, V. Karnik, J. Izawa, J. Chin and A. Fenster, "Fusion of MRI to 3D TRUS for mechanically-assisted targeted prostate biopsy: system design and initial clinical experience," Lecture Notes in Computer Science **6963**, 121-133 (2011).

50   M.C. Roethke, T.H. Kuru, S. Schultze, D. Tichy, A. Kopp-Schneider, M. Fenchel, H.P. Schlemmer, B.A. Hadaschik, "Evaluation of the ESUR PI-RADS scoring system for multiparametric MRI of the prostate with targeted MR/TRUS fusion-guided biopsy at 3.0 Tesla," European Radiology **24**(2), 344-352 (2014).

51   P. Puech, O. Rouviere, R. Renard-Penna, A. Villers, P. Devos, M. Colombel, M.O. Bitker, X. Leroy, F. Mege-Lechevallier, E. Comperat, A. Ouzzane and L. Lemaitre, "Prostate cancer diagnosis: multiparametric MR-targeted biopsy with

cognitive and transrectal US-MR fusion guidance versus systematic biopsy--prospective multicentre study," Radiology **268**(2), 461-469 (2013).

52   S. Natarajan, L.S. Marks, D.J. Margolis, J. Huang, M.L. Macairan, P. Lieu and A. Fenster, "Clinical application of a 3D ultrasound-guided prostate biopsy system," Urologic Oncology **29**(3), 334-342 (2011).

53   D. Volkin, B. Turkbey, A.N. Hoang, S. Rais-Bahrami, N. Yerram, A. Walton-Diaz, J.W. Nix, B.J. Wood, P.L. Choyke and P.A. Pinto, "Multiparametric magnetic resonance imaging (MRI) and subsequent MRI/ultrasonography fusion-guided biopsy increase the detection of anteriorly located prostate cancers," BJU International **114**(6b), E43-E49 (2014).

54   P.P. Tonttila, J. Lantto, E. Paakko, U. Piippo, S. Kauppila, E. Lammentausta, P. Ohtonen and M.H. Vaarala, "Prebiopsy multiparametric magnetic resonance imaging for prostate cancer diagnosis in biopsy-naive men with suspected prostate cancer based on elevated prostate-specific antigen values: results from a randomized prospective blinded controlled trial," European Urology **69**(3), 419-425 (2016).

55   R.C. Susil, K. Camphausen, P. Choyke, E.R. McVeigh, G.S. Gustafson, H. Ning, R.W. Miller and E. Atalar, "System for prostate brachytherapy and biopsy in a standard 1.5 T MRI scanner," Magnetic Resonance in Medicine **52**(3), 683-687 (2004).

56   A. Krieger, R.C. Susil, C. Menard, J.A. Coleman, G. Fichtinger, E. Atalar and L.L. Whitcomb, "Design of a novel MRI compatible manipulator for image guided prostate interventions," IEEE Transactions on Bio-Medical Engineering **52**(2), 306-313 (2005).

57   R.C. Susil, C. Menard, A. Krieger, J.A. Coleman, K. Camphausen, P. Choyke, G. Fichtinger, L.L. Whitcomb, C.N. Coleman and E. Atalar, "Transrectal prostate biopsy and fiducial marker placement in a standard 1.5T magnetic resonance imaging scanner," Urology **175**(1), 113-120 (2006).

58   P. Blumenfeld, N. Hata, S. DiMaio, K. Zou, S. Haker, G. Fichtinger and C.M. Tempany, "Transperineal prostate biopsy under magnetic resonance image guidance: a needle placement accuracy study," JMRI: Journal of Magnetic Resonance Imaging **26**(3), 688-694 (2007).

59   K.M. Pondman, J.J. Futterer, B. ten Haken, L.J. Schultze Kool, J.A. Witjes, T. Hambrock, K.J. Macura and J.O., Barentsz, "MR-Guided biopsy of the prostate: an overview of techniques and a systematic review," European Urology **54**, 517-527 (2008).

60   M. Roethke, A.G. Anastasiadis, M. Lichy, M. Werner, P. Wagner, S. Kruck, C.D. Claussen, A. Stenzl, H.P. Schlemmer and D. Schilling, "MRI-guided prostate biopsy detects clinically significant cancer: analysis of a cohort of 100 patients after previous negative TRUS biopsy," World Journal of Urology **30**(2), 213-218 (2012).

61   S. Kaufmann, S. Kruck, U. Kramer, S. Gatidis, A. Stenzl, M. Roethke, M. Scharpf, and D. Schilling, "Direct comparison of targeted MRI-guided biopsy with systematic transrectal ultrasound-guided biopsy in patients with previous negative prostate biopsies," Urologia Internationalis **94**(3), 319-325 (2015).

62   T. Hambrock, D.M. Somford, C. Hoeks, S.A.W. Bouwense, H. Huisman, D. Yakar, I.M. van Oort, J.A. Witjes, J.J. Futterer and J.O. Barentsz, "Magnetic Resonance Imaging guided prostate biopsy in men with repeat negative biopsies and increased prostate specific antigen," Urology **183**(2), 520-528 (2010).

63   D. Beyersdroff, A. Winkel, B. Hamm, S. Lenk, S.A. Loening, M. Taupitz, "MR Imaging–guided prostate biopsy with a closed MR Unit at 1.5 T: initial results," Radiology **234**(2), 576-581 (2005).

64   A.G. Anastasiadis, M.P. Lichy, U. Nagele, M.A. Kuczyk, A.S. Merseburger, J. Hennenlotter, S. Corvin, K.D. Sievert, C.D. Claussen, A. Stenzl and H.P. Schlemmer, "MRI-guided biopsy of the prostate increases diagnostic performance in men with elevated or increasing PSA levels after previous negative TRUS biopsies," European Urology **50**(4), 738-749 (2006).

65   Clinically Localized Prostate Cancer: AUA/ASTRO/SUO Guideline (2017).

66   V. Scattoni, A. Zlotta, R. Montironi, C. Schulman, P. Rigatti and F. Montorsi, "Extended and saturation prostatic biopsy in the diagnosis and characterisation of prostate cancer: a critical analysis of the literature," European urology **52**(5), 1309-1322 (2007).

67   J.P. Sedelaar, P.L. Vijverberg, T.M. De Reijke, J.J. de la Rosette, P.J. Kil, J.G. Braeckman and A.J. Hendrikx, "Transrectal ultrasound in the diagnosis of prostate cancer: state of the art and perspectives," European Urology **40**(3), 275-284 (2001).

68   B. Djavan, V. Ravery, A. Zlotta, P. Dobronski, M. Dobronski, M. Fakhari, C. Seitz, M. Susani, A. Borkowski, L. Boccon-Gibod, C.C. Schulman and M. Marberger, "Prospective evaluation of prostate cancer detected on biopsies 1, 2, 3 and 4: when should we stop?," Urology **166**(5), 1679-1683 (2001).

69   K.L. Zakian, S. Eberhardt, H. Hricak, A. Shukla-Dave, S. Kleinmann, M. Murunganandham, K. Sircar, M.W. Kattan, V.E. Reuter, P.T. Scardino and J.A.

Koutcher, "Transition zone prostate cancer: metabolic characteristics at 1H MR spectroscopic imaging--initial results," Radiology **229**(1), 241-247 (2003).

70   K.L. Zakian, K. Sircar, H. Hricak, H.N. Chen, A. Shukla-Dave, S. Eberhardt, M. Murunganandham, L. Ebora, M.W. Kattan, V.E. Reuter, P.T. Scardino and J.A. Koutcher, "Correlation of proton MR spectroscopic imaging with gleason score based on step-section pathologic analysis after radical prostatectomy," Radiology **234**(3), 804-814 (2005).

71   M. Anwar, A.C. Westphalen, A.J. Jung, S.M. Noworolski, J.P. Simko, J. Kurhanewicz, M. Roach, P.R. Carroll and F.V. Coakley, "Role of endorectal MR imaging and MR spectroscopic imaging in defining treatable intraprostatic tumour foci in prostate cancer: quantitative analysis of imaging contour compared to whole-mount histopathology," Radiotherapy and Oncology **110**(2), 303-308 (2014).

72   L.H. Chen, H. Ho, R. Lazaro, J. Yuen, W.S. Ng and C. Cheng, "Optimum slicing of radical prostatectomy specimens for correlation between histopathology and medical images," International Journal of Computer Assisted Radiology and Surgery **5**(5), 471-487 (2010).

73   E. Gibson, C. Crukley, M. Gaed, J.A. Gomez, M. Moussa, J.L. Chin, G.S. Bauman, A. Fenster and A.D. Ward, "Registration of prostate histology images to ex vivo MR images via strand-shaped fiducials," JMRI: Journal of Magnetic Resonance Imaging **36**(6), 1402-1412 (2012).

74   A.D. Ward, C. Crukley, C.A. McKenzie, J. Montreuil, E. Gibson, C. Romagnoli, J.A. Gomez, M. Moussa, J. Chin, G. Bauman and A. Fenster, "Prostate: registration of digital histopathologic images to in vivo MR images acquired by using endorectal receive coil," Radiology **263**(3), 856-864 (2012).

75   Y. Sun, J. Yuan, W. Qiu, M. Rajchl, C. Romagnoli and A. Fenster, "Three-dimensional nonrigid MR-TRUS registration using dual optimization," IEEE Transactions on Medical Imaging **34**(5), 1085-1095 (2015).

76   M. Baumann, P. Mozer, V. Daanen and J. Troccaz, "Prostate biopsy tracking with deformation estimation," Medical Image Analysis **16**(3), 562-576 (2012).

77   S. Xu, J. Kruecker, B. Turkbey, N. Glossop, A.K. Singh, P. Choyke, P. Pinto and B.J. Wood, "Real-time MRI-TRUS fusion for guidance of targeted prostate biopsies," Computer Aided Surgery **13**(5), 255-264 (2008).

78   B.A. Hadaschik, T.H. Kuru, C. Tulea, P. Rieker, I.V. Popeneciu, T. Simpfendorfer, J. Huber, P. Zogal, D. Teber, S. Pahernik, M. Roethke, P. Zamecnik, W. Roth, G. Sakas, H.P. Schlemmer and M. Hohenfellner, "A novel

stereotactic prostate biopsy system integrating pre-interventional magnetic resonance imaging and live ultrasound fusion," Urology **186**(6), 2214-2220 (2011).

[79]   V.V. Karnik, A. Fenster, J. Bax, C. Romagnoli and A.D. Ward, "Evaluation of intersession 3D-TRUS to 3D-TRUS image registration for repeat prostate biopsies," Medical Physics **38**(4), 1832-1843 (2011).

[80]   M. Valerio, I. Donaldson, M. Emberton, B. Ehdaie, B.A. Hadaschik, L.S. Marks, P. Mozer, A.R. Rastinehad, H.U. Ahmed, "Detection of clinically significant prostate cancer using magnetic resonance imaging-ultrasound fusion targeted biopsy: a systematic review," European Urology **68**(1), 8-19 (2015).

[81]   B.K. Park, J.W. Park, S.Y. Park, C.K. Kim, H.M. Lee, S.S. Jeon, S.I. Seo, B.C. Jeong and H.Y. Choi, "Prospective evaluation of 3-T MRI performed before initial transrectal ultrasound-guided prostate biopsy in patients with high prostate-specific antigen and no previous biopsy," AJR: American Journal of Roentgenology **197**(5), W876-881 (2011).

[82]   D.W. Cool, X. Zhang, C. Romagnoli, J.I. Izawa, W.M. Romano and A. Fenster, "Evaluation of MRI-TRUS fusion versus cognitive registration accuracy for MRI-targeted, TRUS-guided prostate biopsy," AJR: American Journal of Roentgenology **204**(1), 83-91 (2015).

[83]   N.B. Delongchamps, M. Peyromaure, A. Schull, F. Beuvon, N. Bouazza, T. Flam, M. Zerbib, N. Muradyan, P. Legman and F. Cornud, "Prebiopsy magnetic resonance imaging and prostate cancer detection: comparison of random and targeted biopsies," Urology **189**(2), 493-499 (2013).

[84]   W.J. van de Ven, C.A. Hulsbergen-van de Kaa, T. Hambrock, J.O. Barentsz and H.J. Huisman, "Simulated required accuracy of image registration tools for targeting high-grade cancer components with prostate biopsies," European Radiology **23**(5), 1401-1407 (2013).

Chapter 2

2 Magnetic resonance imaging-targeted, 3D transrectal ultrasound-guided fusion biopsy for prostate cancer: quantifying the impact of needle delivery error on diagnosis[*]

2.1 Introduction

Prostate cancer (PCa) is the most common non-cutaneous cancer in North American men[1,2]. The current clinical standard for PCa diagnosis is two-dimensional (2D) transrectal ultrasound (TRUS)-guided biopsy. As PCa is seldom detectable on ultrasound, an extended sextant template is commonly used to guide 18-gauge core biopsy needles to extract 12 tissue samples (hereinafter referred to as *cores*) for microscopic examination by a pathologist to assess the presence and Gleason grade[3] of cancer. Methods have been proposed to optimize 2D TRUS-guided biopsy targeting strategy[4,5]. However, these systematic approaches do not allow for biopsy target

---

optimization on a per-patient basis, and clinical biopsy has a false negative rate of up to 23%[6]. A negative biopsy in conjunction with a rising prostate-specific antigen (PSA) level measured on blood tests may precipitate referral for repeat biopsy to obtain positive confirmation of cancer, if present. Additionally, 2D TRUS-guided biopsy may underestimate the Gleason score, which is related to the aggressiveness of the cancer. A 15-year clinical study involving 1670 men demonstrated that biopsy Gleason score was undergraded in 32% of the subjects, as compared to grading on radical prostatectomy specimens[7]. Accurate biopsy needle targeting and guidance to obtain sufficient tumour tissue for reliable assessment of the presence and Gleason grade of cancer could reduce patient discomfort due to repeat biopsy and support the early diagnosis of prostate cancer while it remains small and curable.

Futterer et al.[8] showed that multiparametric magnetic resonance imaging (MRI) can support PCa detection and localisation, and has also been used for in-bore needle guidance[9-13]. Emerging multiparametric MRI guidelines and scoring schemes[14] are an important step forward in standardizing the interpretation of prostate MRI for definition of suitable targets for needle biopsy, and recommend the use of T2-weighted[14,15] dynamic contrast-enhanced T1-weighted[16,17], and diffusion weighted[18,19] sequences. In addition, apparent diffusion coefficient maps derived from diffusion-weighted MRI have been shown to be predictive of Gleason grade[20,21], raising the possibility of targeting biopsies only to regions suspicious for high-grade cancer on MRI.

3D TRUS-guided biopsy systems have been developed to improve upon the spatial information of 2D TRUS and allow for MRI targeting via image registration[22-26]. One such *fusion biopsy* system[22] has shown improved positive core rates of 30.4% (compared to 7.1% for 2D TRUS) and 42.3% (compared to 25.6% for 2D TRUS)[27] for moderate and high suspicion lesions, respectively, suggesting the value of MRI-targeted biopsy and motivating further optimization of this procedure. In contrast to MRI, the use of TRUS for needle guidance has the advantage of low cost, widespread availability, real-time imaging, and compatibility with standard biopsy needles. It is also compatible with the close access to the TRUS probe entry point required to accurately position biopsy needles, with patient positioning that is concordant with the usual training of the urologist. Both approaches involve the registration of target regions delineated on diagnostic quality preprocedural multiparametric MRI with the needle guidance imaging (either TRUS or a rapidly acquired intra-procedural T2-weighted image on which tumours are poorly visualised), and a means for compensating for prostate motion during needle insertion.

A recent study by van de Ven et al.[28] provides insight into a potential avenue for further improvement of the positive core rate. The authors estimated the maximum allowable target registration error (TRE) of MRI-3D TRUS registration for correct grading of 95% of ADC-determined high Gleason grade tumour components of peripheral zone PCa with fusion biopsy of sphere-shaped tumours[28]. The results of that study lead to the observation that the positive core rate is related to the biopsy system error in delivering the needle to the intended tumour target (henceforth referred to as the

needle delivery error). Based on this observation, one point of view is that a fusion biopsy system must deliver needles to targets with no more than some maximum needle delivery error to provide a clinically useful positive core rate for all tumours of clinically significant sizes. Another perspective is that for a fusion biopsy system with a given needle delivery error, some (larger) tumours can be sampled with a clinically desired probability (e.g. 95%) in a single biopsy core, and other (smaller) tumours will require more than one attempt (i.e. more than one core targeted at the tumour at different time points during the procedure) in order to achieve the clinically desired probability of sampling the tumour in at least one of the cores taken. In principle, if we determine the number of core samples required for each tumour in a practical biopsy scenario (within a reasonable limit for the number of biopsy cores), we could increase the positive yield of contemporary fusion biopsy systems by optimizing the number and within-tumour placement of targets for each tumour.

As a step toward optimization of prostate fusion biopsy targeting, the objective of this paper was to quantify the probability of obtaining a positive sample from MRI-defined prostate tumours in one biopsy core, under the assumption that the physician aims for the optimal within-tumour needle target. Since prostate tumours are often irregularly shaped[29], we made no assumptions regarding tumour shape and instead used the shapes of human prostate tumours as contoured by experts in 3D on MRI. We also investigated the effect of needle delivery error along the needle axis on the measured tumour burden as determined by percentage core involvement on the pathology report.

2.2 Materials and Methods

2.2.1 Materials

Images were retrospectively obtained from 49 patients (mean ± std age: 61.2 ± 7.5 years) who were enrolled in prospective MRI-3D TRUS fusion prostate biopsy studies at our institution between February 2011 and July 2012. Inclusion criteria were: PSA > 4 ng/mL, high clinical suspicion of PCa over prostatitis and no prior diagnosis of PCa. Multiparametric 3T MR images [T2-weighted, diffusion-weighted (from which an apparent diffusion coefficient map was calculated) and T1-weighted dynamic contrast enhanced] were collected from all patients using a Discovery MR750 (GE Healthcare, Waukesha, WI, USA) using an endorectal receive coil (Prostate eCoil, Medrad, Inc., Warrendale, PA, USA). On the day of MRI, a 3D TRUS image was acquired from each patient using an HDI-5000 ultrasound machine via tracked axial rotation[22] of an end-firing C9-5 5-9 MHz TRUS transducer probe (Philips Medical Systems, Seattle, WA, USA).

2.2.2 Tumour contouring on MRI

All prostate MR images were prospectively reviewed in advance of biopsy by a radiologist & radiology resident each with 7 years of prostate MRI experience (including assessment of > 150 prostate MRI studies each) to identify any concerning lesions requiring MRI-TRUS fusion biopsy. The concern for malignancy was assessed for each

lesion using information from all MR sequences, with particular attention paid to

apparent diffusion coefficient (ADC) findings for lesions located within the peripheral

zone. 81 lesions with indeterminate to high suspicion for malignancy were identified and

selected for targeted biopsy. All lesions were manually contoured in the coordinate

system of the T2-weighted MRI that was used for MRI-3D TRUS fusion. Although

information from the ADC map was used to help determine the contour delineation, the

ADC sequence was not used for fusion with 3D TRUS as the susceptibility of the

diffusion imaging makes the ADC prostate prone to spatial distortion and therefore was

not delineated as part of the original MRI-TRUS fusion biopsy study. The boundaries of

these regions were represented in 3D using triangle meshes and were registered into the

3D TRUS context using an iterative closest point prostate surface based registration

method[30]; point correspondence was established by mapping each point on the MRI

prostate surface to the closest point (in terms of 3D Euclidean distance) on the 3D TRUS

prostate surface. The registered triangle meshes were then rasterized to 3D binary images

with voxel size <1 mm using the marching cubes algorithm[31]. These meshes enclose

volumes ranging from 0.18 cm^3 to 5.22 cm^3 (mean $\pm$ std volume: 0.81 $\pm$ 0.75 cm^3).

Table 2-1 shows the number of meshes with volumes in the range of 0 to 1 cm^3, 1 to 2

cm^3, and $\geq$ 2 cm^3 respectively. All subsequent calculations described in this paper were

performed on these 3D binary meshes within the 3D TRUS spatial context. In the

description of the methods that follows, a positive tumour sample is defined as an

instance where the centre point of the biopsy core intersects with the tumour region on

the 3D binary image.

Table 2-1: Volume ranges of the contour meshes used in this study

Volume range (cm^3)	Number of tumours
$0 < $ Volume < 1	61
$1 \leq $ Volume < 2	16
Volume ≥ 2	4

2.2.3 Probability of positive tumour sampling for given needle delivery error

To calculate the probability of obtaining a positive sample from each tumour with one biopsy attempt, we considered every point within the tumour region as a candidate target point, and used the 3D binary image of the tumour in conjunction with our error model to estimate the probability of obtaining a positive sample using each candidate target point. Specifically, we centred a 3D Gaussian ($\mu = [0,0,0]$ mm) distribution onto every candidate target point within each tumour. The standard deviation σ modeled the biopsy system's root mean squared error ($RMSE$) (mm) in delivering a needle tip to a desired target location, with $\sigma = \frac{RMSE}{\sqrt{3}}$ as described by Hu et al.[32]. The probability of obtaining a tissue sample from each tumour was calculated by integrating the distribution function over the domain of the 3D tumour within its binary image. This procedure was repeated for each point within each tumour region as a candidate biopsy target, with the point of maximum probability P selected as the optimal target. P was calculated for each

tumour as a function of the overall root-mean-squared (RMS) error of the biopsy system and is defined as

$$P(\sigma, T) = \sum_{i=1}^{M} \sum_{j=1}^{N} \sum_{k=1}^{L} G_\sigma(i,j,k) \ \ s.t. \ (i,j,k) \in T,$$

where G is the 3D array form of the zero-mean Gaussian distribution described above, of size $M \times N \times L$, and $T \in \mathbb{Z}^2$ represents the domain defined by the contoured 3D suspicious region in the TRUS context.

(A) (B) (C)
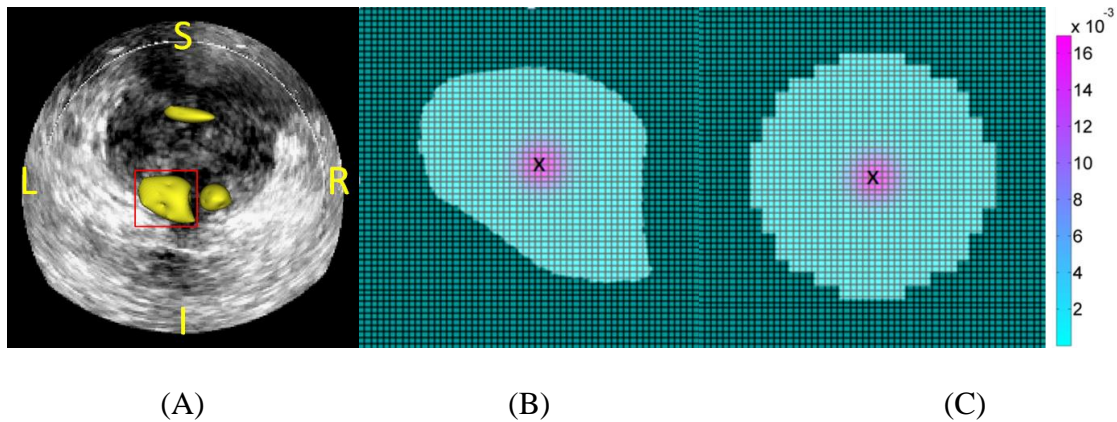
Figure 2-1: (A) Three suspicious regions contoured on MRI, registered to 3D TRUS. **(B)** A Gaussian distribution centred onto the biopsy target point of a prostate tumour projection. Note that a 2D tumour projection and 2D distribution are used for clarity of illustration; our calculations used 3D tumour volumes and 3D distributions. **(C)** A Gaussian distribution centred onto the biopsy target point of the same tumour from B, but modeled as a spheroid.

Previous work in this problem domain has been conducted under the assumption of spherical tumour shape[28]. We measured the effect on P of the assumption of spherical tumour shape by comparing the tumour sampling probabilities P obtained without the spherical shape assumption to the corresponding values of P obtained for spherical tumours of equivalent volumes to the 81 tumours in our data set. For consistency with the method described in this section, we computed values of P for spherical tumours using the same method on a 3D binary image representation of the sphere on the same digital grids as used for each of the 81 tumours in our data set (as opposed to computing them analytically).

Lastly, we adapted our algorithm for calculating positive sampling probabilities in one biopsy attempt to provide the probability P_2 of obtaining at least one positive sample when two biopsy cores are targeted to each tumour at the point of maximum probability. Probabilities were added using the properties of non-mutually exclusive events, wherein the probability of at least one positive sample in two biopsy attempts is $P_2 = P(first\ attempt) + P(second\ attempt) - P(first\ and\ second\ attempt)$.

2.2.4 Maximum needle delivery error for a given tumour sampling probability

For each tumour in our sample, we estimated the maximum $RMSE$ giving at least 95% probability of a positive tumour sample in one biopsy core using the algorithm

described in the preceding section. More precisely, we conducted an exhaustive search

over a range of $RMSE$ values from 0.5 mm to 7 mm in steps of 0.005 mm to

find $RMSE' = \frac{\arg max}{RMSE}\left(P\left(RMSE/\sqrt{3}, T\right) = 0.95\right)$. For the corresponding sphere of equal

volume to each tumour, we estimated the same $RMSE$ threshold using the method

described by van de Ven et al.[28]. To model the scenario where the physician aims for the

centre of the tumour, for both the tumours and their corresponding spheres, the needle

target was defined as the tumour centroid. We subtracted the maximum $RMSE$ for each

tumour from the corresponding maximum $RMSE$ for its corresponding sphere to measure

the effect of the spherical tumour shape assumption on the maximum acceptable ($P \geq$

95%) needle delivery error.

To accommodate arbitrary tumour shapes, our approach is numeric, in contrast to

the analytical approach taken by van de Ven et al.[28]. To measure the discrepancies

introduced by our discretization of the calculations, for a range of spherical volumes and

tumour sampling probabilities P, we conducted an exhaustive search to determine the

maximum $RMSE$ that would give at least P probability of a positive tumour sample in

one biopsy core for each value of spherical tumour volume. This method is analogous to

the calculation of the $RMSE$ threshold as a function of hit rate and volume carried out by

van de Ven et al.[28]. More precisely, for each probability value $Q \in$

$\{0.50, 0.51, \dots, 0.98, 0.99\}$ (covering the same probability range as in the paper by van de

Ven et al.[28]) and for binary volumes T_V representing spherical tumours having volumes

ranging from 0.02 mL to 2.0 mL in 0.02 mL increments, we calculated $\sigma^{Q,V} =$

$\underset{\sigma}{\arg\,max}\,(P(\sigma, T_V) = Q)$ and the corresponding $RMSE$ as $RMSE^{Q,V} = \sqrt{3}\sigma^{Q,V}$.[32] To

further investigate the effect of spherical tumour shape assumption on predicted

maximum allowable $RMSE$, we carried out the same calculations of $RMSE$ thresholds for

the tumours in our data set without the assumption of spherical shape, for $Q \in$

$\{0.50, 0.51, \ldots, 0.98, 0.99\}$. We also conducted an exhaustive search to determine the

$RMSE$ value corresponding to P=95% (within 0.5% accuracy) for each tumour, using

both methods. We calculated the mean difference between methods, with the predicted

RMSE values from the method in the paper by van de Ven et al.[28] subtracted from the

predicted RMSE values from our algorithm.

2.2.5 Effect of axial error on measured tumour burden

We investigated the effect of needle delivery error parallel to the ultrasound probe

axis (henceforth *axial error*) on the measured tumour burden according to the percentage

core involvement: the proportion of a core that contains tumour tissue. The interpretation

of the percentage core involvement is a matter of current debate. We base the present

exploration on the Johns Hopkins criteria, wherein a core involvement of ≥ 50% is

interpreted to indicate a level of tumour burden warranting consideration of treatment

beyond active surveillance[33]. We performed a simulation to measure the effect of axial

error on the measured tumour burden. In particular, for the 55 tumours in our data set

which should have a measured percentage core involvement of ≥ 50% if sampled ideally,

we measured the number of such tumours that would incorrectly have a measured percentage core involvement of $< 50\%$, for a range of different values of axial error.

We performed our simulation as follows. The axial probe direction coincides with the z axis in the image space of our 3D TRUS images. Since the biopsy needle is oriented parallel to the ultrasound probe, the biopsy needle is also parallel to the z axis. To simulate the extraction of a tissue core from a binary tumour image in this space, we positioned the needle laterally (along the directions orthogonal to the probe axis) by specifying its (x, y) coordinates, and then specified a z coordinate corresponding to the centre point of the biopsy core. This needle positioning is shown in Fig. 2-2, with axis labels included. We then considered only the image subdomain $(x, y, z \pm 9\ mm)$, corresponding to an 18 mm core (as used in our biopsies) centred at (x, y, z) and orthogonal to the (x, y) plane. For each binary tumour image T, x and y were set to the position corresponding to the thickest point of the tumour along the z direction. The absolute positive core length $L(AE)$ was then computed to be the Euclidean distance between the two most mutually distant "on" pixels in T within the biopsy core subdomain $(x, y, z \pm 9\ mm)$, computed as a function of axial error (AE). The percentage core involvement for an 18 mm core extracted from the ideal spatial location was then calculated as $I(AE) = L(AE)/18mm \times 100\%$. For each tumour T we then found the minimum AE required to incorrectly obtain a percentage core involvement of $< 50\%$ as $AE_{min} = \frac{\arg min}{abs(AE)}\ I(AE) < 50\%$. We performed this minimization by exhaustive search of values of z from 0 mm to 15 mm in steps of 0.1 mm.
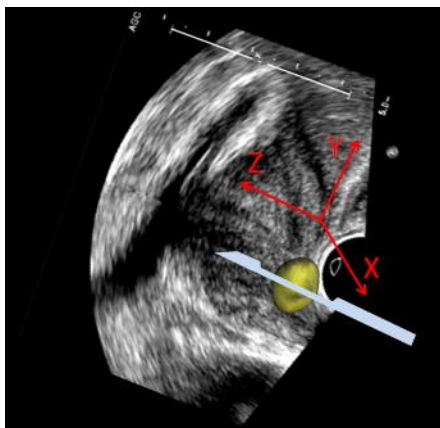
Figure 2-2: Simulated positioning of the biopsy needle at the centre of a tumour volume, with x, y and z directions defined.

2.2.6   Estimation of biopsy system RMSE

The approach presented in this work can in principle be applied to any biopsy system with a measured needle delivery error. However, to provide context for our results, we calculated the needle delivery error of a contemporary fusion biopsy system developed at our institution[22]. Our clinical trial of this system involves several workflow steps, each contributing to needle delivery error. The RMS TREs of each step are enumerated as follows. (1) Pre-procedural MRI-3D TRUS and 3D TRUS-3D TRUS registrations to map MRI-defined tumour surfaces into the 3D TRUS context for targeting: 1.74 mm[23] and 2.36 mm[34], respectively. (2) Intra-procedural 2D-3D TRUS registration for prostate motion compensation during probe navigation and needle guidance: 1.63 mm[35]. (3) Needle guidance error of the biopsy system[22]: 1.0 mm. We

added these errors in quadrature under the assumptions that they are independent and the needle delivery error of the fusion biopsy system could be modeled using a Gaussian distribution. This yielded an estimated overall error in delivering a biopsy needle to an intended target to be 3.5 mm.

2.3 Results

2.3.1 Probability of positive tumour sampling for given needle delivery error

The probability of a positive sample in one biopsy core, P, was calculated for each tumour, for $RMSE = 1$ mm through 6 mm. This is shown in Fig. 2-3(A), where the 81 points for every $RMSE$ on the horizontal axis give the maximum probability of obtaining a positive sample from each tumour for each level of error. For each $RMSE$ level on the horizontal axis, the probability on the vertical axis for tumour T corresponds to $P(\sigma, T)$, where $\sigma = \frac{RMSE}{\sqrt{3}}$. The red curve depicts the mean sampling probability for each value of $RMSE$, and the broken black line depicts a 95% sampling probability. For an $RMSE$ of 3.5 mm (our system's estimated needle delivery error) tumours with $P \geq$ 95% had a mean $\pm$ std volume of 1.67 ± 1.01 cm^3, with a maximum volume of 5.22 cm^3 and a minimum of 0.81 cm^3, and those with $P < 95\%$ had a mean $\pm$ std volume of 0.51 ± 0.21 cm^3, with a maximum volume of 1.52 cm^3 and a minimum of 0.18 cm^3. Both distributions of tumour volume (for $P \geq 95\%$ and $P < 95\%$) passed a normality test;

with failure to reject the null hypothesis that the samples were drawn from normally

distributed populations according to a one-sample Kolmogorov-Smirnov test (p > 0.05).

The difference between these means was statistically significant according to a

heteroscedastic two-tailed t-test (p < 0.0001). This implies that despite the potential

impact of differences in tumour shape on positive sampling probability, tumours with

high (> 95%) probability of positive sampling can be distinguished from those with lower

sampling probability based on tumour volume. The upper bound of the 99% prediction

interval for the tumour volumes with $P < 95\%$ was 1.05 cm^3; this inference provides

some insight into the largest tumours that *cannot* be successfully sampled in one biopsy

core with 95% confidence. To explore the bias and confidence region for the differences

between estimated tumour sampling probabilities with and without the spherical

assumption, Fig. 2-4 shows a Bland-Altman plot of these differences at $RMSE = 3.5$

mm; the observed positive bias is reflective of the overestimation of sampling probability

resulting from the spherical assumption. Fig. 2-3(B) shows the differences in

probabilities of a positive sample in one biopsy core arising from the use of the spherical

assumption of tumour shapes, versus no spherical shape assumption. The red curve

depicts the mean difference for each value of $RMSE$. The use of the spherical tumour

assumption results in a consistent overestimation of tumour sampling probability.

However, the amount of overestimation varies with the RMSE of the biopsy system. For

instance, at 1.5 mm RMSE, the overestimation was relatively small, with mean ± SD of

0.5±0.2% (range 0.0% to 1.9%). At 4 mm RMSE, the overestimation was larger, with

mean ± SD of 3.4±2.6% (range 0.0% to 15.4%). The mean difference of the predicted

RMSE values from the van de Ven method, subtracted from the predicted RMSE values from our algorithm was -0.0046 mm, and the maximum difference observed was -0.075 mm. This implies that our algorithm under the assumption of spherical tumour shapes produces the same results as the algorithm used by van de Ven et al., to within 0.1 mm error.

Fig. 2-5 shows the probabilities of obtaining at least one positive sample from each tumour when two biopsy attempts are made, targeted at the point of maximum probability, for $RMSE = 1$ mm through 6 mm.
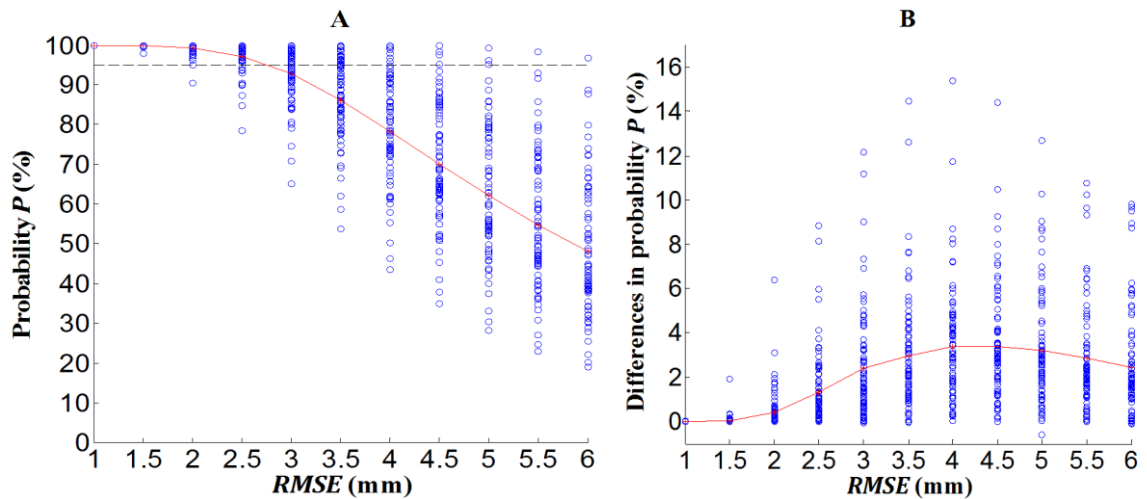
Figure 2-3: (A) Probability of obtaining a positive core sample for 81 3D tumours in one biopsy attempt, for RMSE from 1 to 6 mm. **(B)** Probabilities of a positive core sample in **(A)** with no spherical assumption, subtracted from the probabilities of a positive core sample under the spherical tumour assumption. Calculated for 81 3D tumours, for RMSE from 1 to 6 mm.
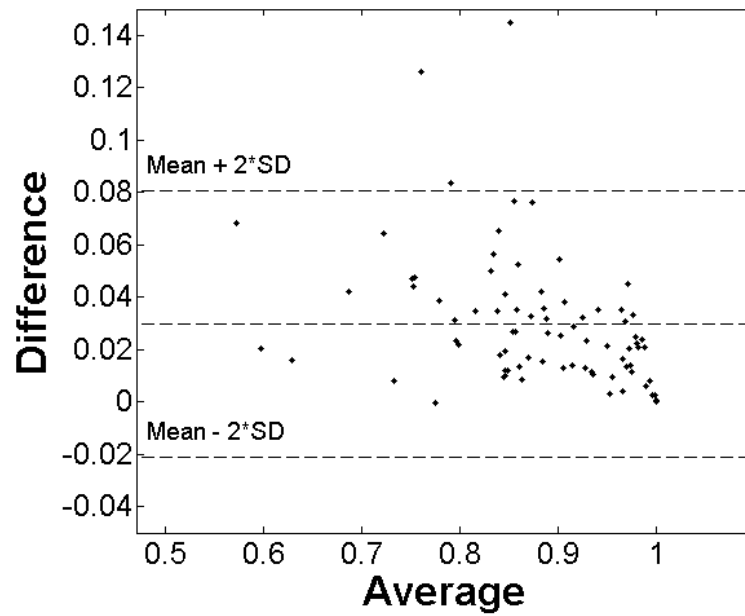
Figure 2-4: Plot of Bland-Altman analysis showing the differences between estimated tumour sampling probabilities with and without the spherical assumption, at RMSE = 3.5 mm.
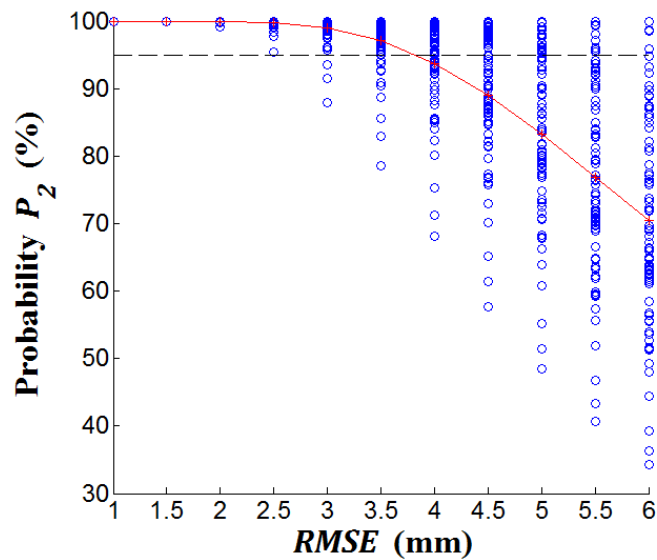
Figure 2-5: Probability of obtaining at least one positive core sample for 81 3D tumours in two biopsy attempts, for RMSE from 1 to 6 mm.

2.3.2   Maximum needle delivery error for a given tumour

sampling probability

Fig. 2-6(A) shows the maximum *RMSE* such that a positive sample will be obtained from each tumour in one biopsy core, with no assumption of spherical shape. The distribution of predicted *RMSE* thresholds from Fig. 2-6(A) passed a normality test, and failed to reject the null hypothesis that the sample was drawn from a normally distributed population according to a one-sample Kolmogorov-Smirnov test ($p > 0.05$). The lower bound of the 95% prediction interval for the *RMSE* thresholds was 1.6 mm, and this inference provides some insight into the maximum needle delivery error such that 95% of tumours will be sampled in one biopsy core. Fig. 2-6(B) indicates the differences in maximum *RMSE* estimated when making the assumption of spherical tumour shape, versus not making this assumption. The values on the horizontal axis show the maximum *RMSE* without the spherical assumption, minus the maximum *RMSE* with the spherical assumption. Negative values on the x axis indicate instances where making the assumption of spherical shape over-estimates the maximum allowable *RMSE* to achieve a 95% probability of sampling each tumour using a single biopsy core. Over-estimation occurred in all but one tumour.
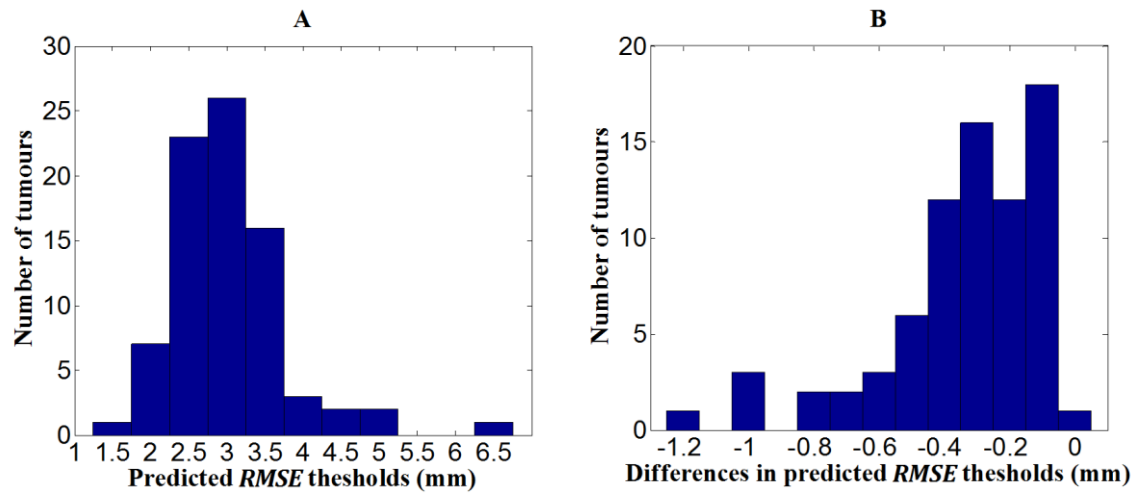
Figure 2-6: (A) Histogram of the maximum allowable RMSE values to achieve a 95% probability of sampling each tumour using a single biopsy core, predicted by our algorithm using no assumption of spherical tumour shapes. **(B)** Histogram of the differences obtained by subtracting the thresholds predicted under the assumption of spherical tumour shapes from the thresholds given in **(A)**.

Fig. 2-7 shows the RMS error threshold as a function of desired tumour sampling probability and tumour volume, under the assumption of spherical tumour shapes, calculated using our discrete approach. The white numbers in black circles indicate the 2 mm through 8 mm *RMSE* isocontours for spherical tumours. Each row of small numbers of 2 mm through 8 mm corresponds to one of the 81 non-spherical tumours in our data set, having a volume corresponding to the position of this row on the vertical axis. For instance, the row indicated by the shaded box corresponds to one tumour in our data set with a volume of 1.48 mL. If the maximum permissible *RMSE*s for sampling this non-spherical tumour with each probability level Q agreed with those for a spherical tumour

of the same volume, then its $RMSE$ integer transition points indicated by the small

numbers 7 mm through 3 mm in this row would agree with the isocontours, as in the case

of the 7 mm transition point beside the black star symbol near the bottom of the figure.

However, the spherical assumption in this case resulted in an overestimation of the

maximum permissible $RMSE$. For instance, under the spherical assumption, a system

with a 5 mm $RMSE$ would yield a sampling probability Q of 0.88 (solid vertical arrow), a

9% overestimation of the 0.79 sampling probability estimated (dashed vertical arrow)

when taking the non-spherical shape of the tumour into account. This pattern of

overestimation resulting from the spherical assumption is evident for most tumours in our

data set (i.e. most of the numbers on the plot appear to the left of their corresponding

isocontours). The portion of Fig. 2-7 that is above the horizontal dotted line is similar to

the plot which was published by van de Ven et al.[28] using their analytical approach

(Figure 2 in their article), demonstrating that our method can reproduce the results of that

work in the context of our tests of the spherical tumour shape assumption in this paper.

Due to space considerations, 4 outliers with volume > 2 mL were not included in this

plot.
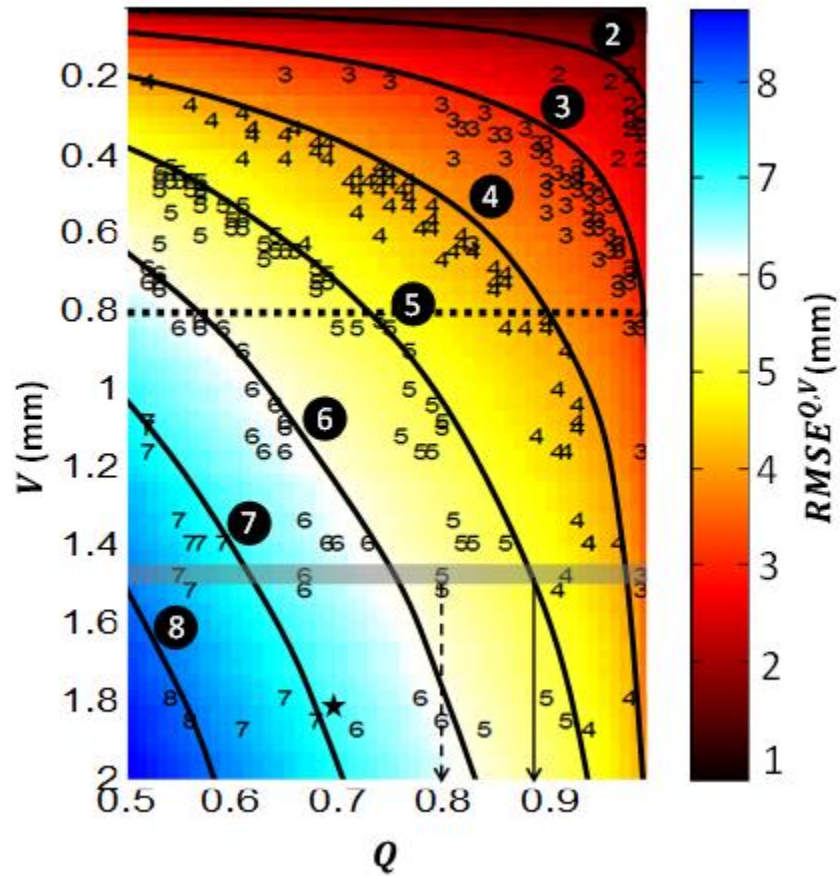
Figure 2-7: Plot showing the relationship between tumour volume V, sampling probability Q, and $RMSE^{Q,V}$ for spherical tumours (colour map and isocontour curves) and for the tumours in our data set without application of the spherical assumption (small digits rendered on the colour map). Note the similarity of the colour map and isocontours above the horizontal dotted line to Figure 2 in the paper by van de Ven et al.[28] See Section 2.3.2 for a detailed description of this figure.

2.3.3 Effect of axial error on measured tumour burden

Fig. 2-8 shows the number of tumours (out of 55 in total) that would be misclassified as $< 50\%$ core involvement for each level of AE_{min} on the horizontal axis. No tumours are misclassified for $RMSE \leq 4$ mm, and more than 50% of tumours are misclassified for $RMSE \geq 5.5$ mm.
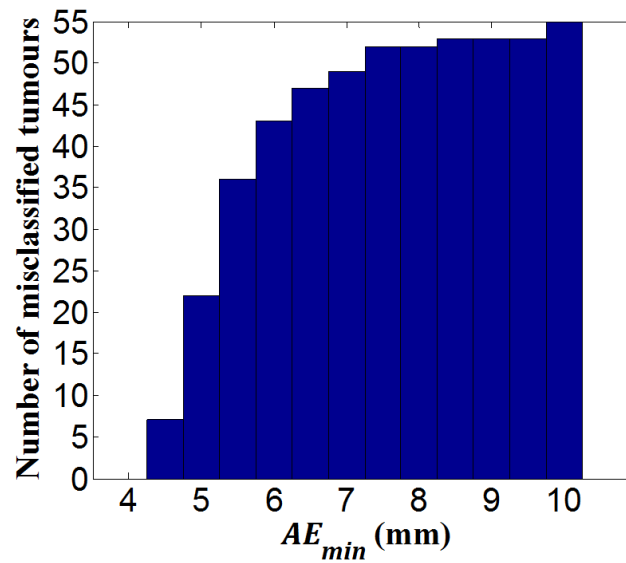
Figure 2-8: Histogram of tumours incorrectly classified as $< 50\%$ core involvement due to axial error (AE_{min}) in biopsy needle delivery.

2.4 Discussion

Context for the results of this paper was provided by a fusion biopsy system developed at our institution[22] for which we estimated an overall needle guidance error of 3.5 mm. However, in principle, the contributions of this paper could be straightforwardly adapted to other fusion biopsy systems or to the MRI guidance context, provided that an estimate of the system's needle guidance error is available.

2.4.1 Probability of positive tumour sampling for given needle delivery error

Fig. 2-3(A) shows that for a $RMSE$ of 3.5 mm, $P \geq 95\%$ for 21 out of 81 tumours, when the optimal target point (having largest P) was targeted by the needle. Therefore, more than one biopsy core must be taken from 74% of the tumours to achieve $P \geq 95\%$ for a biopsy system with an error of 3.5 mm. Fig. 2-5 shows that for a $RMSE$ of 3.5 mm, $P \geq 95\%$ for 68 out of 81 tumours when two biopsy attempts are made for each tumour and the optimal target point was used. Thus the majority of tumours from our study can be sampled in two biopsy cores, with a probability of a 95% or greater. Of the remaining 13 tumours, the largest observed tumour volume was 0.4 cc, suggesting that most tumours of clinically significant sizes[36] could be sampled in two attempts on a system with 3.5 mm $RMSE$.

The upper bound of the 99% prediction interval for volumes of tumours having $P <$ 95% provides a useful rule of thumb that for a biopsy system with 3.5 mm RMS needle delivery error, one cannot expect to sample tumours of approximately 1 cm^3 or smaller with 95% probability with only one biopsy core; multiple biopsy attempts should be made for such tumours at different time points during the procedure. This rule of thumb incorporates the variability in tumour shapes represented in our data set. To maximally increase the probability of achieving a positive sample, one would target different samples within the same lesion, all near to the point of maximum probability for the tumour target. Doing so would require careful instruction, but this task is well within the capability of the trained operator with experience in sampling targets under TRUS guidance. For smaller lesions, the use of MRI-guided biopsy could be considered as an alternative approach in centres where the necessary technologies are available. The superior soft tissue contrast on MRI and potential lesion visibility on the intra-procedural T2W images could potentially obviate the need to make more the one biopsy attempt in order to obtain a sample of smaller tumours. Although this approach requires specialized hardware and longer procedure times (approximate 30-65 min/biopsy) on a modality that could result in substantial cost increases[37-39], if this approach mitigated the need for additional biopsy sessions it could provide a cost reduction over the longer term.

2.4.2 Maximum needle delivery error for a given tumour sampling probability

From Fig. 2-6(B) and Fig. 2-7, we observed that the spherical tumour shape assumption consistently overestimates the maximum allowable error to achieve a 95% tumour sampling probability. From a different perspective, given a fusion biopsy system error, the spherical tumour assumption may lead to an overestimation of positive tumour sampling probabilities. This is likely due to the irregular, non-spherical shapes of prostate tumours, with increasing deviation from sphericity further from 0 on the horizontal axis of Fig. 2-6(B). However, the mean overestimation of tumour sampling probabilities under the assumption of spherical tumour shape was 3% for $RMSE = 3.5$ mm. Therefore, assuming spherical tumour shape may be reasonable for many prostate tumours. In Fig. 2-3(B), there are 3 tumours which show a discrepancy in estimated positive sampling probabilities of more than 10% for at least one of the given $RMSE$ values on the x-axis. The approximate locations of these three tumours within the prostate are right anterior midgland, right anterior apex and right peripheral zone apex respectively. Sphericity measures were determined as the ratio of the surface area of a sphere with the same volume as the given tumour, to the surface area of the tumour. These tumours have sphericity values of 0.793, 0.829 and 0.698 respectively.

Based on the 95% prediction interval for the distribution in Fig. 2-6(A), we determined that a biopsy system would need to have a RMS needle delivery error of no more than 1.6 mm in order to sample 95% of tumours with one core. Considering the

multiple sources of error contributing to needle delivery error in a guided biopsy system, it is reasonable to question the practicality of achieving this level of overall needle delivery error. This observation motivates our perspective that some tumours of clinically significant sizes may require more than one biopsy attempt in order to be sampled during the first biopsy session.

2.4.3 Effect of axial error on measured tumour burden

The histogram shown in Fig. 2-8 indicates that for biopsy systems with needle delivery errors ≥ 4.5 mm, a steeply increasing proportion of patients who may need treatment (percentage core involvement ≥ 50%) could be misclassified as candidates for active surveillance (percentage core involvement < 50%). However, using a contemporary fusion biopsy system such as that developed at our institution[27], with 3.5 mm needle delivery error, none of the tumours in our sample would have been misclassified. Overall, the effect of axial error on measured tumour burden may be mitigated by the 18 mm core length for systems with sufficiently small needle guidance error, but this effect rapidly increases with increasing error.

Although we have interpreted our results in the context of the Johns Hopkins criteria wherein a core involvement ≥ 50% precludes the use of active surveillance, it is important to note that the interpretation of the core involvement measure (specifically, how to measure the length of core involvement, and what threshold to use) is a matter of some controversy. Current interpretation guidelines are based on the assumption that

samples were obtained from clinical standard 2D TRUS-guided biopsy, with its inherent

sampling problems. As accuracy of biopsy continues to increase with improved

interpretation of MRI and other imaging modalities for targeting, and improved systems

for image guidance of the biopsy needle (including both 3D TRUS and MRI guidance

approaches) become available, it is reasonable to expect that for the overall population,

the percentage of core involvement and also the percentage of cores involved may

increase. This will require a recalibration of the criteria for appropriate treatment

selection based on these measures. Thus, it could be valuable to revisit our results

regarding percentage core involvement in the future as interpretation criteria continue to

evolve.

2.4.4 Limitations

The results of this work must be considered in the context of its strengths and

limitations. Although the simulations that we have conducted have relaxed the typically

used assumption of spherical tumour shape and instead used the complex tumour shapes

delineated in 3D by experts on MRI, the needle delivery error model is used subject to a

set of assumptions that may be strong. The use of a zero-mean 3D Gaussian distribution

as the error model implies a lack of systematic error in any of the system components

contributing to the overall needle delivery error. However, it is reasonable to speculate

that some sources of error may be systematic; e.g. image registration steps may be biased

toward alignment of structures to edges apparent in the ultrasound images, which will

tend to be oriented orthogonally to the ultrasound beam direction. Additionally, the use of this error model implies that needle delivery error is spatially isotropic, whereas it is reasonable to conjecture that needle delivery error may be spatially anisotropic, according to the physical constraints of needle insertion angle and considering the elongated nature of the biopsy core itself. The empirical testing of these assumptions and characterization of each source of error in terms of bias and anisotropy in ongoing studies will provide information that will enhance our error model to more realistically reflect the practical biopsy situation. Although the use of this simple error model constitutes a limitation of this work, controlling for this variable and keeping it consistent with previous work does allow for the specific measurement of the effect of the spherical tumour assumption in this work.

Additionally, for our study on the effect of axial error on measured tumour burden, described in Section 2.2.5, we assumed that the thickest point of the tumour along the z-direction was hit by the simulated biopsy core, and investigated how error along the z-direction may affect the calculated percent core involvement. However, this approach does not account for error in the x and y directions. Therefore, this experiment represents a best-case scenario in terms of x and y error, and only investigates how error along the axial direction can affect measured tumour burden. A further investigation on estimated core length in the presence of x,y and z error is warranted.

It should be noted that only contoured lesions selected for biopsy were included in this study, with no preference weighted toward lesions with imaging findings concerning

more aggressive tumour biology, such as those with low ADC values[39]. Although contouring was done in the coordinate system of the T2W images, the ADC was assessed for tumour aggressiveness and this information was incorporated into the decision to target a lesion. However, the tumour contouring performed for this paper was not intended to encompass only the highest-grade portions of the tumours. In the context of prostate cancer diagnosis, it is of utmost importance not only to sample the cancer but also to characterize it, and in particular to obtain samples of tumours that are threatening to the patient (e.g. those containing Gleason grade 4 components). A further study of our research question in the context of tumour contours focused only on aggressive cancer is warranted and would be valuable. Lastly, for small lesions with low ADC values, MRI-guided biopsy could be considered as an alternative to 3D TRUS guidance in centres where the necessary technologies are available.

2.5 Conclusions

In this work, we estimated the probability of obtaining a positive tumour sample from 81 3D suspicious regions contoured on MRI by experts, in a single biopsy core. We observed that for a contemporary fusion biopsy system with 3.5 mm needle guidance error, one cannot expect to sample tumours with volume ≤ 1 cm^3 with 95% probability in only a single attempt. Our findings indicated that more than one core must be taken from the majority of tumours to achieve a sampling probability of 95% or greater for a biopsy system with an overall error ≥ 3.5 mm. In fact, we determined that a biopsy system

would need to have a RMS needle delivery error of no more than 1.6 mm in order to sample 95% of tumours in one core, with $P \geq 95\%$. This motivates our perspective that some tumours of clinically significant volume may require more than one biopsy attempt in order to be sampled during one biopsy session. Due to the 18 mm core length, needle delivery error along the direction of the ultrasound probe axis may have little effect on the measured tumour burden when considering systems with sufficiently small needle guidance error (≤ 4 mm), but this effect rapidly increases with increasing error. Lastly, we observed through comparison with a previously published method that the assumption of spherical tumour shape can lead to slight overestimation positive sampling probabilities. Although this observation was significant ($p < 0.05$), the overestimation varied with biopsy system RMSE and the practical importance of this observation depends on both tumour asphericity and biopsy system needle delivery error. This knowledge generation will support the development of an approach to optimized planning of within-tumour prostate biopsy targets which could support earlier diagnosis of PCa while it remains localized to the prostate and curable.

References

1   *Canadian Cancer Statistics.* Canadian Cancer Society, 2013.

2   R. Siegel, D. Naishadham and A. Jemal, "Cancer Statistics, 2013," CA: Cancer Journal for Clinicians **63**(1), 11-30 (2013).

3   D.F. Gleason, "Classification of prostatic carcinomas," Cancer Chemother Reports **50**(3), 125-128 (1966)

4   M.E. Chen, P. Troncoso, D.A. Johnston, K. Tang, and R.J. Babaian, "Optimization of prostate biopsy strategy using computer based analysis," Urology, **158**(6), 2168-2175 (1997)

5   D. Shen, Z. Lao, J. Zeng, W. Zhang, I.A. Sesterhenn, L. Sun, J.W. Moul, E.H. Herskovits, G. Fichtinger, and C. Davatzikos, "Optimized prostate biopsy via a statistical atlas of cancer spatial distribution," Medical Image Analysis **8**(2), 139-150 (2004).

6   F. Rabbani,, N. Stroumbakis, B.R. Kava, M.S. Cookson, and W.R. Fair, "Incidence and clinical significance of false-negative sextant prostate biopsies" Urology **159**(4), 1247-1250 (1998)

7   A. Rajinikanth, M. Manoharan, C.T. Soloway, F.J. Civantos, and M.S. Soloway, "Trends in Gleason score: concordance between biopsy and prostatectomy over 15 years," Urology **72**(1), 177-182 (2008)

8   J.J. Futterer, S.W. Heijmink, T.W. Scheenen, J. Veltman, H.J. Huisman, P. Vos, C.A. Hulsbergen-Van de Kaa, J.A. Witjes, P.F. Krabbe, A. Heerschap, and J.O. Barentsz, "Prostate cancer localization with dynamic contrast-enhanced MR imaging and proton MR spectroscopic imaging," Radiology **241**(2), 449-458 (2006)

9   A.V. D'Amico, C.M. Tempany, R. Cormack, N. Hata, M. Jinzaki, K. Tuncali, M. Weinstein, and J.P. Richie, "Transperineal magnetic resonance image guided prostate biopsy," Urology **164**(2), 385-387 (2000).

10   P. Blumenfeld, N. Hata, S. DiMaio, K. Zou, S. Haker, G. Fichtinger, and C.M. Tempany, "Transperineal prostate biopsy under magnetic resonance image guidance: a needle placement accuracy study," JMRI: Journal of Magnetic Resonance Imaging **26**(3), 688-694 (2007).

11   J. Cepek, B.A. Chronik, U. Lindner, J. Trachtenberg, S.R. Davidson, J. Bax, and A. Fenster, "A system for MRI-guided transperineal delivery of needles to the prostate for focal therapy," Medical Physics **40**(1), 012304 (2013).

12   A. Krieger, C. Csoma, Iordachital, II, P. Guion, A.K. Singh, G. Fichtinger, and L.L. Whitcomb, "Design and preliminary accuracy studies of an MRI-guided transrectal prostate intervention system," Medical Image Computing and Computer Assisted Interventions **10**(2), 59-67 (2007).

13   N. Hata, M. Jinzaki, D. Kacher, R. Cormak, D. Gering, A. Nabavi, S.G. Silverman, A.V. D'Amico, R. Kikinis, F.A. Jolesz, and C.M. Tempany, "MR imaging-guided prostate biopsy with surgical navigation software: device validation and feasibility," Radiology **220**(1), 263-268 (2001).

14   J.O. Barentsz, J. Richenberg, R. Clements, P. Choyke, S. Verma, G. Villeirs, O. Rouviere, V. Logager and J.J. Futterer, "ESUR prostate MR guidelines 2012," European Radiology **22**(4), 746-757 (2012).

15   A. Sciarra, J.O. Barentsz, A. Bjartell, J. Eastham, H. Hricak, V. Panebianco, and J.A. Witjes, "Advances in magnetic resonance imaging: how they are changing the management of prostate cancer," European Urology **59**(6), 962-977 (2011).

16   M.R. Engelbrecht, J.O. Barentsz, G.J. Jager, M. van der Graaf, A. Heerschap, J.P. Sedelaar, R.G. Aarnink, and J.J. de la Rosette, "Prostate cancer staging using imaging," BJU Int, **86**(1), 123-134 (2000).

17   I. Ocak, M. Bernardo, G. Metzger, T. Barrett, P. Pinto, P.S. Albert, and P.L. Choyke, "Dynamic contrast-enhanced MRI of prostate cancer at 3 T: a study of pharmacokinetic parameters," AJR: American Journal of Roentgenology **189**(4), 849: W192-W201 (2007)

18   H.A. Vargas, O. Akin, T. Franiel, Y. Mazaheri, J. Zheng, C. Moskowitz, K. Udo, J. Eastham and H. Hricak, "Diffusion-weighted endorectal MR imaging at 3T for prostate cancer: tumour detection and assessment of aggressiveness," Radiology **259**(3), 775-784 (2011).

19   B. Turkbey, V.P. Shah, Y. Pang, M. Bernado, S. Xu, J. Kruecker, J. Locklin, A.A. Baccala, A.R. Rastinehad, M.J. Merino, J.H. Shih, B.J. Wood, P.A. Pinto and P.L. Choyke., "Is apparent diffusion coefficient associated with clinical risk scores for prostate cancers that are visible on 3-T MR images?," Radiology **258**(2), 488-495 (2011).

20   Y. Itou, K. Nakanishi, Y. Narumi, Y. Nishizawa, and H. Tsukuma, "Clinical utility of apparent diffusion coefficient (ADC) values in patients with prostate cancer: can ADC values contribute to assess the aggressiveness of prostate cancer?" JMRI: Journal of Magnetic Resonance Imaging **33**(1), 167-172 (2011).

21   T. Hambrock, D.M. Somford, H.J. Huisman, I.M. van Oort, J.A. Witjes, C.A. Hulsbergen-van de Kaa, T. Scheenen and J.O. Barentsz, "Relationship between

apparent diffusion coefficients at 3.0-T MR imaging and Gleason grade in peripheral zone prostate cancer," Radiology **259**(2), 453-461 (2011).

[22] J. Bax, D. Cool, L. Gardi, K. Knight, D. Smith, J. Montreuil, S. Sherebrin, C. Romagnoli and A. Fenster, "Mechanically assisted 3D ultrasound guided prostate biopsy system," Medical Physics **35**(12), 5397-5410 (2008).

[23] Y. Sun, J. Yuan, M. Rajchl, W. Qiu, C. Romagnoli and A. Fenster, "Efficient Convex Optimization Approach to 3D Non-Rigid MR-TRUS Registration," Lecture Notes in Computer Science **8149** (2013).

[24] M. Baumann, P. Mozer, V. Daanen and J. Troccaz, "Prostate biopsy tracking with deformation estimation," Medical Image Analysis **16**(3), 562-576 (2012).

[25] S. Xu, J. Kruecker, B. Turkbey, N. Glossop, A.K. Singh, P. Choyke, P. Pinto and B.J. Wood, "Real-time MRI-TRUS fusion for guidance of targeted prostate biopsies," Computer Aided Surgery **13**(5), 255-264 (2008).

[26] B.A. Hadaschik, T.H. Kuru, C. Tulea, P. Rieker, I.V. Popeneciu, T. Simpfendorfer, J. Huber, P. Zogal, D. Teber, S. Pahernik, M. Roethke, P. Zamecnik, W. Roth, G. Sakas, H.P. Schlemmer and M. Hohenfellner, "A novel stereotactic prostate biopsy system integrating pre-interventional magnetic resonance imaging and live ultrasound fusion," Urology **186**(6), 2214-2220 (2011).

[27] D.W. Cool, J. Bax, C. Romagnoli, A.D. Ward, L. Gardi, V. Karnik, J. Izawa, J. Chin and A. Fenster, "Fusion of MRI to 3D TRUS for mechanically-assisted targeted prostate biopsy: system design and initial clinical experience," Lecture Notes in Computer Science **6963**, 121-133 (2011).

[28] W.J. van de Ven, C.A. Hulsbergen-van de Kaa, T. Hambrock, J.O. Barentsz and H.J. Huisman, "Simulated required accuracy of image registration tools for targeting high-grade cancer components with prostate biopsies," European Radiology **23**(5), 1401-1407 (2013).

[29] L.E. Quint, J.S. van Erp, P.H. Bland, S.H. Mandell, E.A. Del Buono, H.B. Grossman, G.M. Glazer, and P.W. Gikas, "Carcinoma of the prostate: MR images obtained with body coils do not accurately reflect tumour volume," AJR: American Journal of Roentgenology **156**(3), 511-516 (1991).

[30] P.J. Besl and N.D. Mckay, "A method for registration of 3-D shapes," IEEE Transactions on Pattern Analysis and Machine Intelligence **14**(2), 239-256 (1992).

31   W.E. Lorensen and H.E. Cline, "Marching cubes: a high resolution 3D surface construction algorithm," Computer Graphics **21**(4), 163-169 (1987).

32   Y. Hu, H.U. Ahmed, Z. Taylor, C. Allen, M. Emberton, D. Hawkes, and D. Barratt, "MR to ultrasound registration for image-guided prostate interventions," Medical Image Analysis **16**(3), 687-703 (2012).

33   Epstein, J.I., "Prognostic significance of tumour volume in radical prostatectomy and needle biopsy specimens," Urology **186**(3), 790-797 (2011).

34   V.V. Karnik, A. Fenster, J. Bax, C. Romagnoli and A.D. Ward, "Evaluation of intersession 3D-TRUS to 3D-TRUS image registration for repeat prostate biopsies," Medical Physics **38**(4), 1832-1843 (2011).

35   T. De Silva, A. Fenster, D.W. Cool, L. Gardi, C. Romagnoli, J. Samarabandu and A.D. Ward, "2D-3D rigid registration to compensate for prostate motion during 3D TRUS-guided biopsy," Medical Physics **40**(2), 022904 (2013).

36   J.I. Epstein, P.C. Walsh, M. Carmichael and C.B. Brendler, "Pathologic and clinical findings to predict tumour extent of nonpalpable (stage T1c) prostate cancer," JAMA, The Journal of the American Medical Association **271**(5), 368-374 (1994).

37   C.M. Hoeks, M.G. Schouten, J.G. Bomers, S.P. Hoogendoorn, C.A. Hulsbergen-van de Kaa, T. Hambrock, H. Vergunst, J.P. Sedelaar, J.J. Futterer and J.O. Barentsz, "Three-Tesla magnetic resonance-guided prostate biopsy in men with increased prostate-specific antigen and repeated, negative, random, systematic, transrectal ultrasound biopsies: detection of clinically significant prostate cancers," European Urology **62**(5), 902-909 (2012).

38   A.G. Anastasiadis, M.P. Lichy, U. Nagele, M.A. Kuczyk, A.S. Merseburger, J. Hennenlotter, S. Corvin, K.D. Sievert, C.D. Claussen, A. Stenzl, and H.P. Schlemmer, "MRI-guided biopsy of the prostate increases diagnostic performance in men with elevated or increasing PSA levels after previous negative TRUS biopsies," European Urology **50**(4), 738-749 (2006).

39   T. Hambrock, C. Hoeks, C. Hulsbergen-van de Kaa, T. Scheenen, J. Futterer, S. Bouwense, I. van Oort, F. Schroder, H. Huisman, and J. Barentsz, "Prospective assessment of prostate cancer aggressiveness using 3-T diffusion-weighted magnetic resonance imaging-guided biopsies versus a systematic 10-core transrectal ultrasound prostate biopsy cohort," European Urology **61**(1), 177-184 (2012).

Chapter 3

3 A comparison of prostate tumour targeting strategies using magnetic resonance imaging-targeted, transrectal ultrasound-guided fusion biopsy[*]

3.1 Introduction

2D transrectal ultrasound (TRUS)-guided systematic biopsy is the current clinical standard for prostate cancer (PCa) diagnosis. However, as PCa is generally not detectable on ultrasound, a sextant or extended-sextant scheme is used to guide the biopsy needle to extract 6 to 12 tissue samples (cores) for pathologist examination in order to assess the presence and Gleason grade[1] of cancer. However, this approach has been shown to have a 21–47% false negative rate and therefore many patients return to the clinic for repeat biopsies[2,3]. Additionally, this biopsy method may either underestimate or overestimate the true Gleason score of a patient's cancer[4]. Furthermore, it has been shown that 25–

---

[*] This chapter has been previously published as P.R. Martin et al., "A comparison of prostate tumour targeting strategies using magnetic resonance imaging-targeted, transrectal ultrasound-guided fusion biopsy," Medical Physics **45**(3), 1018-1028 (2018).

37% of men who are placed on active surveillance after receiving 2D TRUS-guided systematic biopsy are removed from surveillance to receive treatment within 5 years[5,6]. This may be due to underestimation of tumour grade on initial biopsy, interval changes in the tumour histology, and/or patients opting for definitive treatment.

It has been shown that multiparametric MRI (mpMRI) is an effective tool for PCa detection and localization[7]. The development of 3D TRUS-guided biopsy systems allows for improved spatial information relative to 2D TRUS, and MRI targeting via image registration (Fig. 3-1). These systems also avoid the cost of in-bore MRI-guided biopsy and enable implementation in an office setting. A 3D TRUS biopsy system with MRI-3D TRUS fusion ("fusion biopsy") has been shown to produce significantly higher (p < 0.01) positive biopsy core rates, mean Gleason scores and tumour volumes sampled, compared to 2D TRUS-guided 12-core systematic biopsy[8]. A systematic review was conducted by Valerio et al, collecting 14 papers which compared MRI-TRUS fusion targeted biopsy versus 2D TRUS-guided systematic biopsy. It was found that MRI-TRUS fusion biopsy detected more clinically significant cancers using fewer cores compared with systematic biopsy (median 33%, range 13-50% for fusion biopsy; median 24%, range 5%-52% for systematic biopsy). Fusion biopsy also led to the detection of some clinically significant cancers that would have been missed by standard biopsy alone (median 9%, range 5-16%)[9]. Conversely, Tontilla et al.[10] did not observe any significant improvement in terms of clinically significant cancer detection rate from the use of MRI-TRUS fusion targeted biopsy vs. the extended sextant standard for target selection. However, it is worth noting that of the three operating clinicians in their study (with 5, 10 and 15 years of 2D-TRUS

guided systematic prostate biopsy experience respectively), none had any prior experience with targeted biopsies.

While this work focuses on MRI-TRUS fusion using image registration software, another approach to TRUS-guided biopsy of prostate MRI-defined lesions is "cognitive registration." This approach involves intuitive visual alignment between MRI lesions and TRUS guidance[11]. However, consensus has not yet been reached regarding the superiority of the cognitive vs. software fusion approaches. Two studies reporting that biopsy targeting of clinically significant MRI lesions using cognitive registration resulted in inferior cancer detection rates compared with MRI-TRUS fusion[12,13], while another study found no significant difference in cancer detection rates between the two approaches[14]. Further investigation is warranted, as it may be that small but still clinical significant tumours may benefit more from MRI-TRUS fusion over cognitive registration, compared with larger tumours.

Although fusion biopsy has generally shown increased positive core rates over traditional 2D-TRUS guided systematic biopsy, we believe there is further room for improvement of the method of target selection for this procedure. In particular, this biopsy targeting approach may be further improved by investigating the overall uncertainty in delivering a biopsy needle to intended point target locations *within each 3D contoured lesion*.
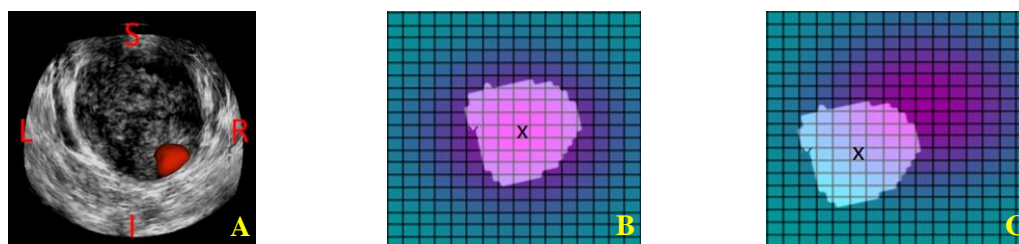
Figure 3-1: (A) A red suspicious region contoured on MRI, registered to 3D TRUS. **(B)** An isotropic Gaussian distribution centreed onto the biopsy target point of a prostate tumour projection. Note that a 2D tumour projection and 2D distribution are used for clarity of illustration; our calculations used 3D tumour volumes and 3D distributions. **(C)** A Gaussian distribution with non-zero systematic error; hence it has been shifted off-centre from the biopsy target point.

There have been two recent studies that provide insight into potential avenues for improving the positive core rate of targeted prostate biopsy. The study by van de Ven et al.[15] estimated the maximum target registration error allowed from MRI-3D TRUS registration for correct Gleason grading of 95% of peripheral zone PCa with fusion biopsy, assuming sphere-shaped tumours. Furthermore, our previous study using radiologist-contoured lesions[16] determined that for a fusion biopsy system with a given needle delivery error, some larger tumours can be sampled with a clinically desired probability (e.g. 95%) in a single biopsy core, and other smaller tumours will require more than one targeted core to achieve the clinically desired probability of sampling the tumour in at least one of the cores taken. The rationale for this perspective is that in principle, *the positive yield of contemporary fusion biopsy systems can be increased by*

optimizing the number and within-tumour placement of targets for each tumour, with consideration given to taking a reasonable number of cores in a practical biopsy scenario. In our previous work[16] and in this work, we have made no assumptions on tumour shape and instead used the shapes of human prostate tumours as contoured by expert readers in 3D using MRI.

Our previous study was intended as a preliminary step toward our goal of increasing the positive yield of fusion prostate biopsy systems, and therefore our experiments were built on a set of assumptions that must be relaxed to more accurately reflect the uncertainties involved in a fusion biopsy procedure. Our previous error model assumed an overall needle delivery error that was isotropic and contained no systematic components. However, both systematic and random errors have been measured in our fusion biopsy system[17], and it is reasonable to consider that such errors could be present in any percutaneous needle delivery device. It is the purpose of this work to relax these assumptions, and investigate the effects of this more complex error model on predicted tumour sampling probabilities. Also, in our previous work[16], we investigated the effect of needle delivery error along the needle axis (henceforth referred to as the axial direction) on the measured tumour burden as determined by percentage core involvement on the pathology report. However, this approach only considered error in the axial direction, and not in either the lateral or elevational directions when estimating the percent core involvement obtained. Therefore, in this work, we investigated the effect of 3D needle delivery error on the probability of successfully sampling a tumour and of obtaining a desired percent core involvement for each biopsy attempt. Lastly, in our previous work

we modeled the tumour centroid as the needle target location for all biopsy attempts. In this work, we investigate a new targeting strategy, henceforth referred to as "ring" targeting, with the intent of compensating for systematic error present in biopsy systems. This targeting strategy is discussed in Section 2.2.3.

Of the sources of error discussed in our previous work, we suspect image registration between preprocedural and intraprocedural imaging to be a substantial contributor to systematic error in biopsy needle placement. A 3D nonrigid MR-TRUS registration method was shown to have a median whole gland target registration error (TRE) of 1.76 mm (range 0.5 – 3.25 mm)[18], while an intersession 3D TRUS-3D TRUS registration method has been shown to have an average whole gland TRE of 2.15 mm (range 0.3 – 5.9 mm)[17]. In this work, we considered systematic errors $\leq$ 6 mm to practically achievable for clinically available MRI-TRUS fusion biopsy systems.

We investigated the following research questions in this chapter. (1) For practically achievable random and systematic error magnitudes associated with fusion biopsy, in what instances does a ring targeting strategy provide a higher probability of obtaining cancer-positive biopsy sample compared to centroid targeting, and vice-versa? (2) In what instances does a ring targeting strategy provide a higher probability of obtaining a 50% core involvement from select tumours compared to centroid targeting, and vice-versa?

3.2 Materials and Methods

3.2.1 Materials

3.2.1.1 Patient characteristics

The study was approved by the research ethics board of our institution, and written informed consent was obtained from all patients prior to enrolment. Images were obtained from 49 patients (mean ± std age: 61.2 ± 7.5 years). Inclusion criteria were: PSA > 4 ng/mL, high clinical suspicion of PCa over prostatitis, and no prior diagnosis of PCa.

3.2.1.2 Imaging

3 Tesla mpMR images (T2W, diffusion weighted and T1W dynamic contrast enhanced) were collected from the patients using a Discovery MR750 (GE Healthcare, Waukesha, WI, USA) with an endorectal coil (Prostate eCoil, Medrad, Inc., Warrendale, PA, USA). On the day of MR imaging, a 3D TRUS image was acquired from each patient using an HDI-5000 ultrasound machine via tracked axial rotation[19] of an end-firing C9-5 5–9 MHz TRUS transducer probe (Philips Medical Systems, Seattle, WA, USA).

3.2.2 Tumour contouring on MRI

All prostate mpMR images were reviewed prior to biopsy by a radiologist (C.R.) and radiology resident (D.C.) to identify any suspicious lesions requiring MRI-TRUS fusion biopsy. Both had 7 years of prostate MRI experience, including assessment of more than 150 prostate MRI studies each. All lesions were manually contoured in the coordinate system of the T2-weighted MRI that was used for MRI-3D TRUS fusion. However, the concern for malignancy was assessed using information from all MR sequences. Particular attention was paid to apparent diffusion coefficient (ADC) findings for lesions located within the peripheral zone. 81 lesions with indeterminate to high suspicion for malignancy were selected for targeted fusion biopsy. Although information from the ADC map was used to help determine the contour delineation, the ADC sequence was not used for fusion with 3D TRUS. This is due to the susceptibility of the diffusion imaging, which makes the ADC map prone to spatial distortion and therefore was not delineated as part of the original MRI-TRUS fusion biopsy study.

The boundaries of these regions were represented in 3D using triangle meshes and were registered into the 3D TRUS context using an iterative closest point prostate surface based registration method[20]; point correspondence was established by mapping each point on the MRI prostate surface to the closest point (in terms of 3D Euclidean distance) on the 3D TRUS prostate surface. The registered triangle meshes were then rasterized to 3D binary images with voxel size <1 mm. These binary images enclose volumes ranging from 0.18 cm^3 to 5.22 cm^3 (mean $\pm$ std volume: 0.81 $\pm$ 0.75 cm^3). These volumes were split into 3 groups, referred to as small tumours (volume < 0.5 cm^3), medium tumours

(0.5 cm^3 < volume < 1 cm^3) and large tumours (volume > 1 cm^3). Table 3-1 shows the

descriptive statistics of tumour sizes for the small, medium and large tumour groups. The

maximum diameter in the lateral-elevational plane was also measured for each tumour,

and the mean values for each tumour group are reported in Table 3-1 (denoted as mean L-

E maximum diameter). All subsequent calculations described in this paper were

performed on these 3D binary images within the 3D TRUS spatial context. In the

description of the methods that follows, a positive tumour sample is defined as an

instance where some portion of the 18 mm long standard biopsy needle core intersects

with the tumour region on the 3D binary image.

Table 3-1: Descriptive statistics of tumour sizes in the three volume groups used in this study.

	Small tumours (Vol ≤ 0.5 cm^3)	Medium tumours (0.5 cm^3 < Vol < 1 cm^3)	Large tumours (Vol ≥ 1 cm^3)
N	35	26	20
Mean volume ± Standard deviation (cm^3)	0.39 ± 0.089	0.66 ± 0.11	1.76 ± 1.02
Max volume (cm^3)	0.50	0.91	5.22
Min volume (cm^3)	0.18	0.51	1.01
Mean L-E maximum diameter ± Standard deviation (cm)	1.09 ± 0.17	1.35 ± 0.16	1.99 ± 0.38
Max L-E maximum diameter (cm)	1.50	1.79	2.82
Min L-E maximum diameter (cm)	0.78	1.10	1.46

3.2.3 Targeting strategies

All simulations for this work were conducted using one of two targeting strategies, described in the following paragraphs.

We tested the centroid targeting strategy (Fig. 3-2A), wherein we simulated targeting the centroid of the tumours for each biopsy attempt. We expected that this approach would produce the best results for simulations with an absence of systematic error.

We also tested a "ring" targeting strategy (Fig. 3-2B) for all simulations that included a non-zero systematic error. In this approach, all targets were selected surrounding the tumour in the lateral-elevational plane, separated by equal arc length around a circle of radius SystMag, concentric to the tumour centroid (Fig. 3-2B), where SystMag is the systematic error magnitude. We selected the first target at a distance of SystMag from the tumour centroid. This target was selected at a random angle θ ($0 \leq \theta < 2\pi$) as measured from patient right. We expected that this approach would produce better results relative to the centroid targeting scheme in the presence of a non-zero systematic error.
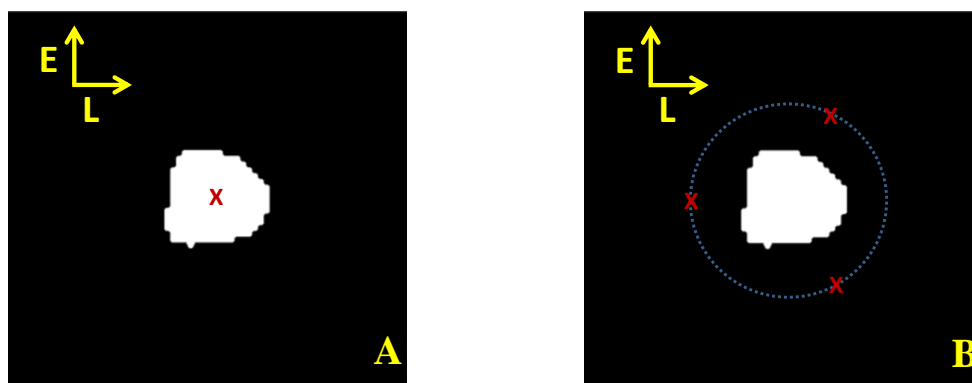
Figure 3-2: **(A)** In the centroid targeting strategy, we modeled the tumour centroid as the biopsy target for each attempt. **(B)** In the ring targeting strategy, we modeled the target locations on a ring in the lateral-elevational plane (shown as L-E above). The ring was centred on the tumour centroid, and its radius was equal to the magnitude of systematic error in the lateral-elevational plane. Targets were spaced at equal arc lengths on the ring. This example shows 3 biopsy attempts.

Figure 3-3 shows the software interface of a 3D MRI-TRUS fusion biopsy system[19], illustrating the biopsy needle in relation to the prostate and two fused MR-defined lesions in both 2D and 3D. The real-time display of 3D fusion biopsy systems such as this one would allow easy incorporation of the two targeting strategies discussed in this section.
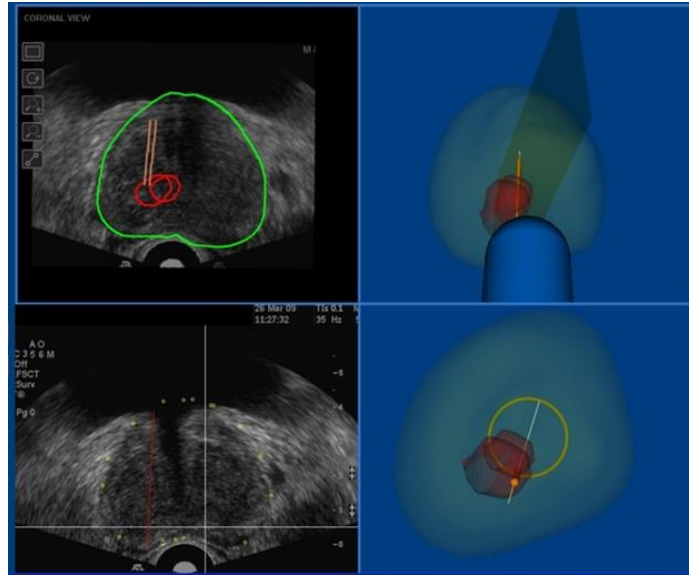
Figure 3-3: The software interface of a 3D MR-TRUS fusion biopsy system.

3.2.4 Description of simulation algorithm

Targets t were selected as described in Section 3.2.3, where the set of targets is denoted $T \subset \mathbb{R}^3$. The isotropic standard deviation σ of the Gaussian distribution modeled the biopsy system's root mean squared needle delivery error (henceforth referred to as RMSE), where RMSE = $|\sigma|$. The mean of the Gaussian distribution g was determined by

$$SystOffset = \begin{pmatrix} \sqrt{\frac{2}{3}} * SystMag * \cos(SystAngle), \\ \sqrt{\frac{2}{3}} * SystMag * \sin(SystAngle), \\ \sqrt{\frac{1}{3}} * SystMag \end{pmatrix}, \qquad (1)$$

where SystAngle is the angle of the systematic error $\in [0,2\pi]$ as measured from the lateral direction (Fig. 3-2) and SystMag is the magnitude of the systematic error. This distribution was centred onto each biopsy target, and

$$g: \mathbb{R}^3 \times T \times \mathbb{R}^3 \times \mathbb{R}^3 \to \mathbb{R},$$

$$g(x, t, SystOffset, \Sigma) = \frac{1}{\sqrt{|\Sigma|(2\pi)^3}} e^{-\frac{1}{2}((x+t)-SystOffset)(\Sigma)^{-1}((x+t)-SystOffset)'}, \quad (2)$$

where $x = [x_1, x_2, x_3]$ represents the spatial coordinates of the distribution and

$$\Sigma = \begin{bmatrix} |\sigma|^2 & 0 & 0 \\ 0 & |\sigma|^2 & 0 \\ 0 & 0 & |\sigma|^2 \end{bmatrix}.$$

The set S contains the points sampled from the Gaussian distribution, each point representing the resultant location of the centre of the biopsy cores after firing the needle at a target, where

$$s: G \to \mathbb{R}^3, \text{ and}$$

$s(g) =$ randomly sampled point from Gaussian distribution g using the accept-reject Monte Carlo sampling method[21].

The set of lesions, L is represented by 3D binary images defined within the domain Ω where 1s indicate tumour tissue, i.e. $\Omega \subset \mathbb{Z}^3$ and

$$l: \Omega \to \{0,1\}.$$

Next, function p determined whether the desired core involvement, c was achieved for each biopsy attempt, as follows

$$p: S \times L \times \mathbb{R}^+ \to \{0,1\} \text{ and}$$

$$p(s, l, c) = \begin{cases} 1 \ if \ sampling \ lesion \ l \ at \ point \ s \ yields \ core \ involvement \geq c \\ 0 \ otherwise \end{cases}. \quad (3)$$

We then defined the function "any core positive," $acp(T, l, SystOffset, RMSE) = \{0,1\}$ to determine whether core involvement $\geq c$ was achieved for any of the biopsy targets contained within set T, as described by the following algorithm.

$P = \{\}$

$for\ i = 1\ to\ |T|$

$\qquad P = \{P\ p(s(g(t_i, SystOffset, RMSE)), l, c)\}$

$end\ for$

$if\ \exists p \in P == 1\ acp = 1, else\ acp = 0$

Finally, we repeated this simulation 1000 times per tumour, and the "positive core fraction" or PCF was evaluated as follows:

$pcf: T \times L \times \mathbb{R}^3 \times \mathbb{R}^3 \rightarrow [0,1]$, where

$pcf(T, l, SystOffset, RMSE) = \frac{1}{1000}\sum_{sim=1}^{1000} acp(T, l, SystOffset, RMSE).$ \qquad (4)

3.2.5 Investigating probability of obtaining a cancer-positive sample

First, we investigated the positive core fraction obtained from each lesion with the goal of obtaining biopsy cores that contain some portion of the lesion tissue, i.e. core involvement > 0 ($c > 0$). We calculated PCF for all 81 lesions, for systematic error magnitude (SystMag) ranging from 1 to 6 mm, and RMSE ranging from 1 to 6 mm. We determined this for both ring and centroid targeting schemes with the number of targets $|T|$ ranging from 2 to 4. We then determined the median PCF across all tumours in the

small, medium and large groups respectively, for each systematic error magnitude and RMSE, and each number of biopsy targets under both targeting schemes. In order to account for varying lesion shapes, we then averaged each of these results over 4 systematic error angles (SystAngle), $\frac{\pi}{4}$, $\frac{3\pi}{4}$, $\frac{5\pi}{4}$ and $\frac{7\pi}{4}$.

3.2.6 Investigating probability of obtaining a 50% core involvement

One common criterion for determining risk stratification for PCa patients is the measure of percent core involvement, or the proportion of the biopsy needle core that contains tumour tissue after obtaining a cancer-positive biopsy sample (in this work we assumed an 18 mm long needle core). Under current guidelines for PCa risk[22,23], a patient's cancer cannot be classified as very low risk when one or more cancer-positive samples are obtained with a ≥ 50% core involvement, even if all other conditions for very low risk disease are satisfied. Therefore, we repeated the process described in Section 3.2.5, but in order to determine the PCF values associated with obtaining a core involvement ≥ 50%. In this experiment, we only used the tumours in our study that were large enough in the axial direction to obtain such a core involvement. Table 3-2 shows the number of tumours in each volume group that are large enough to obtain a 50% core involvement.

Table 3-2: Number of tumours from each volume group large enough to obtain a 50% core involvement.

Tumour volume group	Number of tumours where $\geq$ 50% core involvement is possible
Small (Vol < 0.5 cm^3)	15
Medium (0.5 cm^3 $\leq$ Vol < 1 cm^3)	20
Large (Vol $\geq$ 1 cm^3)	20

3.2.7 Comparing targeting strategies

Both the PCF associated with obtaining a cancer positive sample, and the PCF associated with obtaining a $\geq$ 50% core involvement were calculated for 2 to 4 biopsy attempts ($|T|$), for both targeting strategies and for the small, medium and large tumour groups. The median PCF across all tumours in each group was calculated for each targeting strategy and for both systematic error magnitude (SystMag) and RMSE ranging from 1 to 6 mm. The median PCF observed for the centroid targeting strategy was then plotted alongside the median PCF observed using the ring targeting strategy.

3.3 Results

3.3.1 Probability of a obtaining a cancer positive biopsy sample

Figure 3-4 shows the median PCF of obtaining biopsy cores with core involvement > 0 across all 81 tumours, for both the ring and centroid targeting strategies. Red boxes indicate situations where the ring targeting strategy yields a higher sampling probability, blue boxes indicate instances where centroid targeting has the higher probability, and green indicates no difference. Asterisks indicate a significant difference in sampling probabilities between both targeting strategies as determined by two-sided Wilcoxon signed rank test ($p < 0.05$). For instance, if we observe Fig. 3-4a, for a systematic error of 6 mm and a RMSE of 1 mm, ring targeting provides a tumour sampling probability of 73% while centroid targeting achieves a probability of 52%. Therefore, as $73\% > 52\%$, this box is coloured red to indicate that ring targeting outperforms centroid targeting. Similarly, for a systematic error of 3 mm and RMSE of 6 mm, ring targeting achieves a sampling probability of 74% while we observe a 76% probability under centroid targeting. As $74\% < 76\%$, this box is coloured blue to indicate that centroid targeting outperforms the ring approach in this instance.
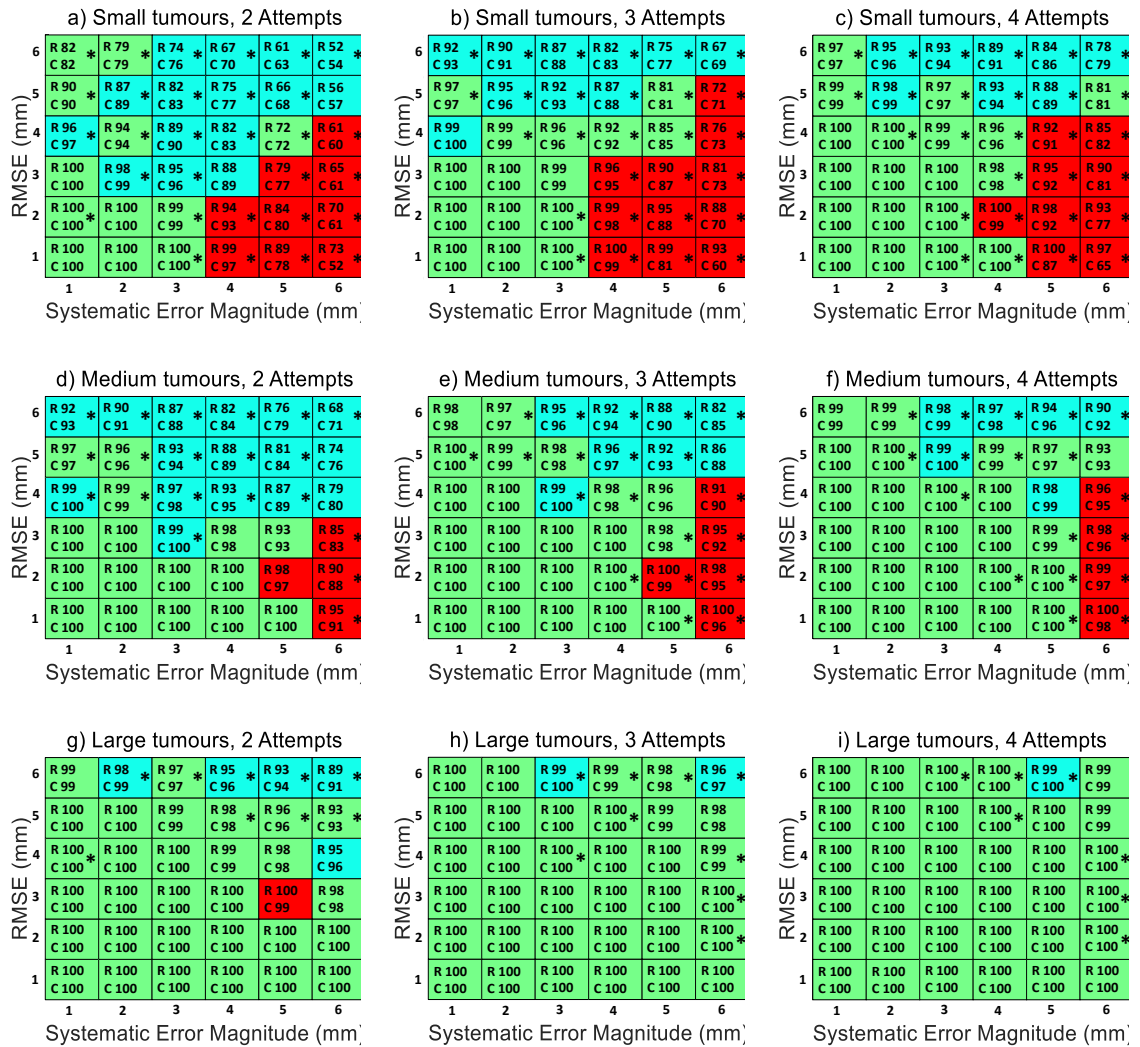
Figure 3-4: Median positive core fraction across all 81 tumours, obtained through ring targeting (R) and centroid targeting (C), given RMSE and systematic error magnitude in mm. Asterisks indicate significant differences (p<0.05).

Fig. 3-5(A-C) highlights a situation where systematic error dominates over random error. These plots show the PCF achieved through both targeting strategies for 2, 3 and 4 biopsy attempts in the situation where Systematic Error Magnitude = 6 mm and RMSE = 2 mm. Conversely, Fig. 3-5(D-F) shows a comparison between the PCF

achieved through both targeting strategies for 2, 3 and 4 biopsy attempts in the situation

where Systematic Error Magnitude = 2 mm and RMSE = 6 mm.
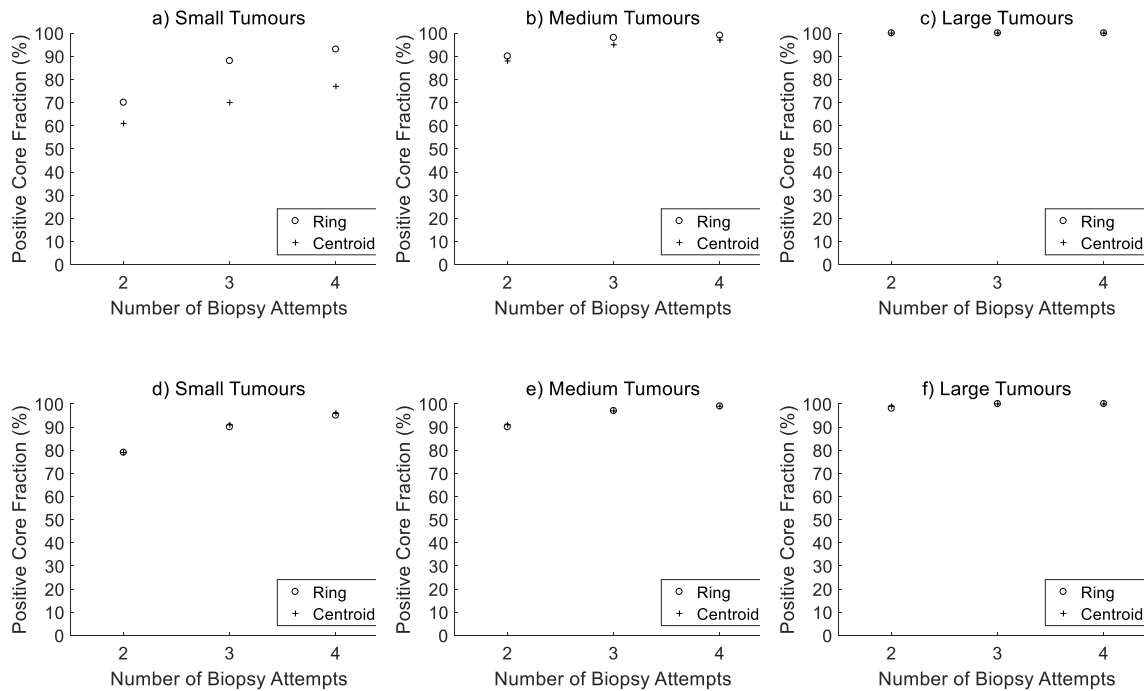
Figure 3-5: PCF achieved through ring targeting and centroid targeting for 2, 3 and 4
biopsy attempts when **a-c)** Systematic Error Magnitude = 6 mm and RMSE = 2 mm and
d-f) Systematic Error Magnitude = 2 mm and RMSE = 6 mm

Lastly, Table 3-3 shows the maximum tumour sampling probability increases achieved

through ring targeting over centroid targeting for each tumour volume group and for 2, 3

and 4 biopsy attempts, followed by the maximum probability increases achieved through

centroid targeting over the ring method.

Table 3-3: Trends observed in tumour sample PCF achieved through ring targeting versus centroid targeting.

	Maximum probability increase achieved by ring over centroid (%)			Maximum probability increase achieved by centroid over ring (%)		
2 Attempts	21	4	1	3	3	2
3 Attempts	33	4	0	2	3	1
4 Attempts	32	2	0	2	2	1
	Small tumours	Medium tumours	Large tumours	Small tumours	Medium tumours	Large tumours

3.3.2 Probability of obtaining a 50% core involvement

Next, the median PCF of biopsy cores containing a 50% core involvement or greater was determined from the tumours in each group that were large enough (in the axial direction) to obtain such a core involvement (55 out of 81 tumours). Again, the median PCF across all 55 tumours was calculated for systematic error and RMSE ranging from 1 to 6 mm (Fig. 3-6). Red boxes indicate situations where the ring targeting strategy yields a higher sampling probability, blue indicates instances where centroid targeting has the higher probability, and green indicates no difference. Asterisks indicate a significant difference in sampling probabilities between both targeting strategies as determined by two-sided Wilcoxon signed rank test ($p < 0.05$).
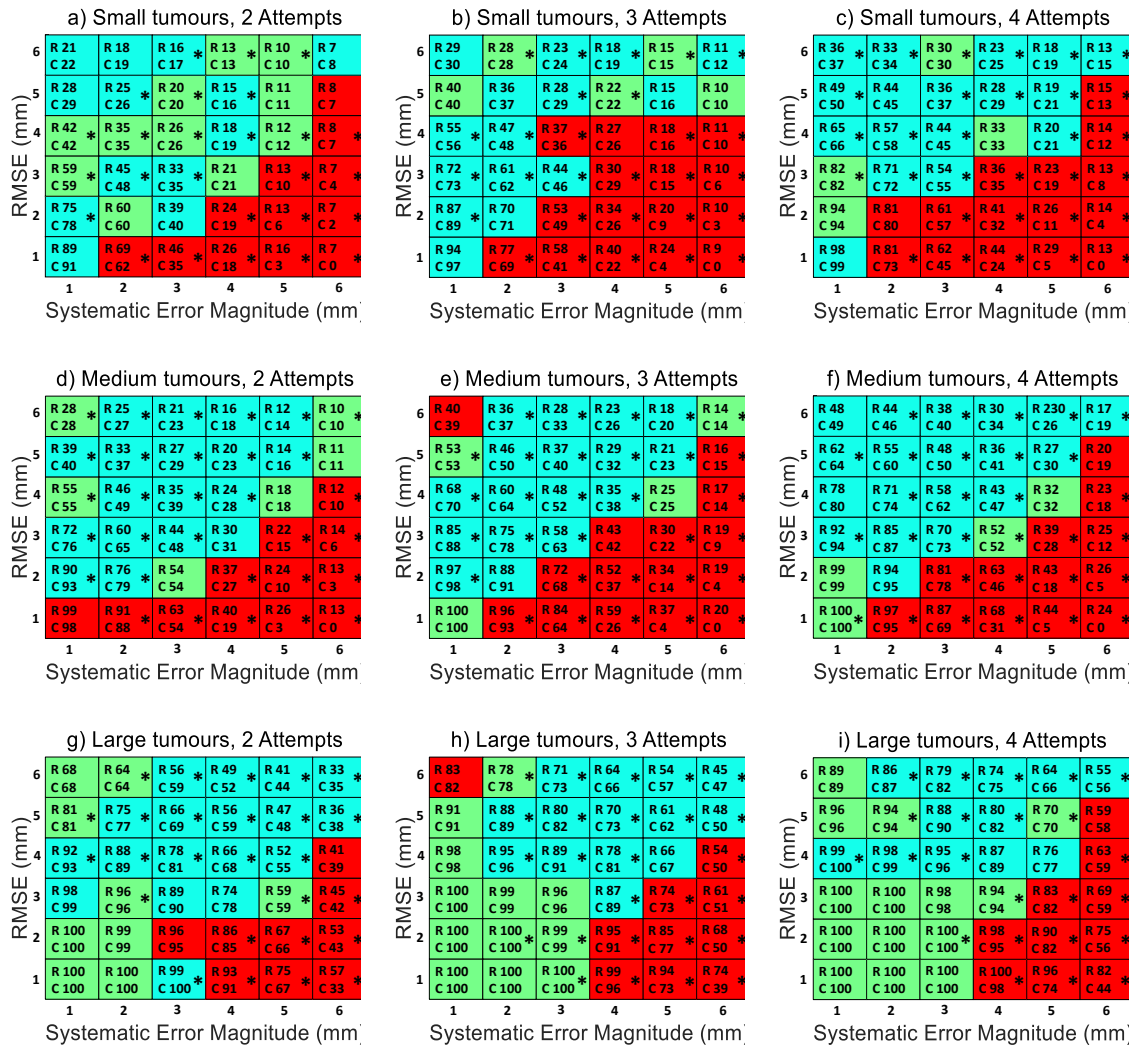
Figure 3-6: Median 50% core involvement Positive Core Fraction across 55 tumours, obtained through both ring targeting (denoted "R") and centroid targeting (denoted "C"), given RMSE and systematic error magnitude in mm. Asterisks indicate significant differences (p<0.05).

Figure 3-7A-C shows a comparison between the 50% core involvement PCF achieved through both targeting strategies for 2, 3 and 4 biopsy attempts in the situation where Systematic Error Magnitude = 2 mm and RMSE = 6 mm.

Figure 3-7D-F shows a comparison between the PCF achieved through both targeting strategies for 2, 3 and 4 biopsy attempts in the situation where Systematic Error Magnitude = 2 mm and RMSE = 6 mm.
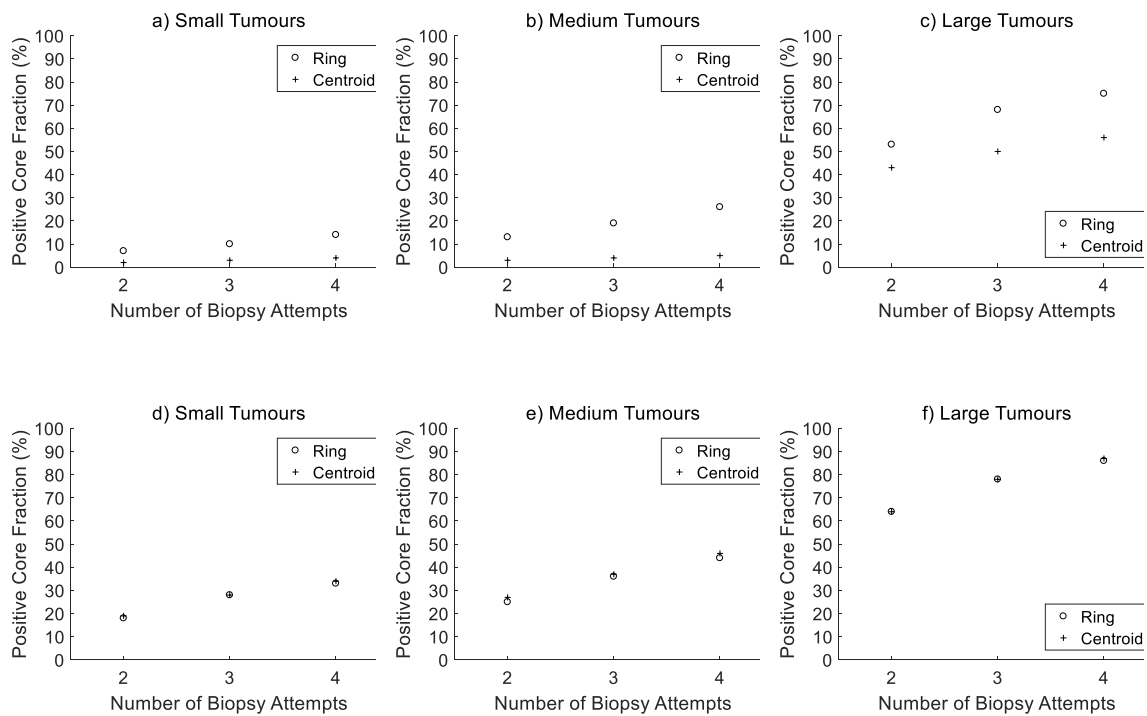

Figure 3-7: PCF of 50% core involvement achieved through ring targeting and centroid targeting for 2, 3 and 4 biopsy attempts when **A-C)** Systematic Error Magnitude = 6 mm and RMSE = 2 mm and **D-F)** Systematic Error Magnitude = 2 mm and RMSE = 6 mm.

Similar to Table 3-3 in Section 3.4.1, Table 3-4 shows the maximum 50% core involvement probability increases achieved through ring targeting over centroid targeting for each tumour volume group and for 2, 3 and 4 biopsy attempts, followed by the maximum probability increases achieved through centroid targeting over the ring method.

Table 3-4: Trends observed in 50% core involvement PCF achieved through ring targeting versus centroid targeting.

	Maximum probability increase achieved by ring over centroid (%)			Maximum probability increase achieved by centroid over ring (%)		
2 Attempts	13	23	24	3	5	3
3 Attempts	20	33	35	3	5	3
4 Attempts	24	39	38	2	5	3
	Small tumours	Medium tumours	Large tumours	Small tumours	Medium tumours	Large tumours

3.4 Discussion

It has been demonstrated that targeted fusion biopsy shows an increase over systematic TRUS-guided biopsy in both cancer-positive core rate and clinically significant cancer detection rate among PCa patients[8,14,24-28], samples more cancer per biopsy core for lesions of low, moderate and high suspicion for PCa[29] and also shows an increase in the cancer detection rate of anterior lesions specifically[26]. However, to the best of our knowledge there exists a gap in research with regards to the effect of within-lesion point targeting strategies coupled with the uncertainty in delivering a biopsy needle to intended target locations within each 3D contoured lesion. We believe this may partially explain the discordance between reported study results; while most studies show an improvement in cancer detection rates through fusion biopsy over standard extended

sextant biopsy, at least one study did not show any improvement[10]. Interestingly, it has also been shown that median prostate volume was significantly higher in patients with negative biopsy results after undergoing fusion biopsy[24] and that the fusion biopsy cancer detection rates decrease with increasing prostate volume[28], indicating that cancer-positive biopsy cores may be more difficult to obtain in patients with larger prostates under the current ad-hoc target selection methods used for fusion biopsies.

We expanded on our previous work[16] by including the presence of systematic error in our error model. Furthermore, we investigated a "ring" targeting strategy with the intention of compensating for a systematic error of known magnitude, but unknown direction. This allowed us to observe which biopsy system error characteristics lead to better performance under ring targeting, and which allow better performance under centroid targeting.

3.4.1 Probability of obtaining a cancer positive biopsy sample

We observed that for small tumours, ring targeting tends to outperform centroid targeting when systematic error magnitude dominates RMSE. This increase in probability becomes larger as we move from 2 to 3 biopsy attempts, but the amount of probability increase levels off between 3 and 4 biopsy attempts (Fig. 3-5a). For medium tumours, this effect is largely reduced. For large tumours, we see virtually no difference in sampling probabilities between the two targeting methods. We expect that this is because tumour sampling probabilities are so high in these instances for medium and large

tumours (PCF $\geq$ 83% for medium tumours when systematic error $\leq$ 6 mm and RMSE $\leq$ 3 mm, and PCF $\geq$ 98% for large tumours over the same error range), that room for improvement between targeting strategies is limited.

When RMSE dominates over systematic error, we generally observed some very modest improvements in PCF ($\leq$ 3%) achieved through centroid targeting over ring targeting for small and medium tumours. For large tumours, the difference was $\leq$ 2%.

For small tumours, substantially larger probability increases were achieved through ring targeting over centroid as opposed to vice-versa. This trend was not observed for medium tumours where the largest difference in PCF between the centroid and ring targeting strategies was 4%, nor was it observed for large tumours where the greatest difference in PCF was 1%.

3.4.2 Probability of obtaining a 50% core involvement

We observed that when systematic error magnitude $\geq$ RMSE for small and medium tumours, ring targeting tends to outperform centroid targeting in terms of PCF of 50% core involvement samples. However, for these small and medium tumours, as systematic error increases to 5 mm and above, this difference between PCF of ring and centroid targeting begins to approach 0. We expect this is because at this level of systematic error, the median probability of obtaining a 50% core involvement approaches 0 for both targeting strategies.

We did not observe this same trend for the large tumour group, as these tumours are large enough such that PCF of 50% core involvement remains >30% for both targeting strategies and for all RMSE and systematic error magnitudes $\leq$ 6 mm. We observe that for large tumours, ring targeting tends to outperform centroid targeting when systematic error magnitude $\geq$ 4 mm and RMSE $\leq$ 2 mm.

As in Section 3.4.1, we generally observed a very modest improvement through centroid targeting over ring targeting in 50% core involvement PCF ($\leq$ 5%) for small, medium and large tumours when RMSE dominates over systematic error. Overall, substantially larger probability increases are achieved through ring targeting over centroid as opposed to vice-versa for small, medium and large tumours.

3.4.3 Clinical relevance

The overall goal of this work was to determine translational lessons that can be quickly incorporated into the workflow of within-lesion target selection for fusion prostate biopsy. We envision that manufacturer-provided error estimates for any MRI targeted, 3D TRUS-guided fusion prostate biopsy system can be used in conjunction with our results in order to allow any physician performing a targeted biopsy to determine which targeting strategy should provide the higher probability of sampling the desired lesion. Therefore, this study highlights the need for manufacturers to provide detailed error information for their biopsy guidance systems, allowing operators to best use their systems.

We believe that additional targeting strategies can continue to be explored in this problem space, including perhaps a combination of centroid and ring targeting in instances where systematic error magnitude does not dominate over RMSE. We also envision that fusion biopsy target locations can be considered in combination with "sextant" systematic biopsy core locations, such that small displacements could be made to existing sextant core locations in order to enable more targeted biopsy attempts with minimal increase in the total number of biopsy cores obtained.

While the core involvement measure investigated in this paper is important for prostate cancer burden estimation under current guidelines for estimating PCa risk[22,23], these guidelines have been developed from the long term results of systematic biopsies. It is worth noting that as more accurate prostate biopsy methods become more widely available, these guidelines may change in order to adapt to new practices.

While this paper represents a first step toward improving the manner in which lesions are targeted using fusion biopsy, a prospective trial will ultimately be needed to determine the improvement in positive yield achieved through optimization of needle target selection. The data presented in this paper could be incorporated into an onboard software module that provides automatic selection of biopsy target locations given the error characteristics of any particular biopsy system. Exploring this possibility is an ongoing focus of our current work.

3.4.4 Limitations

The key limitation of this study is that we used suspicious lesions contoured by radiologists on mpMRI as surrogates for prostatic tumours. Therefore, the lessons taken from our results were reached under the assumption that the radiologist contoured lesions are reflective of true prostate tumour shapes. However, it has been shown that these MR-defined lesions are consistently smaller than the true tumour size as measured on post-prostatectomy histology[30]. Errors introduced in biopsy target selection from these MR-defined lesions may have a substantial effect on cancer detection rates for MRI-TRUS fusion biopsy. Our ongoing work includes the use of digitized radical prostatectomy histology images that have been registered to mpMRI, allowing us to investigate this further.

It should be noted that only contoured lesions that were selected for targeted biopsy were included in this study, with no preference toward regions of high suspicion of aggressive tumour biology. However, while contouring was performed in the coordinate system of the T2W images, apparent diffusion coefficient (ADC) maps obtained from diffusion weighted MR were also assessed for tumour aggressiveness and this information was considered in deciding whether to target lesions.

3.5 Conclusions

In this work, we developed a biopsy simulator for determining biopsy sampling probabilities on 3D tumours in a 3D TRUS-guided fusion biopsy context. We expanded

on our previous work by including the presence of systematic error in our error model. Furthermore, we investigated a "ring" targeting strategy with the intention of compensating for a systematic error of known magnitude, but unknown direction. Our results suggest that the optimal targeting scheme for prostate biopsy depends on the relative levels of systematic and random errors in the system. Where systematic error dominates, a ring targeting scheme may yield improved probability of tumour sampling, particularly for small tumours. We envision that the data presented in this paper can be used to aid in target selection strategies for clinicians performing targeted prostate biopsies on any MRI targeted, 3D TRUS-guided biopsy system.

References

[1]   D.F. Gleason, "Classification of prostatic carcinomas," Cancer Chemotherapy Reports **50**(3), 125-128 (1966).

[2]   H. Singh, E.I. Canto, S.F. Shariat, D. Kadmon, B.J. Miles, T.M. Wheeler and K.M. Slawin, "Predictors of prostate cancer after initial negative systematic 12 core biopsy," Urology **171**(5), 1850-1854 (2004).

[3]   A.V. Taira, G.S. Merrick, R.W. Galbreath, H. Andreini, W. Taubenslag, R. Curtis, W.M. Butler, E. Adamovich and K.E. Wallner, "Performance of transperineal template-guided mapping biopsy in detecting prostate cancer in the initial and repeat biopsy setting," Prostate Cancer and Prostatic Diseases **13**(1), 71-77 (2010).

[4]   A. Rajinikanth, M. Manoharan, C.T. Soloway, F.J. Civantos and M.S. Soloway, "Trends in Gleason score: concordance between biopsy and prostatectomy over 15 years," Urology **72**(1), 177-182 (2008).

[5]   L. Klotz, D. Vesprini, P. Sethukavalan, V. Jethava, L. Zhang, S. Jain, T. Yamamoto, A. Mamedov and A. Loblaw, "Long-term follow-up of a large active surveillance cohort of patients with prostate cancer," Journal of Clinical Oncology **33**(3), 272-277 (2015).

[6]   J.J. Tosoian, M. Mamawala, J.I. Epstein, P. Landis, S. Wolf, B.J. Trock and H.B. Carter, "Intermediate and longer-term outcomes from a prospective active-surveillance program for favorable-risk prostate cancer," Journal of Clinical Oncology **33**(30), 3379-3385 (2015).

[7]   J.J. Futterer, S.W. Heijmink, T.W. Scheenen, J. Veltman, H.J. Huisman, P. Vos, C.A. Hulsbergen-van de Kaa, J.A. Witjes, P.F. Krabbe, A. Heerschap and J.O. Barentsz, "Prostate cancer localization with dynamic contrast-enhanced MR imaging and proton MR spectroscopic imaging," Radiology **241**(2), 449-458 (2006).

[8]   D.W. Cool, J. Bax, C. Romagnoli, A.D. Ward, L. Gardi, V. Karnik, J. Izawa, J. Chin and A. Fenster, "Fusion of MRI to 3D TRUS for mechanically-assisted targeted prostate biopsy: system design and initial clinical experience," Lecture Notes in Computer Science **6963**, 121-133 (2011).

[9]   M. Valerio, I. Donaldson, M. Emberton, B. Ehdaie, B.A. Hadaschik, L.S. Marks, P. Mozer, A.R. Rastinehad, H.U. Ahmed, "Detection of clinically significant prostate cancer using magnetic resonance imaging-ultrasound fusion targeted biopsy: a systematic review," European Urology **68**(1), 8-19 (2015).

10   P.P. Tonttila, J. Lantto, E. Paakko, U. Piippo, S. Kauppila, E. Lammentausta, P. Ohtonen and M.H. Vaarala, "Prebiopsy multiparametric magnetic resonance imaging for prostate cancer diagnosis in biopsy-naive men with suspected prostate cancer based on elevated prostate-specific antigen values: results from a randomized prospective blinded controlled trial," European Urology **69**(3), 419-425 (2016).

11   B.K. Park, J.W. Park, S.Y. Park, C.K. Kim, H.M. Lee, S.S. Jeon, S.I. Seo, B.C. Jeong and H.Y. Choi, "Prospective evaluation of 3-T MRI performed before initial transrectal ultrasound-guided prostate biopsy in patients with high prostate-specific antigen and no previous biopsy," AJR: American Journal of Roentgenology **197**(5), W876-881 (2011).

12   D.W. Cool, X. Zhang, C. Romagnoli, J.I. Izawa, W.M. Romano and A. Fenster, "Evaluation of MRI-TRUS fusion versus cognitive registration accuracy for MRI-targeted, TRUS-guided prostate biopsy," AJR: American Journal of Roentgenology **204**(1), 83-91 (2015).

13   N.B. Delongchamps, M. Peyromaure, A. Schull, F. Beuvon, N. Bouazza, T. Flam, M. Zerbib, N. Muradyan, P. Legman and F. Cornud, "Prebiopsy magnetic resonance imaging and prostate cancer detection: comparison of random and targeted biopsies," Urology **189**(2), 493-499 (2013).

14   P. Puech, O. Rouviere, R. Renard-Penna, A. Villers, P. Devos, M. Colombel, M.O. Bitker, X. Leroy, F. Mege-Lechevallier, E. Comperat, A. Ouzzane and L. Lemaitre, "Prostate cancer diagnosis: multiparametric MR-targeted biopsy with cognitive and transrectal US-MR fusion guidance versus systematic biopsy--prospective multicentre study," Radiology **268**(2), 461-469 (2013).

15   W.J. van de Ven, C.A. Hulsbergen-van de Kaa, T. Hambrock, J.O. Barentsz and H.J. Huisman, "Simulated required accuracy of image registration tools for targeting high-grade cancer components with prostate biopsies," European Radiology **23**(5), 1401-1407 (2013).

16   P.R. Martin, D.W. Cool, C. Romagnoli, A. Fenster and A.D. Ward, "Magnetic resonance imaging-targeted, 3D transrectal ultrasound-guided fusion biopsy for prostate cancer: quantifying the impact of needle delivery error on diagnosis," Medical Physics **41**(7), 073504 (2014).

17   V.V. Karnik, A. Fenster, J. Bax, C. Romagnoli and A.D. Ward, "Evaluation of intersession 3D-TRUS to 3D-TRUS image registration for repeat prostate biopsies," Medical Physics **38**(4), 1832-1843 (2011).

18   Y. Sun, J. Yuan, W. Qiu, M. Rajchl, C. Romagnoli and A. Fenster, "Three-dimensional nonrigid MR-TRUS registration using dual optimization," IEEE Transactions on Medical Imaging **34**(5), 1085-1095 (2015).

19   J. Bax, D. Cool, L. Gardi, K. Knight, D. Smith, J. Montreuil, S. Sherebrin, C. Romagnoli and A. Fenster, "Mechanically assisted 3D ultrasound guided prostate biopsy system," Medical Physics **35**(12), 5397-5410 (2008).

20   P.J. Besl and N.D. Mckay, "A method for registration of 3-D shapes," IEEE Transactions on Pattern Analysis and Machine Intelligence **14**(2), 239-256 (1992).

21   G. Casella, C.P. Robert, M.T. Wells, "Generalized accept-reject sampling schemes," Institute of Mathematical Statistics Lecture Notes - Monograph Series **45**, 327-347 (2004).

22   National Comprehensive Cancer Network Clinical Practice Guidelines in Oncology: Prostate Cancer (2017).

23   Clinically Localized Prostate Cancer: AUA/ASTRO/SUO Guideline (2017).

24   M.C. Roethke, T.H. Kuru, S. Schultze, D. Tichy, A. Kopp-Schneider, M. Fenchel, H.P. Schlemmer, B.A. Hadaschik, "Evaluation of the ESUR PI-RADS scoring system for multiparametric MRI of the prostate with targeted MR/TRUS fusion-guided biopsy at 3.0 Tesla," European Radiology **24**(2), 344-352 (2014).

25   S. Natarajan, L.S. Marks, D.J. Margolis, J. Huang, M.L. Macairan, P. Lieu and A. Fenster, "Clinical application of a 3D ultrasound-guided prostate biopsy system," Urologic Oncology **29**(3), 334-342 (2011).

26   D. Volkin, B. Turkbey, A.N. Hoang, S. Rais-Bahrami, N. Yerram, A. Walton-Diaz, J.W. Nix, B.J. Wood, P.L. Choyke and P.A. Pinto, "Multiparametric magnetic resonance imaging (MRI) and subsequent MRI/ultrasonography fusion-guided biopsy increase the detection of anteriorly located prostate cancers," BJU International **114**(6b), E43-E49 (2014).

27   M.M. Siddiqui, S. Rais-Bahrami, H. Truong, L. Stamatakis, S. Vourganti, K. Nix, A.N. Hoang, A. Walton-Diaz, B. Shuch, M. Weintraub, K. Kruecker, H. Amalou, B. Turkbey, M.J. Merino, P.L. Choyke, B.J. Wood and P.A. Pinto, "Magnetic resonance imaging/ultrasound-fusion biopsy significantly upgrades prostate cancer versus systematic 12-core transrectal ultrasound biopsy," European Urology **64**(5), 713-719 (2013).

28   A. Walton Diaz, A.N. Hoang, B. Turkbey, C.W. Hong, H. Truong, T. Sterling, S. Rais-Bahrami, M.M. Siddiqui, L. Stamatakis, S. Vourganti, J. Nix, J. Logan, C. Harris, M. Weintraub, C. Chua, M.J. Merino, P. Choyke, B.J. Wood and P.A. Pinto, "Can magnetic resonance-ultrasound fusion biopsy improve cancer detection in enlarged prostates?," Urology **190**(6), 2020-2025 (2013).

29   P.A. Pinto, P.H. Chung, A.R. Rastinehad, A.A. Baccala, J. Kruecker, C.J. Benjamin, S. Xu, P. Yan, S. Kadoury, C. Chua, J.K. Locklin, B. Turkbey, J.H. Shih, S.P. Gates, C. Buckner, G. Bratslavsky, W.M. Linehan, N.D. Glossop, P.L. Choyke and B.J. Wood, "Magnetic resonance imaging/ultrasound fusion guided prostate biopsy improves cancer detection following transrectal ultrasound biopsy and correlates with multiparametric magnetic resonance imaging," Urology **186**(4), 1281-1285 (2011).

30   E. Gibson, G.S. Bauman, C. Romagnoli, D.W. Cool, M. Bastian-Jordan, Z. Kassam, M. Gaed, M. Moussa, J.A. Gomez, S.E. Pautler, J.L. Chin, C. Crukley, M.A. Haider, A. Fenster and A.D Ward, "Toward prostate cancer contouring guidelines on magnetic resonance imaging: dominant lesion gross and clinical target volume coverage via accurate histology fusion," International Journal of Radiation Oncology, Biology, Physics **96**(1), 188-196 (2016).

Chapter 4

4 Investigating the impact of prostate biopsy needle delivery error on pathologic cancer risk assessment[*]

4.1 Introduction

2D transrectal ultrasound (TRUS)-guided biopsy is the clinical standard for prostate cancer (PCa) diagnosis. As PCa is often not detectable on ultrasound, a systematic extended-sextant targeting scheme is used for needle guidance, involving 6 to 12 tissue samples (cores) obtained via biopsy. However, this procedure has a false negative rate of 21–47% and many patients require repeat biopsies[1,2]. Additionally, this biopsy method has been shown to misrepresent the true Gleason score of a patient's cancer[3]. While augmented approaches for systematic template biopsy have been proposed[4], multiparametric MRI (mpMRI) is an accepted tool for PCa detection and localization[5,6], which allows for a targeted biopsy approach. Therefore, MRI-targeted, 3D TRUS-guided "fusion" biopsy systems have been developed to allow for magnetic

---

[*]This chapter is adapted from the manuscript entitled "Investigating the impact of prostate biopsy guidance error on pathologic cancer risk assessment" by P.R. Martin et al., *SPIE Journal of Medical Imaging* (under review).

resonance imaging targeting via image registration. One specific fusion biopsy system[7] has shown improved positive core rates of 30.4% (compared to 7.1% for 2D TRUS) and 42.3% (compared to 25.6% for 2D TRUS) for moderate and highly suspicious lesions, respectively[8]. Furthermore, a systematic review of 14 papers comparing fusion biopsy with 2D TRUS-guided systematic biopsy found that the use of fusion biopsy led to the detection of more clinically significant cancers using fewer biopsy cores when compared with 2D TRUS-guided systematic biopsy[9]. There has been one study where the authors did not observe a significant increase in the clinically significant cancer detection rate when performing fusion biopsy compared with systematic biopsy; however, none of the three clinicians participating in this study (with 5, 10 and 15 years of 2D TRUS-guided systematic biopsy experience, respectively) had prior experience with performing targeted biopsies[10].

Although fusion biopsy has led to increased positive core rates, there may be further room for improvement of the method for target selection in this procedure. Our previous work showed that an improved positive core rate could be obtained by optimizing the number of samples taken from each target, according to lesion size and shape, and the error characteristics of the biopsy system[11,12]. We showed that if one can determine the number of core samples required for each tumour in a practical biopsy scenario (within a reasonable limit for the number of biopsy cores), the positive yield of contemporary fusion biopsy systems could be increased by optimizing the number of biopsy attempts for each suspicious lesion. However, accurate characterization of a patient's prostate cancer depends not only on the presence of cancer in the biopsy sample,

but critically also on the proportion of cancer contained in each biopsy core (referred to as the "percent core involvement")[13,14] and the presence of high-grade cancer in the cores. There is evidence of a relationship between the apparent diffusion coefficient (ADC) values on prostate MRI and Gleason grade[15,16]; suggesting a benefit to targeting biopsy using ADC to maximize the yield of high-grade cancer, if present. Previous work in this field has estimated the necessary biopsy accuracy for targeting regions of ADC maps suspected to harbor high-grade cancer[17].

Although strides have been made toward understanding how to optimize biopsy targeting in these previous studies[11,12,17], an important limitation is that MRI-defined regions of suspicion were used as biopsy simulation targets, without histologic confirmation of the core involvements and high-grade cancer yield resulting from biopsy simulation. In this work, we address this by using histologically confirmed PCa tumours as contoured on digital histology images by genitourinary pathologists to conduct biopsy simulations and report core involvement and high-grade cancer yield as a function of biopsy system error. By using histology image contours to define tumour targeting, this work models idealized tumour targeting, wherein boundary delineation on the planning image is exactly concordant with lesions on histopathology. Results from our simulations thus represent a best-case scenario, since lesions contoured by experts on MRI are generally not volumetrically concordant with true histologic lesions[18,19]. As histology slices are inherently 2D and oriented approximately axially, our simulations were conducted in 2D under the assumption that prostate tumour size and shape are invariant

to slicing angle. This is a necessary compromise to reap the benefits of the enhanced core involvement and grade information provided by histology imaging, compared to MRI.

We investigated the following research questions in this paper: (1) What is the relationship between needle delivery error and percent core involvement, for lesions of all Gleason grades, and for high-grade lesions? (2) What is the relationship between needle delivery error and proportion of biopsy attempts that miss the target for lesions of all Gleason grades, and for high-grade lesions? (3) What is the relationship between the number of biopsy attempts made on each tumour target, and the probability of successfully obtaining a tumour sample in at least one of the attempts?

4.2 Materials

4.2.1 Patient characteristics

52 specimens were obtained after radical prostatectomy. Inclusion criteria: patient age ≥18 years, histologically confirmed clinical PCa stage T1 or T2, and ≥ 1 tumour focus with maximum diameter ≥ 5 mm. Exclusion criteria: prior PCa therapy, use of 5-alpha reductase inhibitors within 6 months of study start, contrast agent allergy, sickle cell/other anemias, hip prosthesis, inability to comply with imaging, pelvic sources of artifacts, and MRI contraindications.

4.2.2 Digital histology imaging and contouring

After standard whole-mount paraffin embedding, 4 μm thick sections were cut from the prostate midgland and stained with hematoxylin and eosin. The slides were digitized at 0.5 μm/pixel on a ScanScope GL (Aperio Technologies, Vista, CA) scanner. PCa was contoured by a physician trained in PCa morphology with contouring confirmed by a genitourinary pathologist (Fig. 4-1). PCa foci of different Gleason scores were differentiated from one another based on contour colour.
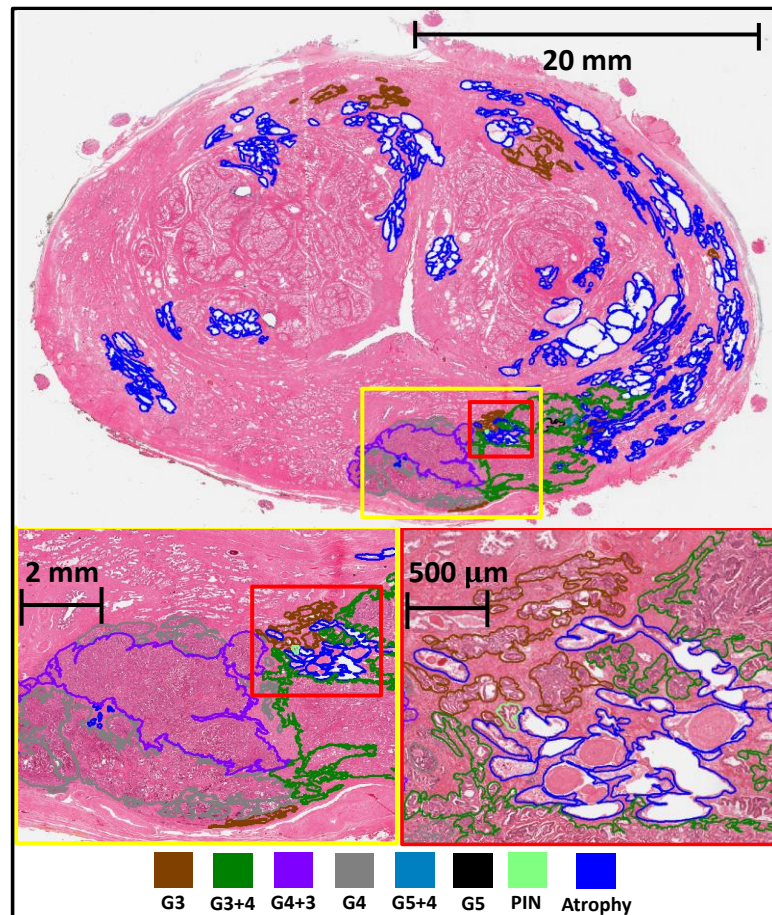

Figure 4-1: Illustrating the level of detail used for histopathology contours in this study.

4.3 Methods

4.3.1 Image preparation for simulation

All contour masks were downsampled to a 30 μm isotropic pixel size. We extracted regions containing cancer of all Gleason grades (Fig. 4-2B), and regions containing only high-grade cancer (Gleason 4+3 and above; Fig. 4-2C). Dilation and erosion with a 600 μm square structuring element was performed on each mask to connect nearby foci, followed by hole filling (Fig. 4-2D). Resulting foci with maximum diameter ≥ 5 mm were retained (after applying a 1.047 linear correction to each diameter to adjust for shrinkage due to formalin fixation[20]). This captures all clinically significant tumours that may be plausibly visible on MRI. This yielded 307 foci of all Gleason grades, and 75 high grade foci. Descriptive statistics of foci sizes for both groups are given in Table 4-1, where the diameter measure refers to the maximum length of each lesion.
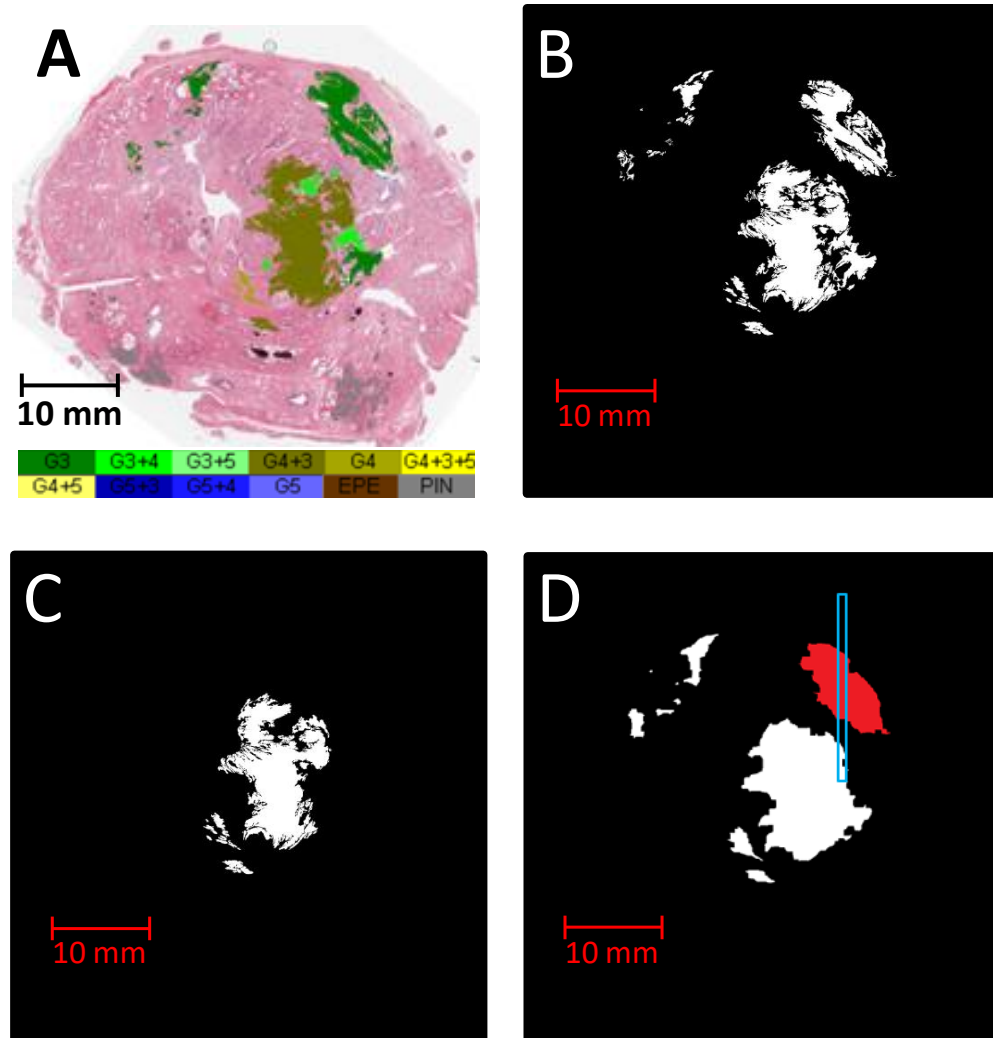
Figure 4-2: (A) Image showing the prostate with contoured regions overlaid. **(B)** Binary image of showing cancer of all Gleason grades. **(C)** High grade cancer only. **(D)** After defining overall foci from the fine-scale contours in Fig 4-2B; with a blue simulated biopsy core overlaid onto a red target tumour. Note that this core contains cancer from the targeted tumour, and also from the posterior tumour that was not targeted.

Table 4-1: Descriptive statistics of foci sizes in all grade and high grade groups.

	All grade lesions	High grade lesions
N	307	75
Mean surface area $\pm$ Standard deviation (mm^2)	68.6 $\pm$ 138.2	108.6 $\pm$ 234.0
Max surface area (mm^2)	1309.0	1309.0
Min surface area (mm^2)	5.6	5.9
Mean diameter $\pm$ Standard deviation (mm)	14.0 $\pm$ 9.1	14.8 $\pm$ 12.1
Max diameter (mm)	56.3	56.3
Min diameter (mm)	5.1	5.3

4.3.2 Biopsy simulation

We modeled the biopsy system's root mean squared needle delivery error (RMSE) using a 2D Gaussian distribution with $\mu = [0,0]$ and an isotropic 2D σ. The magnitude of σ modeled the RMSE in delivering the centre of the needle core to a target location. All simulations were performed using our in-house biopsy simulation platform described in Chapter 3,[12] adapted to run on the 2D histology images used in this study. For each simulation, the centroid of the tumour was chosen as the biopsy target and the

biopsy needle was oriented in the posteroanterior direction (approximating a transrectal approach). The simulated final location of the biopsy needle centre was determined by a random offset from the target, drawn from the Gaussian distribution corresponding to the chosen RMSE. The angle of the needle was held constant. The contents of the 18 mm long biopsy core were then recorded for each of 1000 simulations per target.

4.3.3 Experiments

We conducted three experiments to address the research questions (enumerated as in the Introduction).

(1) *Relationship of needle delivery error and percent core involvement:* We simulated biopsy on the 307 tumour foci containing all Gleason grades, for RMSE = 1 to 6 mm, with one biopsy attempt per tumour. For each tumour at each RMSE level, this yielded 1,000 core length values between 0 mm and 18 mm, representing the amount of cancer found in the simulated core. We subtracted the 5th percentile core length from the 95th percentile core length to obtain a nonparametric measure of variability in core length across the 1,000 simulated biopsies (henceforth the *5–95 percentile core involvement range*). We performed the same simulation on the 75 tumour foci containing only high-grade cancer.

(2) *Relationship between needle delivery error and proportion of biopsy attempts that miss the target:* We used the core involvement data obtained from Experiment 1 to

calculate the proportion of biopsy cores from each 1,000-simulation run that entirely missed each tumour (i.e., core involvement of 0 mm). This was performed for the group of tumours of all grades and the high-grade tumour group, for RMSE = 1 to 6 mm and one biopsy attempt per tumour.

(3) *Relationship between the number of biopsy attempts and the probability of obtaining a tumour sample:* We used the procedure described in Experiment 1 to simulate 1, 2, and 3 biopsy attempts on each of the lesions in the all-grade tumour group, as well as the high-grade only tumours. We calculated the proportion of the 1,000 simulations per tumour that resulted in a cancer positive sample, for RMSE = 1 to 6 mm.

4.4 Results

4.4.1 Experiment 1 – Relationship of needle delivery error and percent core involvement

Fig. 4-3A and 4-3B show the 5–95 percentile core involvement ranges as a function of RMSE for the groups of all Gleason grade lesions and high-grade lesions, respectively. All median 5–95 percentile core involvement values in Fig. 4-3A are significantly different from each other ($p < 0.05$; Wilcoxon signed rank test). Furthermore, all medians in Fig. 4-3B are significantly different from each other ($p < 0.05$; Wilcoxon signed rank test). Significant differences were also detected between the

5–95 percentile core involvement values for lesions of all grades (Fig. 4-3A) and high-grade lesions (Fig. 4-3B) at corresponding RMSE values when RMSE $\geq$ 4 mm ($p < 0.05$; Wilcoxon rank sum test); the median 5–95 percentile core involvement values were higher for high-grade lesions. When RMSE $\leq$ 3 mm, there were no significant differences observed between lesions of all grades and high grade lesions ($p > 0.05$; Wilcoxon rank sum test). For Fig. 4-3A, Pearson correlation coefficients showed a positive correlation ($0.15 \leq \sigma \leq 0.44$, $p < 0.05$) between the 5–95 percentile core involvement and tumour diameter for RMSE $\geq$ 4 mm, with no significant correlations for RMSE $\leq$ 3 mm. For Fig. 4-3B, we observed a significant positive Pearson correlation ($0.25 \leq \sigma \leq 0.40$, $p < 0.05$) between the 5–95 percentile core involvement and tumour diameter for RMSE $\geq$ 5 mm, with no significant correlations for RMSE $\leq$ 4 mm.
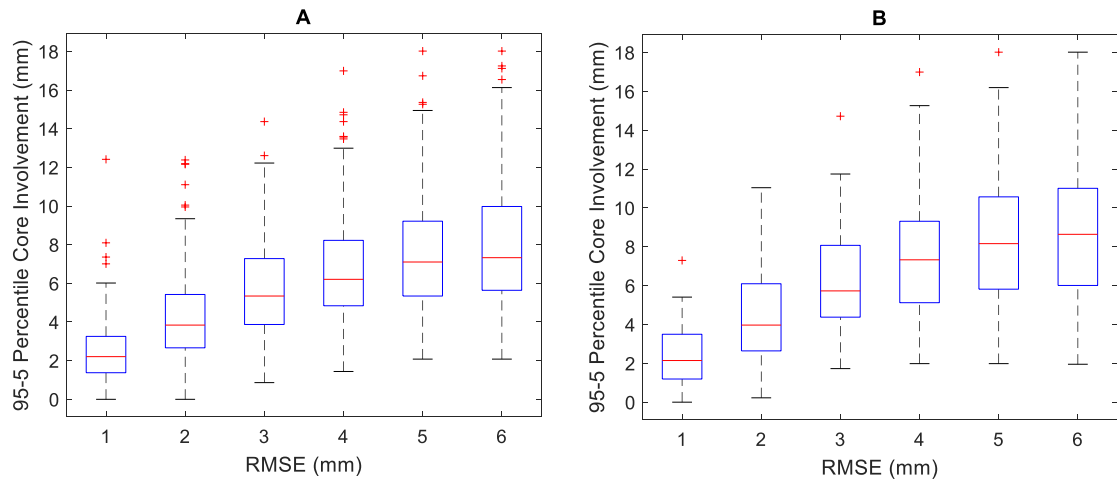
Figure 4-3: 95–5 percentile core involvement range values, for RMSE = 1 to 6 mm, calculated for **(A)** lesions of all Gleason grades and **(B)** high-grade lesions. Whiskers indicate the largest and smallest values within [median, median + (1.5 × inter-quartile range)] and [median – (1.5 × inter-quartile range), median] respectively, while red glyphs indicate outliers outside of this range.

4.4.2 Experiment 2 – Relationship between needle delivery error and proportion of biopsy attempts that miss the target

Figs. 4-4A and 4-4B show the proportion of tumour misses per 1,000 simulations as a function of RMSE for the group of all Gleason grade lesions and high-grade lesions, respectively. All median proportions of tumour misses in Fig. 4-4A are significantly different from each other ($p < 0.05$; Wilcoxon signed rank test). This is also true for the medians in Fig. 4-4B ($p < 0.05$; Wilcoxon signed rank test). However, there were no significant differences detected between the proportions of tumour misses for all-grade

(Fig. 4-3A) and high-grade (Fig. 4-3B) lesions at corresponding RMSE levels ($p > 0.05$; Wilcoxon rank sum test). For Fig. 4-4A, Pearson correlation coefficients showed a negative correlation ($-0.63 < \sigma < -0.17$, $p < 0.05$) between tumour diameter and proportion of missed biopsy attempts for all levels of RMSE. For Fig. 4-4B, Pearson correlation coefficients showed a negative correlation ($-0.65 < \sigma < -0.30$, $p < 0.05$) between tumour diameter and proportion of missed biopsies for all levels of RMSE, with the exception of RMSE = 1 mm where no significant correlation was observed.
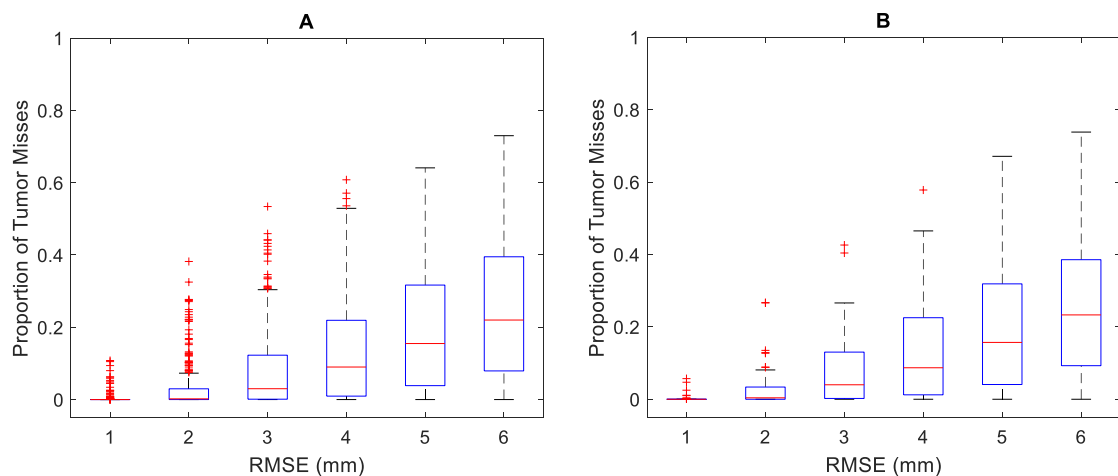

Figure 4-4: The proportion of tumour misses per 1000 simulations calculated for **(A)** all Gleason grade and **(B)** high-grade lesions. Whiskers indicate the largest and smallest values within [median, median + (1.5 × inter-quartile range)] and [median – (1.5 × inter-quartile range), median] respectively, while red glyphs indicate outliers outside of this range.

4.4.3 Experiment 3 – Relationship between number of biopsy attempts and probability of a tumour sample

Fig. 4-5 shows the percentages of cancer-positive cores as a function of RMSE, for 1–3 biopsy attempts. Fig. 4-5A shows these results for 307 lesions of all Gleason grades, where the median percentages of positive tumour samples for one, two and three attempts are all significantly different ($p < 0.05$, Wilcoxon signed rank test). Fig. 4-5B shows results for the 75 high-grade lesions, and again the median percentages of positive tumour samples for one, two and three attempts are all significantly different ($p < 0.05$, Wilcoxon signed rank test), with the exception of the median sampling percentages for two and three biopsy attempts when RMSE = 1 mm. Furthermore, no significant differences were observed between the proportions of positive samples for one, two and three biopsy attempts on all-grade and high-grade lesions at corresponding RMSE levels ($p > 0.05$; Wilcoxon rank sum test).
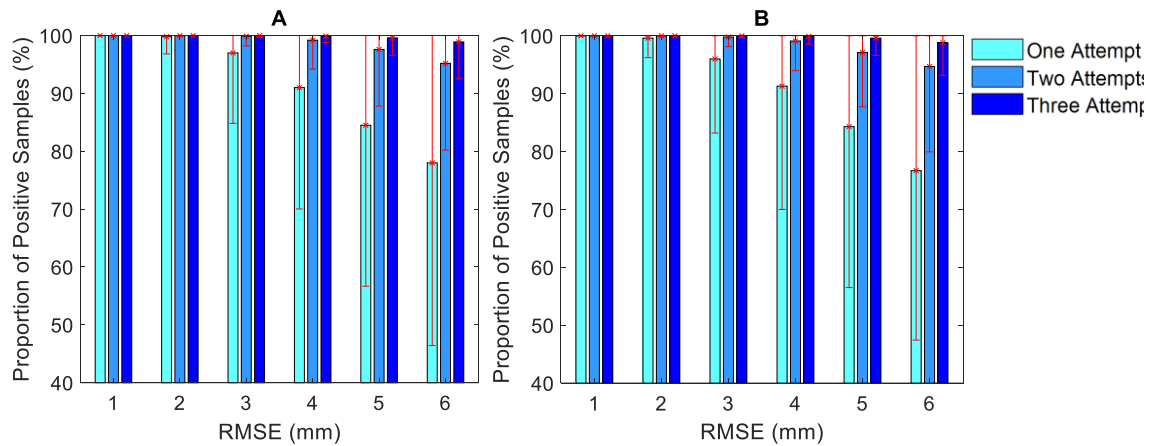
Figure 4-5: The median ± interquartile range rate of cancer positive samples per 1000 biopsy simulations, for **(A)** 307 lesions of all Gleason grades and **(B)** 75 high-grade lesions, as a function of RMSE for one, two and three biopsy attempts.

4.5 Discussion

4.5.1 Experiment 1 – Relationship of needle delivery error and percent core involvement

We observed that different needle delivery errors have different levels of impact on the variability in observed core involvement (Fig. 4-3A), with the greatest changes occurring between a RMSE of 1 mm and 4 mm. At an RMSE = 4 mm (as has been observed in practice[11]), we observed a median 95–5 percentile core involvement range of 6.2 mm for each biopsy attempt, with a maximum value of 17.0 mm. Considering a typical total core length of 18 mm, this median range of variability constitutes more than

1/3 of a full 18 mm long prostate biopsy core. This observation is important in the context of the use of percent core involvement as a means for determining appropriateness of active surveillance[13,14]; the same patient could have very different percent core involvement values from biopsies taken in immediate succession, even with biopsies aimed at the same tumour targets. These differences could be large enough to influence the decision of active surveillance vs. definitive treatment[14]. For high-grade tumours (Fig. 4-3B), we observed a similar pattern with a median 5–95 percentile core involvement range of 7.3 mm at RMSE = 4 mm, with a maximum value of 17.0 mm.

Based on our observation of a positive correlation between the 95–5 percentile core involvement range and tumour diameter reported in Section 4.4.1, this implies greater variability in core involvement arising from needle delivery error for larger tumours. Although this may seem counterintuitive (as larger tumours should be easier to hit), because an on-target biopsy of a large tumour yields a longer core length than for a small tumour, there is a greater potential range of core involvement lengths for large tumours.

Comparing Fig. 4-3A to Fig. 4-3B, we did observe significant differences between all- and high-grade tumours for this measurement when RMSE ≥ 4 mm. For lesions of all grades, we observed median 95–5 percentile core involvement values of 6.2, 7.1 and 7.3 mm, and maximum values of 17.0, 18.0 and 18.0 mm, for RMSE values of 4, 5 and 6 mm respectively. Likewise for high-grade lesions, we observed median 95–5 percentile core involvement values of 7.3, 8.1 and 8.6 mm, and maximum values of 17.0,

18.0 and 18.0 mm, for RMSE values of 4, 5 and 6 mm respectively. These results imply

that when RMSE ≥ 4 mm, targeting of high-grade lesions may lead to an increase in core

involvement variability observed after repeated biopsy attempts when compared to

lesions of all grades. However, this difference is rather small, with an average difference

in 95–5 percentile core involvement of ~1 mm observed between the two lesion groups.

It must also be noted that in the event that a sample of high-grade cancer is obtained

through biopsy, the core involvement measure may be rendered moot. For example, a

biopsy core which contains PCa with a Gleason Score of 7 but a core involvement < 50%

would still be deemed to be clinically significant by the NCCN Clinical Practice

Guidelines for Prostate Cancer[14]. No significant differences were observed when RMSE

≤ 3 mm.

4.5.2 Experiment 2 – Relationship between needle delivery error and proportion of biopsy attempts that miss the target

We observed that increasing needle delivery error leads to an increase in the

proportion of biopsy attempts that will entirely miss the tumour, for both all-grade and

high-grade tumours. The median proportion of misses monotonically increased as RMSE

increased. At RMSE = 4 mm, a median of 9% of the simulated biopsy attempts missed all

cancer and contained only non-cancerous tissue samples (Fig. 4-4A). However, the

spread of this proportion is large and a maximum percentage of 61% of biopsy attempts

missed all tumour tissue at this level of RMSE. The same trend was observed for the group of high-grade lesions as well, with a median percentage of 9% and maximum of 58% of biopsy attempts missing all cancer tissue. This corroborates our results demonstrating the need for more than one biopsy attempt to successfully sample smaller tumours, as discussed in Section 4.5.3.

We also observed a significant negative correlation between tumour diameter and proportion of biopsy attempts where the tumour is entirely missed. This implies that the larger a tumour's diameter, the more likely some portion of it will be sampled by the biopsy needle, which is an expected result.

We did not observe significant differences between all- and high-grade tumours for this measurement. However, our inability to detect significant differences between proportions of tumour misses for all-grade and high-grade tumours was not surprising, as no significant difference was observed in tumour surface area or diameter between lesions of the all grade and high grade groups ($p > 0.05$; Wilcoxon rank sum test).

4.5.3 Experiment 3 – Relationship between number of biopsy attempts and probability of a tumour sample

Fig. 4-5A shows that for RMSE $\geq$ 3 mm, a significantly higher median tumour sampling probability is achieved when two biopsy attempts are made as opposed to one.

Probability increases of 3%, 8%, 13% and 17% were observed between one and two biopsy attempts for RMSE values of 3, 4, 5 and 6 mm respectively. Furthermore, probability increases of 3%, 9%, 15% and 21% can be obtained over this same RMSE range when making three biopsy attempts relative to one. In comparing Fig. 4-5A and 4-5B, no significant differences were observed between all-grade and high-grade lesions with respect to this measurement, for one, two or three biopsy attempts.

The results shown in Fig. 4-5 are concordant (within 5%) with estimated sampling probabilities in our previously published work that used MRI-defined biopsy targets in 3D[11] for RMSE $\leq$ 3 mm. For RMSE $\geq$ 4, mm, the sampling probabilities in this work are higher than our previous experiments (<25% greater). This discrepancy could be explained by simulation of biopsy using 2D lesions in this work as opposed to 3D, and also the presence of microscopic cancerous regions on histology that are generally invisible on MRI; these will be captured within the biopsy cores in simulations conducted in this paper but not in those conducted in our previous work.

4.5.4 Clinical Relevance

To the best of our knowledge, this is the first study to demonstrate a significant effect of prostate biopsy needle guidance error on the percent core involvement of high-grade cancer and cancer of all grades, using gold standard histology imaging. Furthermore, this is the first study to compare the core involvements obtained when

specifically targeting high grade cancer versus cancers of all grades. This was made possible by the unprecedented level of detail of the histology tumour contouring and spatial localization of different intra-tumoural Gleason grades. Our data showed that for expected needle guidance errors, repeated biopsies of the same target can yield percent core involvement measures with sufficient variability to influence the decision for active surveillance vs. definitive treatment. Our data also shows that this issue may be mitigated by making more than one biopsy attempt at selected tumour targets.

4.5.5 Limitations

Although the use of histology imaging for simulated biopsy affords the ability to characterize percent core involvement and distribution of cancer grades in the core using a recognized gold standard, due to clinical limitations histology images are 2D, sliced approximately in the axial orientation, and acquired sparsely throughout the midgland (every 3–5 mm). Thus, the conclusions of this study are made under the assumption that apparent prostate tumour size and shape are invariant to tissue slicing orientation. This study is therefore complementary to previous work addressing these research questions using lesion contours on MRI, which are 3D but subject to inaccuracy and observer variability[11,12,17].

4.6 Conclusions

Image-guided prostate biopsy can target needles to suspicious areas within the prostate with the aim of obtaining an earlier definitive diagnosis and treatment plan. Our data, based on gold standard radical prostatectomy histology, demonstrated that needle delivery error can have a substantial impact on the probability of obtaining a sample and on the percent core involvement when a sample is obtained, for both high-grade cancer and cancers of all grades. We also observed that when RMSE $\geq$ 4 mm, targeting of high-grade lesions may result in higher core involvement variability observed after repeated biopsy attempts when compared to lesions of all grades. These parameters are important to patient risk stratification and the decision to pursue active surveillance vs. definitive treatment. This issue can be mitigated by making multiple biopsy attempts at selected targets, increasing the probability of obtaining a sample that correctly characterizes the extent and grade of the patient's cancer.

References

1   H. Singh, E.I. Canto, S.F. Shariat, D. Kadmon, B.J. Miles, T.M. Wheeler and K.M. Slawin, "Predictors of prostate cancer after initial negative systematic 12 core biopsy," Urology **171**(5), 1850-1854 (2004).

2   A.V. Taira, G.S. Merrick, R.W. Galbreath, H. Andreini, W. Taubenslag, R. Curtis, W.M. Butler, E. Adamovich and K.E. Wallner, "Performance of transperineal template-guided mapping biopsy in detecting prostate cancer in the initial and repeat biopsy setting," Prostate Cancer and Prostatic Diseases **13**(1), 71-77 (2010).

3   A. Rajinikanth, M. Manoharan, C.T. Soloway, F.J. Civantos and M.S. Soloway, "Trends in Gleason score: concordance between biopsy and prostatectomy over 15 years," Urology **72**(1), 177-182 (2008).

4   Y. Hu, H.U. Ahmed, Z. Taylor, C. Allen, M. Emberton, D. Hawkes, and D. Barratt, "MR to ultrasound registration for image-guided prostate interventions," Medical Image Analysis **16**(3), 687-703 (2012).

5   J.J. Futterer, S.W. Heijmink, T.W. Scheenen, J. Veltman, H.J. Huisman, P. Vos, C.A. Hulsbergen-van de Kaa, J.A. Witjes, P.F. Krabbe, A. Heerschap and J.O. Barentsz, "Prostate cancer localization with dynamic contrast-enhanced MR imaging and proton MR spectroscopic imaging," Radiology **241**(2), 449-458 (2006).

6   J.C. Weinreb, J.O. Barentsz, P.L. Choyke, F. Cornud, M.A. Haider, K.J. Macura, D. Margolis, M.D. Schnall, F. Shtern, C.M. Tempany, H.C. Thoeny and S. Verma, "PI-RADS Prostate Imaging - Reporting and Data System: 2015, Version 2," European Urology **69**(1), 16-40 (2016).

7   J. Bax, D. Cool, L. Gardi, K. Knight, D. Smith, J. Montreuil, S. Sherebrin, C. Romagnoli and A. Fenster, "Mechanically assisted 3D ultrasound guided prostate biopsy system," Medical Physics **35**(12), 5397-5410 (2008).

8   D.W. Cool, X. Zhang, C. Romagnoli, J.I. Izawa, W.M. Romano and A. Fenster, "Evaluation of MRI-TRUS fusion versus cognitive registration accuracy for MRI-targeted, TRUS-guided prostate biopsy," AJR: American Journal of Roentgenology **204**(1), 83-91 (2015).

9   M. Valerio, I. Donaldson, M. Emberton, et al., "Detection of Clinically Significant Prostate Cancer Using Magnetic Resonance Imaging-Ultrasound

Fusion Targeted Biopsy: A Systematic Review," European Urology **68**, 8-19 (2015).

10   P.P. Tonttila, J. Lantto, E. Paakko, U. Piippo, S. Kauppila, E. Lammentausta, P. Ohtonen and M.H. Vaarala, "Prebiopsy multiparametric magnetic resonance imaging for prostate cancer diagnosis in biopsy-naive men with suspected prostate cancer based on elevated prostate-specific antigen values: results from a randomized prospective blinded controlled trial," European Urology **69**(3), 419-425 (2016).

11   P.R. Martin, D.W. Cool, C. Romagnoli, A. Fenster and A.D. Ward, "Magnetic resonance imaging-targeted, 3D transrectal ultrasound-guided fusion biopsy for prostate cancer: quantifying the impact of needle delivery error on diagnosis," Medical Physics **41**(7), 073504 (2014).

12   P.R. Martin, D.W. Cool, A. Fenster, A.D. Ward, "A comparison of prostate tumour targeting strategies using magnetic resonance imaging-targeted, transrectal ultrasound-guided fusion biopsy," Medical Physics **45**(3), 1018-1028 (2018).

13   J.I. Epstein, P.C. Walsh, M. Carmichael and C.B. Brendler, "Pathologic and clinical findings to predict tumour extent of nonpalpable (stage T1c) prostate cancer," JAMA, The Journal of the American Medical Association **271**(5), 368-374 (1994).

14   National Comprehensive Cancer Network Clinical Practice Guidelines in Oncology: Prostate Cancer (2017).

15   T. Hambrock, D.M. Somford, H.J. Huisman, I.M. van Oort, J.A. Witjes, C.A. Hulsbergen-van de Kaa, T. Scheenen and J.O. Barentsz, "Relationship between apparent diffusion coefficients at 3.0-T MR imaging and Gleason grade in peripheral zone prostate cancer," Radiology **259**(2), 453-461 (2011).

16   Y. Itou, K. Nakanishi, Y. Narumi, Y. Nishizawa, and H. Tsukuma, "Clinical utility of apparent diffusion coefficient (ADC) values in patients with prostate cancer: can ADC values contribute to assess the aggressiveness of prostate cancer?" JMRI: Journal of Magnetic Resonance Imaging **33**(1), 167-172 (2011).

17   W.J. van de Ven, C.A. Hulsbergen-van de Kaa, T. Hambrock, J.O. Barentsz and H.J. Huisman, "Simulated required accuracy of image registration tools for targeting high-grade cancer components with prostate biopsies," European Radiology **23**(5), 1401-1407 (2013).

18   M.G. Salarian, M. Shahedi, M. Gaed, J.A. Gomez, M. Moussa, C. Romagnoli, D.W. Cool, M. Bastian-Jordan, J.L. Chin, S. Pautler, G.S. Bauman and A.D.

Ward, "Accuracy and variability of tumour burden measurement on multi-parametric MRI," SPIE Medical Imaging Proceedings 9041, 90410I (2014).

[19]   E. Gibson, G.S. Bauman, C. Romagnoli, D.W. Cool, M. Bastian-Jordan, Z. Kassam, M. Gaed, M. Moussa, J.A. Gomez, S.E. Pautler, J.L. Chin, C. Crukley, M.A. Haider, A. Fenster and A.D Ward, "Toward prostate cancer contouring guidelines on magnetic resonance imaging: dominant lesion gross and clinical target volume coverage via accurate histology fusion," International Journal of Radiation Oncology, Biology, Physics **96**(1), 188-196 (2016).

[20]   S. Jonmarker, A. Valdman, A. Lindberg, M. Hellstrom, L. Egevad, "Tissue shrinkage after fixation with formalin injection of prostatectomy specimens," Virchows Archiv **449**(3), 297-301 (2006).

Chapter 5

5 Conclusions and future work suggestions

5.1 Overview of rationale for research project:

Prior to this work, there has been substantial research showing the advantages of
MRI-targeted 3D TRUS-guided fusion biopsy over 2D TRUS-guided systematic biopsy.
These fusion biopsy systems were developed with the purpose of improving upon the
spatial information provided by 2D TRUS, and also to allow for targeting of lesions
defined on MRI during biopsy, using image registration[1-5]. To date, there have been
numerous studies which have shown an increase in cancer-positive core rates for fusion
biopsy, relative to systematic TRUS-guided biopsy[6-10]. A systematic review was also
conducted comparing 3D TRUS-guided fusion biopsy with 2D TRUS-guided systematic
biopsy, and it was found that fusion biopsy detected more clinically significant cancers
using fewer cores compared with systematic biopsy (median 33% cancer-positive core
rate, range 13-50% for fusion biopsy; median 24% cancer-positive core rate, range 5%-
52% for systematic biopsy)[11]. Furthermore, a recent multicentre and randomized trial at
25 centres in 11 countries found the use of MRI prior to biopsy led to fewer men
undergoing biopsy, and the use of MRI-targeted fusion biopsy led to less overdetection of

clinically insignificant cancer, with fewer biopsy cores obtained compared with standard 2D TRUS-guided systematic biopsy[12]. This study also showed a significant increase in the detection of clinically significant cancer when fusion biopsy was used, compared with the standard systematic biopsy group[12].

While it is not a focus of this thesis, another approach to TRUS-guided biopsy of prostate MRI-defined lesions is "cognitive registration." This approach involves intuitive visual alignment between MRI lesions and TRUS guidance[13]. While it has been shown that the use of MRI for cognitive fusion led to an increased detection rate of clinically significant cancer and less overdetection of clinically insignificant cancer compared with systematic biopsy[12], consensus has not yet been reached comparing the efficacy of the cognitive vs. software fusion approaches. Two studies have reported that biopsy targeting of clinically significant MRI lesions using cognitive registration resulted in inferior cancer detection rates compared with MRI-TRUS fusion[14,15], while another study found no significant difference in cancer detection rates between the two approaches[8]. Further investigation is warranted, as the greatest benefit for MRI-TRUS fusion over cognitive registration may be achieved for tumours that are small but still clinical significant.

Despite substantial research being conducted in order to investigate the potential improvements in patient care achieved through the use of fusion prostate biopsy, prior to this thesis, there remained a lack of knowledge in terms of target optimization for placement fusion biopsy needles. At the time of the writing of this thesis, the author is aware of one other study which investigated how fusion biopsy needle delivery error

affects cancer detection, by van de Ven et al.[16] This led to the observation that the positive core rate is related to the biopsy system error in delivering the needle to the intended tumour target. Furthermore, a recent study by Lu et al.[17] showed that for the Artemis fusion biopsy system, cancer detection rates improve as the number of biopsy cores increases from one to five, but no significant increase in detection rate was observed beyond five cores. For cancers of any Gleason grade, positive core rates of 69% and 84% were reported for one biopsy attempt and two biopsy attempts respectively. These results show close agreement with our results presented in Figure 2-3 and Figure 2-5 for a needle delivery error of 5 mm. While we estimated the needle delivery error of the Artemis system to be 3.5 mm in Chapter 2, it should be noted that our error model did not account for needle deflection during biopsy, and in reality this error may be larger than 3.5 mm in practice.

What is envisioned for this field after the completion of the work presented in this thesis, is that needle delivery error estimates for any MRI targeted, 3D TRUS-guided fusion prostate biopsy system could be used in conjunction with the results presented in this thesis in order to aid any physician performing a targeted biopsy in deciding the number and spatial locations of targeted biopsy needles in order to achieve a desired probability of sampling the lesion being targeted. Specifically, it is envisioned that the lessons presented in this work could be incorporated into an onboard software module that provides automatic selection of biopsy target locations given the error characteristics of any particular biopsy system (see Section 5.2.2).

5.2 Project summary and conclusions

The work presented in this thesis represents several steps toward the overarching goal of more accurate characterization of cancer burden for PCa patients, as well as earlier diagnosis of PCa while it remains confined to the gland and curable. These steps toward this goal were achieved through the development of a fusion biopsy simulation software platform which allowed for the investigation of how needle delivery error of MRI-targeted, 3D TRUS-guided "fusion" prostate biopsy affects the probability of successfully sampling prostatic tumours and the estimation of cancer burden for suspected PCa patients. This work was divided into three chapters, which are summarized below.

In Chapter 2, the probability of obtaining a positive tumour sample in a single biopsy core was estimated for 81 3D suspicious regions contoured on MRI by two radiologists. The results indicated that more than one core must be taken from the majority of tumours to achieve a sampling probability of 95% or greater for a biopsy system with an overall error ≥ 3.5 mm. Furthermore, it was shown that despite the potential impact of differences in tumour shape on positive sampling probability, tumours with high ($> 95\%$) probability of positive sampling can be distinguished from those with lower sampling probability based on tumour volume. The upper bound of the 99% prediction interval for the lesion volumes with sampling probability $< 95\%$ was 1.05 cm^3, which provides some insight into the largest tumours that cannot be successfully sampled in one biopsy core with 95% confidence. It was also observed through

comparison with a previously published method that the assumption of spherical tumour shape can lead to an overestimation of positive sampling probabilities. Although this observation was significant ($p < 0.05$), the overestimation varied with biopsy system RMSE and the practical importance of this observation depends on both tumour asphericity and biopsy system needle delivery error. The results from Chapter 2, especially the finding that multiple biopsy attempts are necessary in order to achieve a sampling probability ≥95% for the majority of prostate lesions defined on MRI, were critical to the justification of development of the biopsy simulation software platform which allowed the simulation of multiple biopsy attempts and different targeting schemes for each lesion, as discussed in Chapter 3.

In Chapter 3, a "ring" targeting strategy was proposed, with the intention of compensating for a systematic error of known magnitude, but unknown direction. The results suggest that the optimal targeting scheme for prostate biopsy depends on the relative levels of systematic and random errors in the system. Where systematic error dominates, a ring targeting scheme may yield improved probability of tumour sampling, particularly for small tumours. Furthermore, the work in Chapter 2 was focused primarily on the probability of obtaining any amount of PCa within the biopsy core, without considering the core involvement (i.e. the proportion of the biopsy core that contains tumour tissue), which is an important measure used to determine the clinical significance of a patient's PCa[188,19]. In Chapter 3, I compared the probabilities of obtaining a core involvement ≥ 50% (from 55 out of the 81 total lesions which were large enough to obtain this core involvement) when using either a ring or centroid

targeting strategy. Similar to the first study in Chapter 3, I found that when systematic

error dominates, a ring targeting scheme may yield improved probability of tumour

sampling. However, the probabilities of obtaining a 50% core involvement were

substantially lower compared with the probabilities of obtaining any amount of PCa

within the core, for both targeting strategies. While this Chapter represents a step toward

improving the manner in which lesions are targeted using fusion biopsy, a prospective

trial will ultimately be needed to determine the improvement in positive yield achieved

through optimization of needle target selection. The data presented in this paper could be

incorporated into an onboard software module that provides the operator with biopsy

target locations given the error characteristics of any particular biopsy system (see

Section 5.2.2).

An important limitation of the work presented in Chapters 2 and 3 is that MRI-

defined regions of suspicion were used as biopsy simulation targets, without histologic

confirmation of the core involvements and high-grade cancer yield resulting from biopsy

simulation. In Chapter 4, I addressed this by using histologically confirmed PCa tumours

as contoured on digital histology images by genitourinary pathologists to conduct biopsy

simulations and report core involvement and high-grade cancer yield as a function of

biopsy system error. By using histology image contours to define tumour targeting, this

work modeled idealized tumour targeting, wherein boundary delineation on the planning

image was exactly concordant with lesions on histopathology. Results from our

simulations thus represented a best-case scenario, since lesions contoured by experts on

MRI are not volumetrically concordant with true histologic lesions**Error! Reference source not**

found.,[21]. As histology slices are inherently 2D and oriented approximately axially, our

simulations were conducted in 2D under the assumption that prostate tumour size and

shape are invariant to slicing angle. This was a necessary compromise to reap the benefits

of the enhanced core involvement and grade information provided by histology imaging,

compared to MRI. Our data, based on gold standard radical prostatectomy histology,

demonstrated that needle delivery error can have a substantial impact on the probability

of obtaining a sample and on the percent core involvement when a sample is obtained, for

both high-grade cancer and cancers of all grades. We also observed that when RMSE $\geq$ 4

mm, targeting of high-grade lesions may result in higher core involvement variability

observed after repeated biopsy attempts when compared to lesions of all grades. It must

be noted that in the event that a sample of high-grade cancer is obtained through biopsy,

the importance of core involvement in estimation of tumour burden may be diminished[18].

However, these parameters are important to patient risk stratification and the decision to

pursue active surveillance vs. definitive treatment. In concordance with the findings

presented in Chapters 2 and 3, I observed that this issue can be mitigated by making

multiple biopsy attempts at selected targets, increasing the probability of obtaining a

sample that correctly characterizes the extent and grade of the patient's cancer.

In this thesis, we have demonstrated the effects of fusion biopsy needle delivery

error on prostatic lesion biopsy sampling probabilities. According to our hypotheses in

Section 1.5.1, more than one biopsy attempt should be necessary to achieve probabilities

$\geq$ 95% of both obtaining a PCa-positive sample, and obtaining a core involvement $\geq$

50% for lesions large enough to obtain a core involvement of that size. It was shown in

Chapter 2 that for a fusion biopsy system random needle delivery error of 3.5 mm, the sampling probability $< 95\%$ for 60 out of 81 lesions (74% of lesions) in the dataset when one biopsy attempt is made. While the study conducted in Chapter 2 was performed using suspicious prostatic lesions contoured on MRI and not pathologist-confirmed PCa from histology, the experiments conducted in Chapter 4 used tumours from gold standard prostate histology to simulate biopsy attempts, and it was shown that the sampling probability $< 95\%$ for 180 out of 307 tumours (59% of tumours) when making one biopsy attempt for a fusion biopsy system with a random needle delivery error of 4 mm. When making two biopsy attempts, sampling probability $< 95\%$ for only 80 out of 307 tumours (26% of tumours), therefore showing that sampling probability $\geq 95\%$ for the majority of PCa tumours when two or more biopsy attempts are made.

In the results presented in Chapter 3, it was observed that for a fusion biopsy system with a random needle delivery error ≥ 4 mm and systematic error ≤ 6 mm, the probability of obtaining a 50% core involvement is $< 95\%$ for the majority of tumours of volume < 1 cm^3 when ≤ 4 biopsy attempts are made, and also for the majority of tumours of volume ≥ 1 cm^3 when ≤ 2 biopsy attempts are made. It was observed that when three biopsy attempts are made for tumours of volume ≥ 1 cm^3, the probability of obtaining a 50% core involvement is $\geq 95\%$ for a fusion biopsy system with a random needle delivery error ≤ 4 mm and a systematic error ≤ 2 mm. Likewise, the probability of obtaining a 50% core involvement is $\geq 95\%$ when four biopsy attempts are made on tumours of volume ≥ 1 cm^3, for a fusion biopsy system with a random needle delivery error ≤ 4 mm and a systematic error ≤ 3 mm. These results were observed for both the

centroid and ring targeting strategies presented in Chapter 3. Therefore, it was observed that multiple biopsy attempts are necessary to achieve a probability $\geq$ 95% of obtaining a 50% core involvement for the majority of tumours in our dataset, including those of volume $\geq$ 1 cm^3.

Thus, *the central hypotheses of this thesis were confirmed* through the findings presented in Chapters 2, 3 and 4.

5.3 Advancements in knowledge achieved through completion of this work

Through the completion of this thesis, we have advanced knowledge in this field by providing: (1) insight into the maximum tumour volume that cannot be successfully sampled in one biopsy core with 95% confidence; (2) evidence that an assumption of spherical tumour shape results in a consistent overestimation of tumour sampling probability; (3) evidence that ring targeting may yield improved probability of tumour sampling for fusion biopsy systems where systematic error dominates over random error; (4) evidence that needle delivery error introduces enough variability in core involvement measures for repeated biopsies of the same tumour target to influence the decision of active surveillance vs. definitive treatment, for both high grade PCa and for PCa of all grades; and (5) evidence that targeting of high grade lesions may result in higher core

involvement variability after repeated biopsy attempts when compared with lesions of all grades.

5.4 Suggestions for future work:

5.4.1 Simulations using prostate histopathology co-registered with MRI

The work presented in this thesis represents, to the best of my knowledge, the first study of its kind to investigate the effects of prostate fusion biopsy needle delivery error on tumour sampling probabilities and cancer burden estimation. However, in the studies presented in this thesis, either radiologist-defined contours on MRI (Chapters 2 and 3) or gold standard radical prostatectomy histology (Chapter 4) were used to determine biopsy needle target locations and evaluate the contents of the simulated biopsy cores. Furthermore, the experiments described within this thesis were conducted under the assumption that needle delivery error is invariant to tumour location within the prostate. While the work detailed in this thesis represents necessary early steps in the investigation of this problem, the next logical step is to use my fusion biopsy simulation software platform to simulate situations which are more closely related to how targeted fusion biopsies are planned and evaluated in a clinical setting.

We have the ability in our research laboratory to accurately fuse whole-mount prostatectomy histology with in-vivo MRI obtained prior to surgery[22,23] (Fig. 5-1). This fusion has been performed for 52 prostatectomy specimens as part of a clinical trial at our centre, where MRI contours have been performed by four radiologists for 18 of those cases to date. This involves the same histology dataset as was used in Chapter 4 of this thesis, and PCa has been contoured on all histology images by a physician trained in PCa morphology, with contouring confirmed by a genitourinary pathologist. Using this dataset of co-registered prostate histology and in vivo MR images, my biopsy simulation platform can be used to determine biopsy target locations using the radiologist-contoured MR image dataset, but then evaluate biopsy core involvement and aggressiveness of PCa in each biopsy core based on the co-registered histology data.
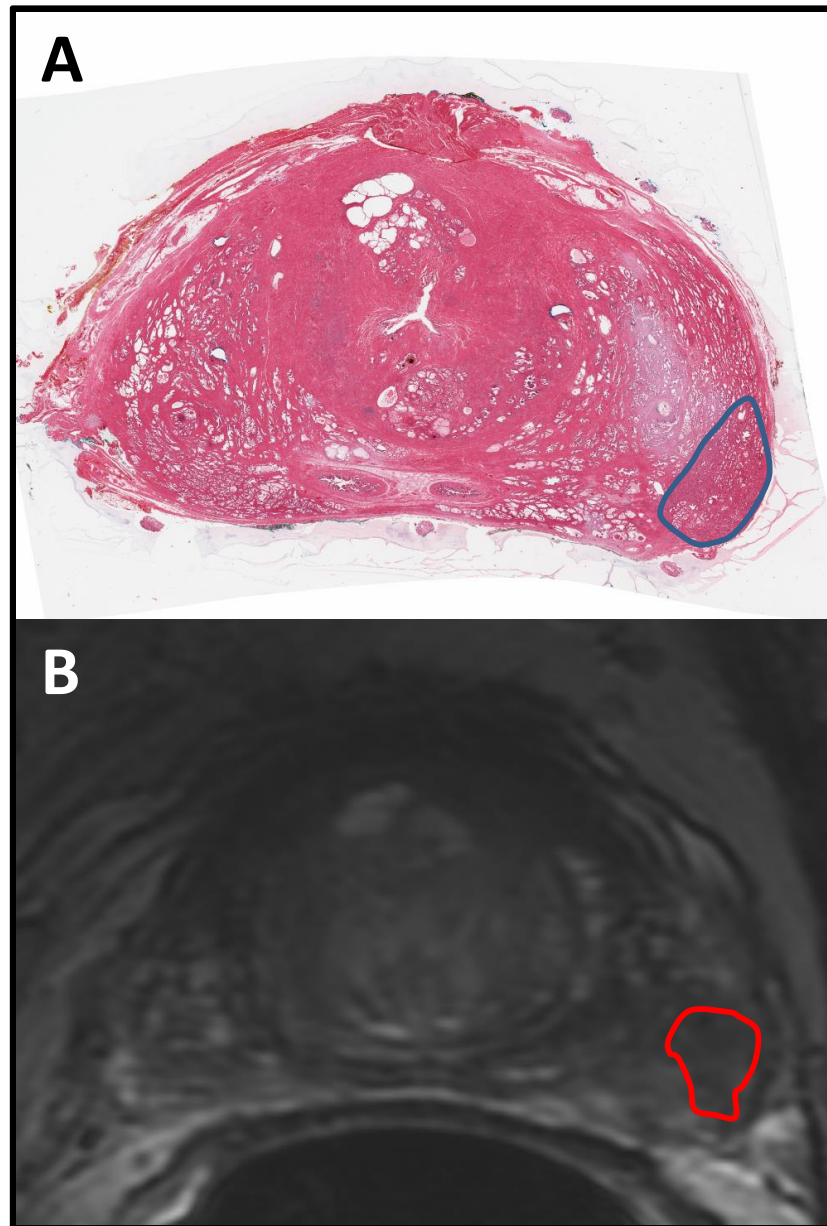
Figure 5-1: Showing co-registration between **(A)** whole-mount prostatectomy histology and **(B)** in-vivo T2W MRI. The location of PCa on histology is delineated in blue, while suspicious lesion delineation performed by a radiologist on MRI is shown in red. While the radiologist was correct in assessing the location of PCa in this case, the lesion margins on MRI do not match with the tumour margins as delineated on histology.

This approach can be used to investigate the following research questions, enumerated 1 through 5 below.

1) When using radiologist-defined contours to select biopsy needle target locations in the presence of biopsy system needle delivery error, what is probability of obtaining a positive sample of PCa of any grade within the biopsy core as evaluated using gold-standard co-registered histology?

2) What is the probability of obtaining a positive sample of high grade PCa (Gleason Score $\geq$ 4+3) within the biopsy core?

3) When using radiologist-defined contours to select biopsy needle target locations, what is the impact of biopsy needle delivery error on the core involvement of PCa obtained within a biopsy core?

4) How do the results from this new prostate biopsy model compare to those presented in this thesis?

5) How can the biopsy tumour targeting strategies proposed in this thesis be adapted to adjust for the misalignment between MRI lesions and PCa tumours?

The findings of this particular study could be used to improve fusion biopsy targeting through the following avenues: (1) determining the maximum tumour volume that cannot be sampled with 95% confidence in a given number of biopsy attempts when performing MRI-targeted 3D TRUS-guided biopsy, evaluated using prostate histology as opposed to evaluated using only MRI-contours as in Chapter 2 of this thesis; (2)

determining the maximum high grade tumour volume that cannot be sampled with 95% confidence in a given number of biopsy attempts; (3) determining the number of biopsy attempts necessary to achieve a 50% core involvement for tumours which are large enough for such a core involvement to be obtained, given lesion volume; and (4) determining potential improvements to the centroid and ring targeting strategies for biopsy needle target selection proposed in this thesis, in order to adjust for misalignment between MRI-lesions and PCa tumours.

5.4.2 Implementation of adapted fusion biopsy targeting strategies in clinic

The findings presented in this work could be directly beneficial in ongoing clinical studies in prostate cancer. Specifically, lessons learned on the topic of prostate biopsy target selection could be translated into clinic through incorporation into the graphical user interface of any fusion biopsy system currently being used to perform targeted prostate biopsies. I envision that the biopsy system display could be updated to indicate the number and spatial locations of biopsy targets necessary to achieve any desired probability of successfully sampling the suspicious lesions contoured on MRI, given the estimated needle delivery error for the particular biopsy system and the size and shape of the lesions to be targeted (Fig. 5-2A).

Alternatively, a less stringent targeting approach could be taken, wherein a colour map is overlaid onto the MR contours indicating the probability of successfully sampling the region of interest (Fig. 5-2B). This would allow the operating clinician to have more freedom in selecting where biopsy needles are placed, given indicated probabilities of a successful sample. Furthermore, these colour maps could continue to update as biopsy cores are taken (i.e. indicating an increase in sampling probability as more biopsy attempts are made). The implementation of such a targeting system has the potential to increase the tumour sampling probability for fusion biopsy systems which are already used in clinical practice.
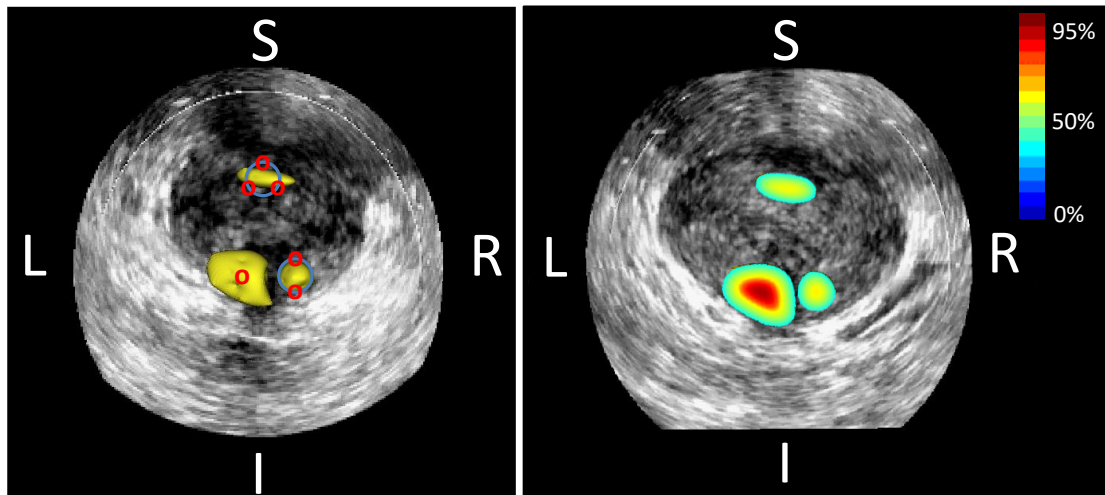
Figure 5-2: A probe's eye view (i.e. looking down the axial direction of a TRUS probe) of 3 suspicious lesions contoured on MRI and registered to 3D TRUS. **(A)** Indicating biopsy target locations using both the centroid and ring targeting strategies (see Chapter 3) in order to achieve the operator's desired probability of obtaining a successful sample from these regions. **(B)** Colour maps overlaid onto the MRI contours indicating the probability of a successful sample given biopsy target location.

References:

[1]   J. Bax, D. Cool, L. Gardi, K. Knight, D. Smith, J. Montreuil, S. Sherebrin, C. Romagnoli and A. Fenster, "Mechanically assisted 3D ultrasound guided prostate biopsy system," Medical Physics **35**(12), 5397-5410 (2008).

[2]   Y. Sun, J. Yuan, W. Qiu, M. Rajchl, C. Romagnoli and A. Fenster, "Three-dimensional nonrigid MR-TRUS registration using dual optimization," IEEE Transactions on Medical Imaging **34**(5), 1085-1095 (2015).

[3]   M. Baumann, P. Mozer, V. Daanen and J. Troccaz, "Prostate biopsy tracking with deformation estimation," Medical Image Analysis **16**(3), 562-576 (2012).

[4]   S. Xu, J. Kruecker, B. Turkbey, N. Glossop, A.K. Singh, P. Choyke, P. Pinto and B.J. Wood, "Real-time MRI-TRUS fusion for guidance of targeted prostate biopsies," Computer Aided Surgery **13**(5), 255-264 (2008).

[5]   B.A. Hadaschik, T.H. Kuru, C. Tulea, P. Rieker, I.V. Popeneciu, T. Simpfendorfer, J. Huber, P. Zogal, D. Teber, S. Pahernik, M. Roethke, P. Zamecnik, W. Roth, G. Sakas, H.P. Schlemmer and M. Hohenfellner, "A novel stereotactic prostate biopsy system integrating pre-interventional magnetic resonance imaging and live ultrasound fusion," Urology **186**(6), 2214-2220 (2011).

[6]   D.W. Cool, J. Bax, C. Romagnoli, A.D. Ward, L. Gardi, V. Karnik, J. Izawa, J. Chin and A. Fenster, "Fusion of MRI to 3D TRUS for mechanically-assisted targeted prostate biopsy: system design and initial clinical experience," Lecture Notes in Computer Science **6963**, 121-133 (2011).

[7]   M.C. Roethke, T.H. Kuru, S. Schultze, D. Tichy, A. Kopp-Schneider, M. Fenchel, H.P. Schlemmer, B.A. Hadaschik, "Evaluation of the ESUR PI-RADS scoring system for multiparametric MRI of the prostate with targeted MR/TRUS fusion-guided biopsy at 3.0 Tesla," European Radiology **24**(2), 344-352 (2014).

[8]   P. Puech, O. Rouviere, R. Renard-Penna, A. Villers, P. Devos, M. Colombel, M.O. Bitker, X. Leroy, F. Mege-Lechevallier, E. Comperat, A. Ouzzane and L. Lemaitre, "Prostate cancer diagnosis: multiparametric MR-targeted biopsy with cognitive and transrectal US-MR fusion guidance versus systematic biopsy--prospective multicentre study," Radiology **268**(2), 461-469 (2013).

[9]   S. Natarajan, L.S. Marks, D.J. Margolis, J. Huang, M.L. Macairan, P. Lieu and A. Fenster, "Clinical application of a 3D ultrasound-guided prostate biopsy system," Urologic Oncology **29**(3), 334-342 (2011).

10   D. Volkin, B. Turkbey, A.N. Hoang, S. Rais-Bahrami, N. Yerram, A. Walton-Diaz, J.W. Nix, B.J. Wood, P.L. Choyke and P.A. Pinto, "Multiparametric magnetic resonance imaging (MRI) and subsequent MRI/ultrasonography fusion-guided biopsy increase the detection of anteriorly located prostate cancers," BJU International **114**(6b), E43-E49 (2014).

11   M. Valerio, I. Donaldson, M. Emberton, B. Ehdaie, B.A. Hadaschik, L.S. Marks, P. Mozer, A.R. Rastinehad, H.U. Ahmed, "Detection of clinically significant prostate cancer using magnetic resonance imaging-ultrasound fusion targeted biopsy: a systematic review," European Urology **68**(1), 8-19 (2015).

12   V. Kasivisvanathan, A.S. Rannikko, M. Borghi, V. Panebianco, L.A. Mynderse, M.H. Vaarala, A. Briganti, L. Budaus, G. Hellawell, R.G. Hindley, M.J. Roobol, S. Eggener, M. Ghei, A. Villers, F. Bladou, G.M. Villeirs, J. Virdi, S. Boxler, G. Robert, P.B. Singh, W. Venderink, B.A. Hadaschik, A. Ruffion, J.C. Hu, D. Margolis, S. Crouzet, L. Klotz, S.S. Taneja, P. Pinto, I. Gill, C. Allen, F. Giganti, A. Freeman, S. Morris, S. Punwani, N.R. Williams, C. Brew-Graves, J. Deeks, Y. Takwoingi, M. Emberton and C.M Moore, "MRI-targeted or standard biopsy for prostate-cancer diagnosis," The New England Journal of Medicine **378**(19), 1767-1777 (2018).

13   B.K. Park, J.W. Park, S.Y. Park, C.K. Kim, H.M. Lee, S.S. Jeon, S.I. Seo, B.C. Jeong and H.Y. Choi, "Prospective evaluation of 3-T MRI performed before initial transrectal ultrasound-guided prostate biopsy in patients with high prostate-specific antigen and no previous biopsy," AJR: American Journal of Roentgenology **197**(5), W876-881 (2011).

14   D.W. Cool, X. Zhang, C. Romagnoli, J.I. Izawa, W.M. Romano and A. Fenster, "Evaluation of MRI-TRUS fusion versus cognitive registration accuracy for MRI-targeted, TRUS-guided prostate biopsy," AJR: American Journal of Roentgenology **204**(1), 83-91 (2015).

15   N.B. Delongchamps, M. Peyromaure, A. Schull, F. Beuvon, N. Bouazza, T. Flam, M. Zerbib, N. Muradyan, P. Legman and F. Cornud, "Prebiopsy magnetic resonance imaging and prostate cancer detection: comparison of random and targeted biopsies," Urology **189**(2), 493-499 (2013).

16   W.J. van de Ven, C.A. Hulsbergen-van de Kaa, T. Hambrock, J.O. Barentsz and H.J. Huisman, "Simulated required accuracy of image registration tools for targeting high-grade cancer components with prostate biopsies," European Radiology **23**(5), 1401-1407 (2013).

17   A. Lu, K. Ghabili, K. Nguyen, M. Leapman and P. Sprenkle, "How many cores are needed to detect clinically significant prostate cancer on targeted MRI-ultrasound fusion biopsy?" Journal of Clinical Oncology **36**(6), 134 (2018).

[18] National Comprehensive Cancer Network Clinical Practice Guidelines in Oncology: Prostate Cancer (2017).

[19] Clinically Localized Prostate Cancer: AUA/ASTRO/SUO Guideline (2017).

[20] M.G. Salarian, M. Shahedi, M. Gaed, J.A. Gomez, M. Moussa, C. Romagnoli, D.W. Cool, M. Bastian-Jordan, J.L. Chin, S. Pautler, G.S. Bauman and A.D. Ward, "Accuracy and variability of tumour burden measurement on multi-parametric MRI," SPIE Medical Imaging Proceedings 9041, 90410I (2014).

[21] E. Gibson, G.S. Bauman, C. Romagnoli, D.W. Cool, M. Bastian-Jordan, Z. Kassam, M. Gaed, M. Moussa, J.A. Gomez, S.E. Pautler, J.L. Chin, C. Crukley, M.A. Haider, A. Fenster and A.D Ward, "Toward prostate cancer contouring guidelines on magnetic resonance imaging: dominant lesion gross and clinical target volume coverage via accurate histology fusion," International Journal of Radiation Oncology, Biology, Physics **96**(1), 188-196 (2016).

[22] E. Gibson, C. Crukley, M. Gaed, J.A. Gomez, M. Moussa, J.L. Chin, G.S. Bauman, A. Fenster and A.D. Ward, "Registration of prostate histology images to ex vivo MR images via strand-shaped fiducials," JMRI: Journal of Magnetic Resonance Imaging **36**(6), 1402-1412 (2012).

[23] A.D. Ward, C. Crukley, C.A. McKenzie, J. Montreuil, E. Gibson, C. Romagnoli, J.A. Gomez, M. Moussa, J. Chin, G. Bauman and A. Fenster, "Prostate: registration of digital histopathologic images to in vivo MR images acquired by using endorectal receive coil," Radiology **263**(3), 856-864 (2012).

Appendices

APPENDIX A – Permission for reproduction of scientific articles

A.1 Permission to reproduce previously published material in Chapter 2

JOHN WILEY AND SONS LICENSE
TERMS AND CONDITIONS

Jun 15, 2018

This Agreement between PETER MARTIN ("You") and John Wiley and Sons ("John Wiley and Sons") consists of your license details and the terms and conditions provided by John Wiley and Sons and Copyright Clearance Center.

License Number	4367080123138
License date	Jun 13, 2018
Licensed Content Publisher	John Wiley and Sons
Licensed Content Publication	Medical Physics
Licensed Content Title	Magnetic resonance imaging-targeted, 3D transrectal ultrasound-guided fusion biopsy for prostate cancer: Quantifying the impact of needle delivery error on diagnosis
Licensed Content Author	Peter R. Martin, Derek W. Cool, Cesare Romagnoli, et al
Licensed Content Date	Nov 30, 2016
Licensed Content Volume	41
Licensed Content Issue	7
Licensed Content Pages	10
Type of use	Dissertation/Thesis
Requestor type	Author of this Wiley article
Format	Print and electronic
Portion	Full article
Will you be translating?	No
Title of your thesis / dissertation	Toward optimization of target planning for magnetic resonance image-targeted, 3D-transrectal ultrasound-guided fusion prostate biopsy
Expected completion date	Aug 2018
Expected size (number of pages)	160
Requestor Location	PETER MARTIN Department of Medical Biophysics The University of Western Ontario London Ontario, ON N6A 3K7 Canada Attn: PETER MARTIN
Publisher Tax ID	EU826007151
Total	0.00 CAD

- The Wiley Materials and all of the intellectual property rights therein shall at all times remain the exclusive property of John Wiley & Sons Inc, the Wiley Companies, or their respective licensors, and your interest therein is only that of having possession of and the right to reproduce the Wiley Materials pursuant to Section 2 herein during the continuance of this Agreement. You agree that you own no right, title or interest in or to the Wiley Materials or any of the intellectual property rights therein. You shall have no rights hereunder other than the license as provided for above in Section 2. No right, license or interest to any trademark, trade name, service mark or other branding ("Marks") of WILEY or its licensors is granted hereunder, and you agree that you shall not assert any such right, license or interest with respect thereto

- NEITHER WILEY NOR ITS LICENSORS MAKES ANY WARRANTY OR REPRESENTATION OF ANY KIND TO YOU OR ANY THIRD PARTY, EXPRESS, IMPLIED OR STATUTORY, WITH RESPECT TO THE MATERIALS OR THE ACCURACY OF ANY INFORMATION CONTAINED IN THE MATERIALS, INCLUDING, WITHOUT LIMITATION, ANY IMPLIED WARRANTY OF MERCHANTABILITY, ACCURACY, SATISFACTORY QUALITY, FITNESS FOR A PARTICULAR PURPOSE, USABILITY, INTEGRATION OR NON-INFRINGEMENT AND ALL SUCH WARRANTIES ARE HEREBY EXCLUDED BY WILEY AND ITS LICENSORS AND WAIVED BY YOU.

- WILEY shall have the right to terminate this Agreement immediately upon breach of this Agreement by you.

- You shall indemnify, defend and hold harmless WILEY, its Licensors and their respective directors, officers, agents and employees, from and against any actual or threatened claims, demands, causes of action or proceedings arising from any breach of this Agreement by you.

- IN NO EVENT SHALL WILEY OR ITS LICENSORS BE LIABLE TO YOU OR ANY OTHER PARTY OR ANY OTHER PERSON OR ENTITY FOR ANY SPECIAL, CONSEQUENTIAL, INCIDENTAL, INDIRECT, EXEMPLARY OR PUNITIVE DAMAGES, HOWEVER CAUSED, ARISING OUT OF OR IN CONNECTION WITH THE DOWNLOADING, PROVISIONING, VIEWING OR USE OF THE MATERIALS REGARDLESS OF THE FORM OF ACTION, WHETHER FOR BREACH OF CONTRACT, BREACH OF WARRANTY, TORT, NEGLIGENCE, INFRINGEMENT OR OTHERWISE (INCLUDING, WITHOUT LIMITATION, DAMAGES BASED ON LOSS OF PROFITS, DATA, FILES, USE, BUSINESS OPPORTUNITY OR CLAIMS OF THIRD PARTIES), AND WHETHER OR NOT THE PARTY HAS BEEN ADVISED OF THE POSSIBILITY OF SUCH DAMAGES. THIS LIMITATION SHALL APPLY NOTWITHSTANDING ANY FAILURE OF ESSENTIAL PURPOSE OF ANY LIMITED REMEDY PROVIDED HEREIN.

- Should any provision of this Agreement be held by a court of competent jurisdiction to be illegal, invalid, or unenforceable, that provision shall be deemed amended to achieve as nearly as possible the same economic effect as the original provision, and the legality, validity and enforceability of the remaining provisions of this Agreement shall not be affected or impaired thereby.

- The failure of either party to enforce any term or condition of this Agreement shall not constitute a waiver of either party's right to enforce each and every term and condition of this Agreement. No breach under this agreement shall be deemed waived or excused by either party unless such waiver or consent is in writing signed by the party granting such waiver or consent. The waiver by or consent of a party to a breach of any provision of this Agreement shall not operate or be construed as a waiver of or consent to any other or subsequent breach by such other party.

- This Agreement may not be assigned (including by operation of law or otherwise) by you without WILEY's prior written consent.

- Any fee required for this permission shall be non-refundable after thirty (30) days from receipt by the CCC.

- These terms and conditions together with CCC's Billing and Payment terms and conditions (which are incorporated herein) form the entire agreement between you and WILEY concerning this licensing transaction and (in the absence of fraud) supersedes all prior agreements and representations of the parties, oral or written. This Agreement may not be amended except in writing signed by both parties. This Agreement shall be binding upon and inure to the benefit of the parties' successors, legal representatives, and authorized assigns.

- In the event of any conflict between your obligations established by these terms and conditions and those established by CCC's Billing and Payment terms and conditions, these terms and conditions shall prevail.

- WILEY expressly reserves all rights not specifically granted in the combination of (i) the license details provided by you and accepted in the course of this licensing transaction, (ii) these terms and conditions and (iii) CCC's Billing and Payment terms and conditions.

- This Agreement will be void if the Type of Use, Format, Circulation, or Requestor Type was misrepresented during the licensing process.

- This Agreement shall be governed by and construed in accordance with the laws of the State of New York, USA, without regards to such state's conflict of law rules. Any legal action, suit or proceeding arising out of or relating to these Terms and Conditions or the breach thereof shall be instituted in a court of competent jurisdiction in New York County in the State of New York in the United States of America and each party hereby consents and submits to the personal jurisdiction of such court, waives any objection to venue in such court and consents to service of process by registered or certified mail, return receipt requested, at the last known address of such party.

A.2 Permission to reproduce previously published material in Chapter 3

TERMS AND CONDITIONS

This copyrighted material is owned by or exclusively licensed to John Wiley & Sons, Inc. or one of its group companies (each a"Wiley Company") or handled on behalf of a society with which a Wiley Company has exclusive publishing rights in relation to a particular work (collectively "WILEY"). By clicking "accept" in connection with completing this licensing transaction, you agree that the following terms and conditions apply to this transaction (along with the billing and payment terms and conditions established by the Copyright Clearance Center Inc., ("CCC's Billing and Payment terms and conditions"), at the time that you opened your RightsLink account (these are available at any time at http://myaccount.copyright.com).

Terms and Conditions

- The materials you have requested permission to reproduce or reuse (the "Wiley Materials") are protected by copyright.

- You are hereby granted a personal, non-exclusive, non-sub licensable (on a stand-alone basis), non-transferable, worldwide, limited license to reproduce the Wiley Materials for the purpose specified in the licensing process. This license, **and any CONTENT (PDF or image file) purchased as part of your order,** is for a one-time use only and limited to any maximum distribution number specified in the license. The first instance of republication or reuse granted by this license must be completed within two years of the date of the grant of this license (although copies prepared before the end date may be distributed thereafter). The Wiley Materials shall not be used in any other manner or for any other purpose, beyond what is granted in the license. Permission is granted subject to an appropriate acknowledgement given to the author, title of the material/book/journal and the publisher. You shall also duplicate the copyright notice that appears in the Wiley publication in your use of the Wiley Material. Permission is also granted on the understanding that nowhere in the text is a previously published source acknowledged for all or part of this Wiley Material. Any third party content is expressly excluded from this permission.

- With respect to the Wiley Materials, all rights are reserved. Except as expressly granted by the terms of the license, no part of the Wiley Materials may be copied, modified, adapted (except for minor reformatting required by the new Publication), translated, reproduced, transferred or distributed, in any form or by any means, and no derivative works may be made based on the Wiley Materials without the prior permission of the respective copyright owner.**For STM Signatory Publishers clearing permission under the terms of the STM Permissions Guidelines only, the terms of the license are extended to include subsequent editions and for editions in other languages, provided such editions are for the work as a whole in situ and does not involve the separate exploitation of the permitted figures or extracts,** You may not alter, remove or suppress in any manner any copyright, trademark or other notices displayed by the Wiley Materials. You may not license, rent, sell, loan, lease, pledge, offer as security, transfer or assign the Wiley Materials on a stand-alone basis, or any of the rights granted to you hereunder to any other person.

- The Wiley Materials and all of the intellectual property rights therein shall at all times remain the exclusive property of John Wiley & Sons Inc, the Wiley Companies, or their respective licensors, and your interest therein is only that of having possession of and the right to reproduce the Wiley Materials pursuant to Section 2 herein during the continuance of this Agreement. You agree that you own no right, title or interest in or to the Wiley Materials or any of the intellectual property rights therein. You shall have no rights hereunder other than the license as provided for above in Section 2. No right, license or interest to any trademark, trade name, service mark or other branding ("Marks") of WILEY or its licensors is granted hereunder, and you agree that you shall not assert any such right, license or interest with respect thereto

- NEITHER WILEY NOR ITS LICENSORS MAKES ANY WARRANTY OR REPRESENTATION OF ANY KIND TO YOU OR ANY THIRD PARTY, EXPRESS, IMPLIED OR STATUTORY, WITH RESPECT TO THE MATERIALS OR THE ACCURACY OF ANY INFORMATION CONTAINED IN THE MATERIALS, INCLUDING, WITHOUT LIMITATION, ANY IMPLIED WARRANTY OF MERCHANTABILITY, ACCURACY, SATISFACTORY QUALITY, FITNESS FOR A PARTICULAR PURPOSE, USABILITY, INTEGRATION OR NON-INFRINGEMENT AND ALL SUCH WARRANTIES ARE HEREBY EXCLUDED BY WILEY AND ITS LICENSORS AND WAIVED BY YOU.

- WILEY shall have the right to terminate this Agreement immediately upon breach of this Agreement by you.

- You shall indemnify, defend and hold harmless WILEY, its Licensors and their respective directors, officers, agents and employees, from and against any actual or threatened claims, demands, causes of action or proceedings arising from any breach of this Agreement by you.

- IN NO EVENT SHALL WILEY OR ITS LICENSORS BE LIABLE TO YOU OR ANY OTHER PARTY OR ANY OTHER PERSON OR ENTITY FOR ANY SPECIAL, CONSEQUENTIAL, INCIDENTAL, INDIRECT, EXEMPLARY OR PUNITIVE DAMAGES, HOWEVER CAUSED, ARISING OUT OF OR IN CONNECTION WITH THE DOWNLOADING, PROVISIONING, VIEWING OR USE OF THE MATERIALS REGARDLESS OF THE FORM OF ACTION, WHETHER FOR BREACH OF CONTRACT, BREACH OF WARRANTY, TORT, NEGLIGENCE, INFRINGEMENT OR OTHERWISE (INCLUDING, WITHOUT LIMITATION, DAMAGES BASED ON LOSS OF PROFITS, DATA, FILES, USE, BUSINESS OPPORTUNITY OR CLAIMS OF THIRD PARTIES), AND WHETHER OR NOT THE PARTY HAS BEEN ADVISED OF THE POSSIBILITY OF SUCH DAMAGES. THIS LIMITATION SHALL APPLY NOTWITHSTANDING ANY FAILURE OF ESSENTIAL PURPOSE OF ANY LIMITED REMEDY PROVIDED HEREIN.

- Should any provision of this Agreement be held by a court of competent jurisdiction to be illegal, invalid, or unenforceable, that provision shall be deemed amended to achieve as nearly as possible the same economic effect as the original provision, and the legality, validity and enforceability of the remaining provisions of this Agreement shall not be affected or impaired thereby.

- The failure of either party to enforce any term or condition of this Agreement shall not constitute a waiver of either party's right to enforce each and every term and condition of this Agreement. No breach under this agreement shall be deemed waived or excused by either party unless such waiver or consent is in writing signed by the party granting such waiver or consent. The waiver by or consent of a party to a breach of any provision of this Agreement shall not operate or be construed as a waiver of or consent to any other or subsequent breach by such other party.

- This Agreement may not be assigned (including by operation of law or otherwise) by you without WILEY's prior written consent.

- Any fee required for this permission shall be non-refundable after thirty (30) days from receipt by the CCC.

- These terms and conditions together with CCC's Billing and Payment terms and conditions (which are incorporated herein) form the entire agreement between you and WILEY concerning this licensing transaction and (in the absence of fraud) supersedes all prior agreements and representations of the parties, oral or written. This Agreement may not be amended except in writing signed by both parties. This Agreement shall be binding upon and inure to the benefit of the parties' successors, legal representatives, and authorized assigns.

- In the event of any conflict between your obligations established by these terms and conditions and those established by CCC's Billing and Payment terms and conditions, these terms and conditions shall prevail.

- WILEY expressly reserves all rights not specifically granted in the combination of (i) the license details provided by you and accepted in the course of this licensing transaction, (ii) these terms and conditions and (iii) CCC's Billing and Payment terms and conditions.

- This Agreement will be void if the Type of Use, Format, Circulation, or Requestor Type was misrepresented during the licensing process.

- This Agreement shall be governed by and construed in accordance with the laws of the State of New York, USA, without regards to such state's conflict of law rules. Any legal action, suit or proceeding arising out of or relating to these Terms and Conditions or the breach thereof shall be instituted in a court of competent jurisdiction in New York County in the State of New York in the United States of America and each party hereby consents and submits to the personal jurisdiction of such court, waives any objection to venue in such court and consents to service of process by registered or certified mail, return receipt requested, at the last known address of such party.

Curriculum Vitae

EDUCATION

2012-Present   **PhD Medical Biophysics, Clinical CAMPEP MSc** (in progress)
Western University, London, Ontario

Supervisor: Aaron D. Ward, PhD
Project Title: *"Toward Optimization of Target Planning for 3D Transrectal Ultrasound-Guided Prostate Biopsy"*

2007-2012   **BSc (Honours) Physics/Applied Mathematics**
Memorial University of Newfoundland, St. John's, Newfoundland & Labrador

Supervisor: Luc Y. Beaulieu, PhD
Honours Thesis Title: *"Correlating surface roughness to the root mean squared roughness, skewness and kurtosis statistical parameters"*

AWARDS, SCHOLARSHIPS AND ACHIEVEMENTS

2017   **Top Oral Presentation Award**
Oncology Research and Education Day, London, ON

2016-2018   **NSERC CGS-D Scholarship ($35,000 annually)**
Held at Western University, London, ON

2016-2018   **Doctoral Excellence Research Award ($10,000)**
Held at Western University, London, ON

2015-2016   **Ontario Graduate Scholarship ($15,000 annually)**
Held at Western University, London, ON

2015   **3rd Place Poster Presentation Award**
Imaging Network Ontario Symposium, London, ON

2015   **CCSRI Travel Award**
Canadian Cancer Society Research Institute, Toronto, ON

2014   **2nd Place Poster Presentation Award**
Imaging Network Ontario Symposium, Toronto, ON

2012-2014   **Computer-Assisted Medical Intervention (CAMI) Trainee**
NSERC Collaborative Research and Training Experience Program
Western University

2012-Present **Western Graduate Research Scholarship**
Western University

2009-2010   **Department of Science Dean's List**
Memorial University of Newfoundland

2007   **Entrance Scholarship**
Memorial University of Newfoundland

RESEARCH

PEER-REVIEWED JOURNAL PUBLICATIONS

1. **Martin P.**, Cool D.W., Fenster A., Ward A.D., "A comparison of prostate tumor targeting strategies using magnetic resonance imaging-targeted, transrectal ultrasound-guided fusion biopsy" Med Phys, 2017 (**Accepted for publication**).

2. Bauman G., **Martin P.**, Thiessen J.D., Taylor R., Moussa M., Gaed M., Rachinsky I., Kassam Z., Chin J., Pautler S., Lee T.Y, Valliant J.F., Ward A., "[^{18}F]- DCFPYL Positron Emission Tomography/Magnetic Resonance Imaging for Localization of Dominant Intraprostatic Foci: First Experience" European Urology Focus 222, https://doi.org/10.1016/j.euf.2016.10.002, 2016.

3. **Martin P.**, Cool D.W., Romagnoli C., Fenster A., Ward A.D., "Magnetic resonance imaging-targeted, 3D transrectal ultrasound-guided fusion biopsy for prostate cancer: quantifying the impact of needle delivery error on diagnosis" Med Phys 41(7), 2014.

CONFERENCE PROCEEDINGS

1. **Martin P.** How does prostate biopsy guidance error impact pathologic cancer risk assessment? SPIE Medical Imaging, February 27-March 3, 2016. San Diego, CA, USA (**podium presentation**).

2. **Martin P.** Optimizing MRI-targeted fusion prostate biopsy: the effect of systematic error and anisotropy on tumour sampling. SPIE Medical Imaging, February 21-26, 2015. Orlando, FL, USA (**podium presentation**).

3. **Martin P.** Toward 3D-guided prostate biopsy target optimization: an estimation of tumour sampling probabilities. SPIE Medical Imaging, February 15–20, 2014. San Diego, CA, USA (**podium presentation**).

REFEREED ABSTRACTS

1. **Martin P.** How should we target prostate tumours using fusion biopsy? COMP Annual Scientific Meeting, July 12-15, 2017. Ottawa, ON (**podium presentation**).

2. **Martin P.** How should we target prostate tumours using fusion biopsy? London Imaging Discovery Day, June 27, 2017. London, ON (poster presentation).

3. **Martin P.** How should we target prostate tumours using fusion biopsy? Oncology Research and Education Day, June 16, 2017. London, ON (**podium presentation**).

4. **Martin P.** How should we target prostate tumours using fusion biopsy? London Health Research Day, March 28, 2017. London, ON (poster presentation).

5. **Martin P.** How should we target prostate tumours using fusion biopsy? Imaging Network Ontario Symposium, March 15-16, 2017. London, ON (poster presentation).

6. **Martin P.** How does prostate biopsy guidance error impact pathologic cancer risk assessment? COMP Annual Scientific Meeting, July 20-23, 2016. St. John's, NL (**podium presentation**).

7. **Martin P.** How does prostate biopsy guidance error impact pathologic cancer risk assessment? London Imaging Discovery Conference, June 21, 2016. London, ON (**podium presentation**).

8. **Martin P.** How does prostate biopsy guidance error impact pathologic cancer risk assessment? Imaging Network Ontario Symposium, March 30-31, 2016. Toronto, ON (poster presentation).

9. **Martin P.** How does prostate biopsy guidance error impact pathologic cancer risk assessment? London Health Research Day, March 29, 2016. London, ON (poster presentation).

10. **Martin P.** Optimizing MRI-targeted fusion prostate biopsy: the effect of systematic error and anisotropy on tumour sampling. IUPESM World Congress on Medical Physics and Biomedical Engineering, June 7-12, 2015. Toronto, ON (**podium presentation**).

11. **Martin P.** Optimizing MRI-targeted fusion prostate biopsy: the effect of systematic error and anisotropy on tumour sampling. Imaging Network Ontario Symposium, March 30-31, 2015. London, ON

12. **Martin P.** Magnetic resonance imaging-targeted, 3D transrectal ultrasound-guided fusion biopsy for prostate cancer: quantifying the impact of needle delivery error on diagnosis. London Imaging Discovery Conference, June 26, 2014. London, ON

13. **Martin P.** Magnetic resonance imaging-targeted, 3D transrectal ultrasound-guided fusion biopsy for prostate cancer: quantifying the impact of needle delivery error on diagnosis. Oncology Research and Education Day, June 20, 2014. London, ON

14. **Martin P.** Magnetic resonance imaging-targeted, 3D transrectal ultrasound-guided fusion biopsy for prostate cancer: quantifying the impact of needle delivery error on diagnosis. Imaging Network Ontario Symposium, March 24, 2014. Toronto, ON (**podium presentation**).

15. **Martin P.** Magnetic resonance imaging-targeted, 3D transrectal ultrasound-guided fusion biopsy for prostate cancer: quantifying the impact of needle delivery error on diagnosis. London Health Research Day, March 18, 2014. London, ON

16. **Martin P.** Toward optimization of Planning for 3D-Guided Prostate Biopsy. Canadian Cancer Research Conference, November 4, 2013. Toronto, ON

17. **Martin P**. Toward optimization of Planning for 3D-Guided Prostate Biopsy. Joint meeting of Canadian Association of Radiation Oncologists and Canadian Organization of Medical Physicists – Innovations in Imaging, September 19, 2013. Montreal, QC (**podium presentation**).

18. **Martin P.** Toward optimization of Planning for 3D-Guided Prostate Biopsy. Oncology Research and Education Day, June 21, 2013. London, ON

19. **Martin P.** Toward optimization of Planning for 3D-Guided Prostate Biopsy. London Imaging Discovery Conference, June 13, 2013. London, ON (**podium presentation**).

20. **Martin P.** Toward optimization of Planning for 3D-Guided Prostate Biopsy. London Health Research Day, March 19, 2013. London, ON

21. **Martin P.** Toward optimization of Planning for 3D-Guided Prostate Biopsy. Imaging Network Ontario Symposium, February 4, 2013. Toronto, ON (**podium presentation**).

LOCAL PRESENTATIONS

1. **Martin P.** How should we target prostate tumours using fusion biopsy?   Imaging Applications in Prostate Cancer Workshop, November 17, 2017. London, ON

2. **Martin P.** How should we target prostate tumours using fusion biopsy? Physicists in Medicine Journal Club, October 25, 2017. London Regional Cancer Program, London, ON

3. **Martin P.** How does prostate biopsy guidance error impact pathologic cancer risk assessment? Imaging Applications in Prostate Cancer Workshop, November 25, 2016. London, ON

4. **Martin P.** How does prostate biopsy guidance error impact pathologic cancer risk assessment? Physicists in Medicine Journal Club, May 9, 2016. London Regional Cancer Program, London, ON

5. **Martin P.** Optimizing MRI-targeted fusion prostate biopsy: the effect of systematic error and anisotropy on tumour sampling. Imaging Applications in Prostate Cancer Workshop, November 21, 2014. London, ON

6. **Martin P.** Optimizing MRI-targeted fusion prostate biopsy: the effect of systematic error and anisotropy on tumour sampling. Physicists in Medicine Journal Club, October 27, 2014. London Regional Cancer Program, London, ON

7. **Martin P.** Magnetic resonance imaging-targeted, 3D transrectal ultrasound-guided fusion biopsy for prostate cancer: quantifying the impact of needle delivery error on diagnosis. Physicists in Medicine Journal Club, April 20, 2014. London Regional Cancer Program, London, ON

8. **Martin P.** Magnetic resonance imaging-targeted, 3D transrectal ultrasound-guided fusion biopsy for prostate cancer: quantifying the impact of needle delivery error on diagnosis. Computer Assisted Medical Interventions Seminar, March 14, 2014. Robarts Research Institute, London, ON

9. **Martin P.** Magnetic resonance imaging-targeted, 3D transrectal ultrasound-guided fusion biopsy for prostate cancer: quantifying the impact of needle delivery error on diagnosis. Imaging Applications in Prostate Cancer Workshop, November 22, 2013. London, ON

10. **Martin P.** Toward optimization of planning for 3D-guided prostate biopsy. Physicists in Medicine Journal Club, April 15, 2013. London Regional Cancer Program, London, ON

11. **Martin P.** Toward optimization of planning for 3D-guided prostate biopsy. Computer Assisted Medical Interventions Seminar, March 15, 2013. Robarts Research Institute, London, ON

TEACHING EXPERIENCE

09/17-12/17   **Weekly quality assurance "QA-ship"**
Performed weekly quality assurance tests on the linear accelerators at London Regional Cancer Program.
London Health Science Centre
Western University

01/15-04/15   **Weekly quality assurance "QA-ship"**
Performed weekly quality assurance tests on the linear accelerators at London Regional Cancer Program.
London Health Science Centre
Western University

01/14-04/14   **Co-developer of graduate Medical Imaging course**
Other co-developers: Eli Gibson, Anthony Lausch, Sarah Mattonen, Kurtis Dekker, Ivan Kosik, Zahra Hosseini, Patricia Johnson, Dr. Tamie Poepping, Dr. Charles McKenzie, Dr. Jerry Battista, Dr. Aaron Ward
Objective: To provide students with practical, hands-on experience implementing previously learned imaging concepts using desktop imaging systems in the context of computed tomography, magnetic resonance, and ultrasound imaging modalities.
Western University

04/11-07/11   **Teaching Assistant**
Developed online tutorial videos for undergraduate physics students
Department of Physics and Physical Oceanography
Memorial University of Newfoundland

09/10-12/10 **Teaching Assistant**
Graded weekly calculus assignments
Department of Mathematics and Statistics
Memorial University of Newfoundland